2-23-2017

Improving Effects of Sampling Time in Fast Adaptation-Based Control Algorithms with Applications

John R. Cooper
University of Connecticut, john.cooper@uconn.edu

Improving Effects of Sampling Time in Fast Adaptation-Based Control Algorithms with Applications

John Cooper, Ph.D.

University of Connecticut, 2017

Over the past decade, $\mathcal{L}_1$ adaptive control has emerged as viable control architecture for systems with unmodeled dynamics and time-varying uncertainties. $\mathcal{L}_1$ control uses a concept known as "fast adaptation" to estimate uncertainties. This means the controller relies on high sampling rates. However, in any real-world application, sampling speed is limited by hardware capabilities. Thus the question of how to obtain better performance at slower sampling rates in fast adaptation-based algorithms has become an important research topic. This dissertation presents two methods of online modeling to solve this problem. The first of these is function approximation using artificial neural networks. This removes the burden of estimating state-dependent nonlinearities from the adaptive law. The second method is a memorizing mechanism which uses an integrator to store estimations from previous time-steps. The benefits of each of these methods are shown analytically and in simulation by comparing performance to an unmodified $\mathcal{L}_1$ controller.

Additionally, a technique for using fast adaptation to perform online optimization is discussed. Engineering systems are often designed to optimize some criteria, but in practice, manufacturing variability and component age cause deviations from the optimal design. Performance-seeking control can be used to re-optimize a system online by changing control inputs based on adaptation. This is useful when two control inputs are implicitly related such that an optimum point exists in the cost function. One input is updated via a gradient search while the other is updated via a Lyapunov-based controller using adaptive parameters for feedback. Simulation results are presented.

Finally, the dissertation contains two case studies: pressure control in aircraft air management systems and satellite orbit stabilization. In air management systems, the relationship between valve angle and downstream pressure is highly nonlinear, and the dynamics are

subject to effects of hysteresis due to dry friction. Man-made satellites are subject to a number of difficult-to-measure disturbance forces such as variations in Earth's gravitational and magnetic fields, aerodynamic drag, and solar radiation pressure. These characteristics lend themselves well to the use of adaptive control. Each case study contains simulation examples and comparisons of different control strategies.

Improving Effects of Sampling Time in Fast Adaptation-Based Control Algorithms with Applications

John Cooper

B.S., University of New Haven, **2010**

A Dissertation

Submitted in Partial Fulfillment of the

Requirements for the Degree of

Doctor of Philosophy

at the

University of Connecticut

2017

APPROVAL PAGE

Doctor of Philosophy Dissertation

Improving Effects of Sampling Time in Fast Adaptation-Based Control Algorithms with Applications

Presented by

John Cooper, B.S.

Major Advisor _____
Chengyu Cao

Associate Advisor _____
Jiong Tang

Associate Advisor _____
Nejat Olgac

Associate Advisor _____
Zhaoyan Fan

Associate Advisor _____
Irene Gregory

Associate Advisor _____
Xu Chen

University of Connecticut
2017

To my son, Julian, and wife, Sasha

Contents

Introduction

Adaptive control has been researched since the 1950's and has recently seen an increase in industrial application [20, 83, 19]. This is a result of the increased capabilities of computer hardware over the course of the last half-century. "Fast adaptation" controllers such as $\mathcal{L}_1$ adaptive control have further advanced the state of the art over the last decade [12, 11]. These algorithms rely on very fast sampling rates to update adaptive parameters at every time-step. This of course places a requirement on the control hardware which cannot be met by many current industrial processors. This dissertation solves this issue by introducing two techniques for increasing performance of fast adaptation-based algorithms in the presence of slow sampling rates.

In order to overcome the loss of performance at slow sampling speeds, it is desirable to have a more accurate state estimation. This reduces the load on the adaptive law, i.e. lower magnitude adaptive parameters are generated. One way to solve this is to perform additional a-priori system identification. However, the main purpose of adaptive control is to determine controller parameters online without spending resources on system identification. Another approach is to perform online modeling. This dissertation presents two methods for incorporating online modeling into an $\mathcal{L}_1$ adaptive controller. The first of these uses the artificial learning of neural networks. A weighted sum of Gaussian radial basis functions is used to approximate the state-dependent component of system uncertainties. The second method is a memorizing mechanism that stores past information by using an integrator in the adaptive law.

In addition to these contributions, this dissertation also introduces a technique that uses fast adaptation to perform online optimization. This can be used in any system where two control inputs are implicitly related. A performance-metric is optimized by updating one of the inputs via a gradient search and the other via a Lyapunov-based controller where the Lyapunov function is composed of adaptive estimates. This method is known as performance-seeking control and is useful in applications in which an engineering system is designed to optimize a criteria, for example fuel efficiency in jet engines. Manufacturing variability and age-related degradation can both play a role in moving the actual system operating point away from the optimum. Performance-seeking control can then be used to re-optimize the system.

Finally, two case studies are presented. The first case study is control of a nonlinear pressure-regulating engine bleed valve in aircraft air management systems. The control valve is subject to hysteresis due to backlash and dry friction. The second case study is satellite orbit stabilization. Man-made satellites are subject to many unknown disturbances including variations in Earth's gravitational and magnetic fields, aerodynamic drag, and solar radiation pressure.

The dissertation is organized as follows: Chapter 1 gives a history of the control engineering field and explains how adaptive control fits into the larger picture. Chapter 2 describes the basic $\mathcal{L}_1$ adaptive control architecture, which the dissertation's major contributions are applied to in Chapters 3 and 4. Chapter 5 describes the performance-seeking controller. Chapters 6 and 7 present the case studies on aircraft air management systems and satellite orbit stabiliization respectively. Finally in 8, conclusions are drawn and directions for future work are proposed.

Chapter 1

History of Control Theory and Literature Review

While the primary topic of this dissertation is adaptive control, specifically fast adaptation-based algorithms, this chapter serves to provide the reader with a comprehensive overview of the history and development of control engineering. This supplies a necessary perspective for the main contributions and required background when comparing adaptive control results to those of traditional controllers.

Control is a branch of engineering and mathematics that studies how to design the input of a system to achieve a desired output. What is meant by "system" in this case is anything that produces an output when given an input. For example, a car can be considered a system where the input is the displacement of the gas pedal, and the output is the car's velocity. Systems to be controlled can take almost any form including, electric circuits, mathematical equations, bank accounts, and many other elements that appear in engineering fields.

Some of the earliest examples of this topic include flow rate control in a water clock and control of the liquid level in a wine vessel. Cornelias Drebbel is credited with creating a temperature control system for an egg incubator as early as the 16th century. Many of the early works in control were motivated by the need to maintain a constant rotational shaft

speed. One such example is the fly-ball governor, which was applied to the steam engine in 1788 by James Wyatt. Each of these systems is described in [51].

1.1 Stability

Stability is the most important aspect of control design. A stable system is one for which a bounded input yields a bounded output. In an unstable system, the output continues to increase toward infinity for any small input. This is obviously undesirable because the system cannot be controlled. The earliest discussion of instability in feedback control came from G.B. Airy in regards to rotational control of a telescope [2]. The first systematic study of stability was performed by J.C. Maxwell in 1868 [50]. In this work, he derived a stability condition for 2nd and 3rd order systems. E.J. Routh later developed a complete stability criteria in 1877 [70].

The Routh stability criterion states that for a system to be stable, each pole must have a negative real part. Since system transfer functions are expressed as ratios of polynomials, each factor of the denominator corresponds to an exponential decay factor in the time-domain response. If a pole has a positive real part, the exponential decay factor becomes an exponential growth factor, and the response becomes unbounded.

In 1927, H.S. Black invented the electronic feedback amplifier at Bell Telephone Laboratories [6, 5]. This invention made long-distance telephoning possible, but resulted in a high-gain feedback loop, which can easily destabilize a system. The system dynamics involved were too complex to apply Routh's stability analysis. This lead Harry Nyquist to develop the Nyquist stability criteria [59]. This criteria uses a Nyquist plot to evaluate stability based on the argument principle. The argument principle states that for a give closed trajectory of the Laplace variable in the complex plane, the evaluation of a system transfer function for each point on the trajectory will encircle the origin only if a pole or zero is enclosed in the trajectory. The Nyquist plot is a plot of the open-loop transfer function

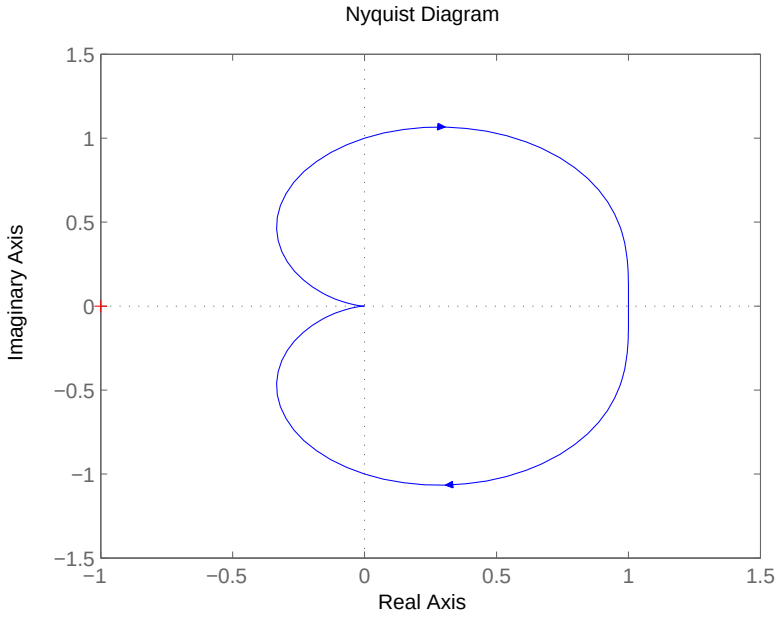

Figure 1.1: Nyquist plot for the system $\frac{1}{s^2+s+1}$.

along a trajectory that encircles the entire right-half of the complex plane. If the Nyquist plot encircles the point -1, then the closed-loop transfer function has a pole or zero in the right-half plane. A clockwise encirclement indicates a zero while a counterclockwise encirclement indicates a pole. Therefore, a clockwise encirclement means the closed-loop system is unstable. Figure 1.1 shows an example of a Nyquist plot.

The Nyquist plot is useful for checking the gain and phase margins to determine stability. The gain margin is the factor by which the control gain can be increased before the system becomes unstable, and the phase margin is the angle by which the transfer function can be rotated by before become unstable.

Not much later than Routh, A.M. Lyapunov studied stability of motion using nonlinear differential equations [49]. This work was published in 1892, but was not introduced to control until circa 1948. Lyapunov stability is concerned with more than simply whether a bounded input yields a bounded output. A system is said to be "uniformly stable" if stability does not depend on initial conditions, "asymptotically stable" if the state approaches an equilibrium state as time increases, and "uniformly asymptotically stable" if the state is

bounded for all time after a certain threshold.

Stability can be determined by Lyapunov's direct method, which can be stated as follows. If there exists a positive definite function of the system states that has a negative semi-definite time derivative (a Lyapunov function), the equilibrium point (where the function is equal to zero) is stable. If the equilibrium point is stable and the Lyapunov function is decrescent, it is uniformly stable. If the point is uniformly stable and the Lyapunov funtion's time derivative is negative definite, the point is uniformly asymptotically stable.

1.2 Classical Control

Using Nyquist stability theory, Bode developed a design methodology for feedback amplifiers [6]. The Bode plots are plots of the magnitude and phase of the open-loop transfer function versus frequency for a sinusoidal input. The gain and phase margins can be quickly read from these plots. The phase margin is the distance the phase is from 180°at the frequency where the magnitude is zero dB. The gain margin is the distance the gain is from 0 dB at the frequency where the phase angle is 180°. Figure 1.2 shows an example pair of Bode plots.

Bode plots are useful for the design of lag/lead compensators, a control architecture in which one pole and one zero are added to the system. Control systems are often required to meet specified stability margins, and Bode plots provide a systematic way to select lag/lead parameters to meet such specifications.

At the same time as the development of the feedback amplifier, feedback control began to be used for industrial processes. These systems consisted of complicated nonlinear dynamics with time-delays between sensors and actuators. The proportional-integral-derivative (PID) controller was developed for these applications [8]. This development was based on experimental results and simplified linear models of the processes to be controlled. In PID, the control signal is generated as the sum of a component proportional to the error signal between reference and measurement, a component proportional to the integral of the error

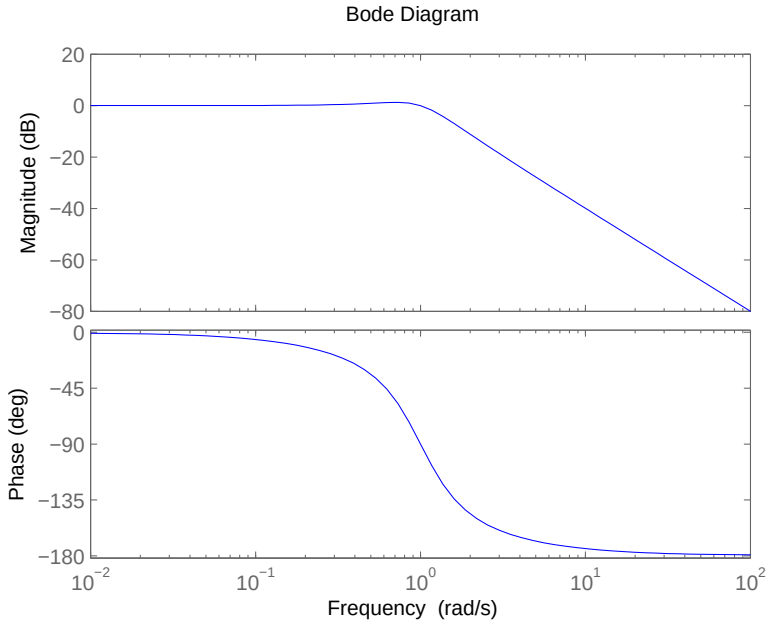

Figure 1.2: Bode plots for the system $\frac{1}{s^2+s+1}$.

signal, and a component proportional to the derivative of the error signal. If only the proportional term is used, a steady-state error will always be present since a nonzero control signal cannot correspond to zero error. Adding the integral term can eliminate error but can make the control signal too aggressive, causing oscillations. The derivative term applies corrective action early on and adds damping to the system. Sensor noise is easily amplified by taking the derivative of a measured signal, thus the signal is usually low-pass filtered before taking the derivative in practice.

Alongside feedback amplifier design and PID, a theory of stochastic processes was being developed by N. Wiener [82]. These three disparate, yet tightly related research areas were finally united in 1947 when MIT Radiation Laboratory published a comprehensive set of techniques for the design of servomechanisms [36].

In 1948, W.R. Evans published an extension to Routh's work which provided a means for graphical analysis of control systems [23]. Unstable aircraft dynamics were a prime motivator for this method. Evans' graphical analysis has come to be known as the root locus method. It is used to determine the range of parameter values for which a closed-loop system is stable.

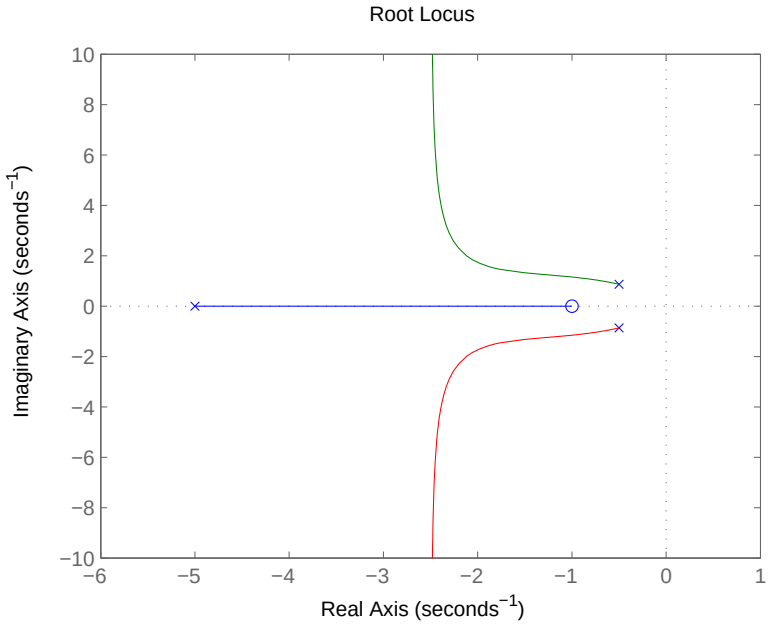

Figure 1.3: Root locus for the system $\frac{1}{s^2+s+1}$ controlled by the compensator $\frac{s+1}{s+5}$.

Each system pole is plotted in the complex plane as the control gain is varied from zero to infinity. Figure 1.3 shows an example of the root locus method. Note that this system is stable for any control gain value since no poles ever cross the imaginary axis.

1.3 Modern Control

The methods described up to this point comprise what is known as *classical control*. Starting in the 1950's, a new branch of control theory known as *modern control* emerged. In modern control, systems are represented in the state space format as opposed to the transfer function format, and analysis is done in the time-domain as opposed to the frequency-domain. These characteristics enable the analysis of nonlinear and time-varying systems. Lyapunov functions are used to determine stability. Notable early works in modern control can be found in [4, 37, 66].

One of the most important themes in control theory over the last half-century has been methods for dealing with uncertainties. Uncertainty can refer to measurement noise, unmod-

eled dynamics, and unknown disturbance. There exist two distinct philosophies in dealing with this issue: robust control and adaptive control. In robust control, the controller design is static, and is given the maximum loop gain within the reference signal frequency spectrum without causing instability [52]. Adaptive control (the main focus of this dissertation) uses time-varying controller parameters that are updated based on measurements.

A popular type of pseudo-adaptive control is known as gain scheduling [41]. Gain scheduled controller parameters are updated based on the detected operating point. Sensor feedback is used to detect the operating point, and the controller gains are determined using a lookup table. In this manner, gains can be updated as quickly as sensors respond to changes. There are a few caveats to this approach. For example, frequent and rapid gain changes can lead to instability. This can be mitigated by placing limits on the parameter change rate. Furthermore, the gains must be computed offline, so feedback cannot correct for errors. Also, gain scheduling is expensive to implement when there is a large number of operating points, and finally in order to detect operating points, additional sensors may be required.

1.4 Adaptive Control

An adaptive controller is one with parameters that are automatically updated online to achieve better performance. Adaptive control is most useful in applications where operating conditions change over time. In these cases, a single, tuned controller parameter value may not yield the desired control performance over the whole range of conditions. An example which was the primary motivation for early adaptive control research in the 1950's is the design of autopilots for high-performance aircraft [31, 54]. For a given Mach number and altitude, aircraft dynamics can be linearized, and a traditional controller can be designed. However, when Mach and altitude deviate sufficiently from the operating point which the system has been linearized for, the linear model is no longer valid, and there is no guarantee that the designed controller will remain stable.

Adaptive control combines a parameter estimator, or adaptive law, with a control law that is designed as if the true values of the parameters are known. These controllers can be classified as either indirect or direct. In indirect adaptive control, plant parameters are estimated and controller parameters are then calculated using the estimations. In direct adaptive control, the plant model is parameterized in terms of the controller parameters, and controller parameters are estimated directly.

The earliest results in adaptive control were mainly experimentally-based with very little theoretical analysis [3]. In 1965, Lyapunov stability was first applied to adaptive controllers [61, 76]. Later, conditions for global stability in adaptive control were established by Goodwin et al. [28].

Model reference adaptive control (MRAC) is one of the most widely known methods of adaptive control [3]. It is a special class of adaptive pole placement control (APPC). The goal of APPC is to design a controller such that closed loop poles are in the desired location in the complex plane. If plant parameters are known, this is an easy task. When they are unknown, they are replaced with adaptively generated estimates.

In MRAC, the designer chooses a reference model which specifies the desired input-output relation of the system. The goal is then to design a parameterized control law such that the closed-loop transfer function is equivalent to the reference model. This can be achieved by canceling the plant zeros and replacing them with the reference model zeros. This of course restricts the system to be minimum phase since canceling a zero with a positive real part would introduce a pole with a positive real part to the system. To find the controller parameters the plant is parameterized as well. If the plant parameters were known, controller parameters could be computed easily. When plant parameters are unknown, the controller parameters are replaced with adaptive estimates which are obtained by either direct or indirect methods. Figure 1.4 shows the basic block-diagram of the MRAC architecture.

The design of the adaptive law can take many forms. A few examples are the sensitivity method, positivity and Lyapunov designs, and gradient or least squares methods. The

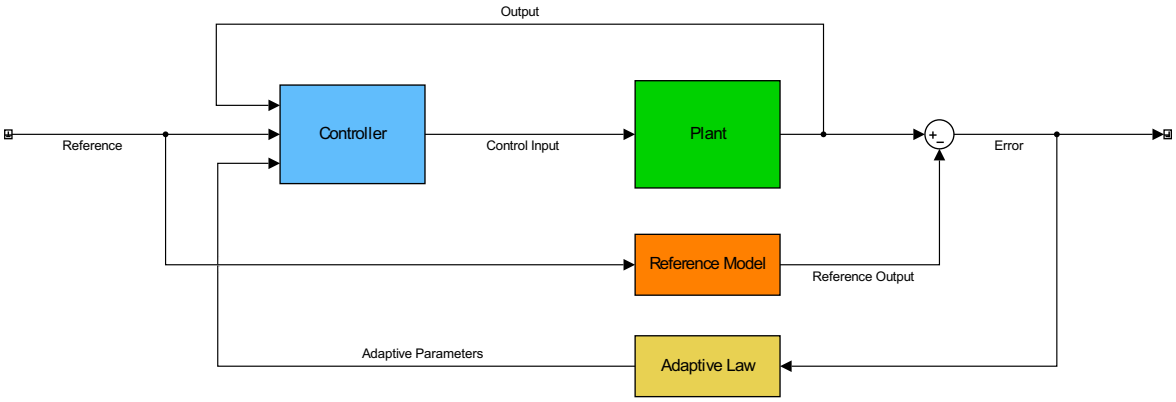

Figure 1.4: MRAC block-diagram

sensitivity method is an adaptive law designed to minimize a certain performance function. For example, this is usually the error between a measured signal and a model output that uses the estimated parameters. Positivity and Lyapunov designs reformulate the adaptive law design as a stability problem [61, 76]. Gradient and least squares methods are based on estimation error costs. These avoid non-implementable sensitivity functions by basing the cost function on the estimation error.

In the mid 1980's, Rohrs et al. showed a lack of robustness in the current adaptive control designs with respect to unmodeled dynamics and disturbances [68]. This was the impetus for developments such as σ-modification [35, 34] and e-modification [57]. Furthermore, backstepping adaptive control was developed as a method to handle more complex nonlinear systems [39].

$\mathcal{L}_1$ adaptive control is a form of indirect adaptive control based on model reference adaptive control (MRAC) which has been developed over the course of the last decade [12, 11]. The $\mathcal{L}_1$ control architecture consists of a state predictor, adaptive law, and control law. The state predictor is a dynamic system that attempts to estimate the system state or output using adaptive parameters. The adaptive law updates the adaptive parameters using a fast adaptation scheme. This means the controller relies on fast sampling rates. The control law then uses the updated parameters to drive the state predictor to track a desired reference. The combination of these components results in the real system output tracking the desired

reference. Adaptive control design usually consists of a trade-off between performance and robustness. The $\mathcal{L}_1$ architecture seeks to conduct this trade-off in a systematic way by decoupling estimation and control. This is done by utilizing fast adaptation such that the accuracy of uncertainty estimation is limited by hardware sampling rates, and robustness is maintained by low-pass filtering the control input. $\mathcal{L}_1$ is the architecture to which the main contributions of this dissertation will be applied to, and it will be discussed in detail in Chapter 2.

Chapter 2

$\mathcal{L}_1$ Adaptive Control

The $\mathcal{L}_1$ controller consists of three components: state predictor, adaptive law, and control law. The state predictor is a dynamic system that tries to match the plant dynamics by using adaptive estimates of system uncertainties. The adaptive law compares the predicted state to the measured state and updates the adaptive estimates to drive the prediction error to zero. The control law is designed to cancel the effects of the adaptive estimates on the state predictor and drive the predicted output to match a desired reference signal. The combination of this control law design with the adaptive law leads to the measured output tracking the desired reference. A block diagram of this architecture is shown in Figure 2.1.

There are a few key differences between the $\mathcal{L}_1$ structure and the MRAC structure shown

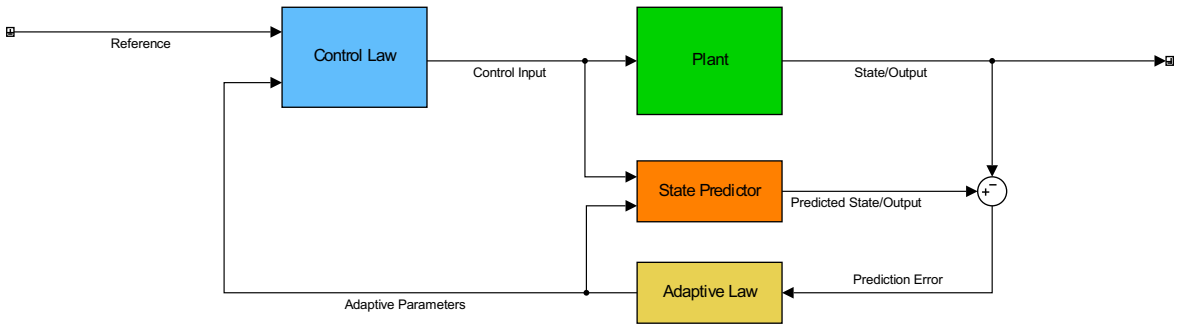

Figure 2.1: $\mathcal{L}_1$ block-diagram

in Figure 1.4. In MRAC, the desired closed-loop dynamics are specified by the reference model, while the $\mathcal{L}_1$ state predictor specifies open-loop dynamics that are controlled via the adaptive law. Furthermore, the control law does not use direct plant feedback as the MRAC controller does.

The following sections describe the three components of the $\mathcal{L}_1$ formulation in detail.

2.1 Problem Formulation

Consider a single-input, single-output (SISO) system with full state feedback,

$$\begin{aligned} \dot{x}(t) &= A_K x(t) + B u_K(t) + \sigma(x,t) \\ y &= Cx(t) \quad x(0) = 0 \end{aligned} \tag{2.1}$$

where $x \in \mathbb{R}^n$ is the state, $t \in \mathbb{R}$ is time, $A_K \in \mathbb{R}^{n \times n}$ is the state matrix, $B \in \mathbb{R}^n$ is the input matrix, $u \in \mathbb{R}$ is the control input, $\sigma \in \mathbb{R}^n$ is a vector of bounded, unknown disturbances, $y \in \mathbb{R}$ in the output, and $C \in \mathbb{R}^{1 \times n}$ is the output matrix.

Assumption 2.1. *A_K, B is controllable.*

Assumption 2.2. *$\exists\, L(\delta) \quad \forall\, \delta > 0$ such that*

$$||\sigma(x,t) - \sigma(\bar{x},t)||_\infty \leq L(\delta)||x - \bar{x}||_\infty \quad \forall\, ||x||_\infty \leq \delta, ||\bar{x}||_\infty \leq \delta \tag{2.2}$$

Assumption 2.3. *$\exists\, B_1$ such that $||\sigma(x,t)||_\infty \leq B_1 \quad \forall\, t \geq 0$.*

Assumption 2.4. *$\exists\, d_{\sigma_x}(\delta) > 0$ and $d_{\sigma_t}(\delta) > 0 \quad \forall\, \delta > 0$ such that*

$$\left|\left|\frac{\partial \sigma(x,t)}{\partial x}\right|\right| \leq d_{\sigma_x}(\delta), \quad \left|\left|\frac{\partial \sigma(x,t)}{\partial t}\right|\right| \leq d_{\sigma_t}(\delta) \quad \forall\, x \text{ such that } ||x||_\infty \leq \delta \tag{2.3}$$

With Assumption 2.1, $\exists K \in \mathbb{R}^{1 \times n}$ such that a nominal control signal, $-Kx(t)$ stabilizes

the system, i.e. $A_K - BK$ is Hurwitz. We can then represent the system in (2.1) as

$$\dot{x}(t) = Ax(t) + Bu(t) + \sigma(x,t) \tag{2.4}$$

where $A = A_K - BK$ and $u(t) = u_K(t) - Kx(t)$. Because $\sigma(x,t)$ is bounded, the system remains controllable in the presence of the uncertainties.

The control objective is for $y(t)$ to track a given reference system while $x(t)$ remains bounded. The reference system dynamics are

$$\begin{aligned} \dot{x}_{des}(t) &= Ax_{des}(t) + BK_g r(t) \\ y_{des}(t) &= Cx_{des}(t) \quad x_{des}(0) = 0 \end{aligned} \tag{2.5}$$

where $x_{des} \in \mathbb{R}^n$ is the reference system state, $K_g = -(CA^{-1}B)^{-1}$, and $r(t)$ is a bounded reference signal with $r(t) \leq ||r||_{\mathcal{L}_\infty}$.

2.2 State Predictor

The state predictor is a dynamic model that matches the structure of the system to be controlled in (2.4),

$$\begin{aligned} \dot{\hat{x}}(t) &= A\hat{x}(t) + Bu(t) + \hat{\sigma}(t) \\ \hat{y} &= C\hat{x}(t) \quad \hat{x}(0) = 0 \end{aligned} \tag{2.6}$$

where $\hat{x} \in \mathbb{R}^n$ is the predicted state, $\hat{\sigma} \in \mathbb{R}^n$ is a vector of adaptive parameters, and $\hat{y}$ is the predicted output. The predicted state is not directly fed back to generate the control signal, $u(t)$. It is instead used to generate the adaptive parameter, $\hat{\sigma}(t)$, based on the error dynamics between it and the real system in (2.4). Full state feedback is still used to define the error dynamics.

2.3 Adaptive Law

The adaptive law is piece-wise constant and is updated at every time-step, i.e. $\hat{\sigma}(t) = \hat{\sigma}(iT)$ where i is an integer such that $iT \leq t < (i+1)T$ and T is the time-step duration.

The adaptive law is obtained by defining the error dynamics. Let the prediction error, $\tilde{x}$ be defined as $\tilde{x}(t) = \hat{x}(t) - x(t)$. Then the error dynamics can be obtained by subtracting (2.4) from (2.6),

$$\dot{\tilde{x}}(t) = A\tilde{x}(t) + \hat{\sigma}(t) - \sigma(x,t) \tag{2.7}$$

(2.7) can be viewed as a system with inputs $\hat{\sigma}(t)$ and $-\sigma(t)$. From linear systems theory, we can write the solution to (2.7) over the interval $[iT, (i+1)T]$ as

$$\tilde{x}(t) = \Phi(T)\tilde{x}(iT) + \int_{iT}^{t} \Phi(t-\tau)\hat{\sigma}(iT)\, d\tau - \int_{iT}^{t} \Phi(t-\tau)\sigma(x,\tau)\, d\tau \tag{2.8}$$

where τ is a dummy variable and $\Phi(T) = e^{AT}$. At $t = (i+1)T$, (2.8) becomes

$$\tilde{x}((i+1)T) = \Phi(T)\tilde{x}(iT) + \int_{0}^{T} \Phi(T-\tau)\hat{\sigma}(iT)\, d\tau - \int_{0}^{T} \Phi(T-\tau)\sigma(x,\tau)\, d\tau \tag{2.9}$$

Note that $\hat{\sigma}(iT)$ does not depend on τ and can thus be taken outside of the integral. We can choose $\hat{\sigma}$ such that its effects on the system drive $\tilde{x}$ to zero at the next time-step by ignoring the third term in (2.7), plugging in $\tilde{x}((i+1)T) = 0$, and solving for $\hat{\sigma}(iT)$. This results in

$$\hat{\sigma}(iT) = \Gamma(T)\tilde{x}(iT), \quad \Gamma(T) = -\left[\int_{0}^{T} \Phi(T-\tau)\, d\tau\right]^{-1} \Phi(T) \tag{2.10}$$

The question of how to obtain $\hat{\sigma}(t)$ for a system without full state feedback has been addressed in [13, 45].

2.4 Control Law

Since we have designed the adaptive law such that $\hat{x}$ tracks x, we can design the control law such that $\hat{y}$ tracks r. The result of these design choices is that y will track r. Let $u(t) = u_1(t) + u_2(t) + u_3(t)$. Then we can rewrite (2.6) as

$$\begin{aligned} \dot{\hat{x}}(t) &= A\hat{x}(t) + B(u_1(t) + u_2(t) + u_3(t)) + \hat{\sigma}(t) \\ \hat{y}(t) &= C\hat{x}(t) \end{aligned} \tag{2.11}$$

u_1 will be used for tracking while u_2 and u_3 will be used to cancel the effects of $\hat{\sigma}$. Using the superposition principle, the relevant system to consider for the design of u_1 becomes

$$\dot{\hat{x}}(t) = A\hat{x}(t) + Bu_1(t) \tag{2.12}$$

$$\hat{y}(t) = C\hat{x}(t) \tag{2.13}$$

At steady-state, we want $\dot{\hat{x}} = 0$ and $\hat{y} = r$. Substituting these into (2.12) and solving for u_1 yields

$$u_1(t) = K_g r(t), \quad K_g = -\left[CA^{-1}B\right]^{-1} \tag{2.14}$$

To design u_2 and u_3, we will first decompose $\hat{\sigma}$ into matched and unmatched components. This is done via the transformation

$$\begin{bmatrix} \hat{\sigma}_1(t) \\ \hat{\sigma}_2(t) \end{bmatrix} = \begin{bmatrix} B & \bar{B} \end{bmatrix}^{-1} \hat{\sigma}(t) \tag{2.15}$$

where $\hat{\sigma}_1 \in \mathbb{R}$ is the matched component of $\hat{\sigma}$, $\hat{\sigma}_2 \in \mathbb{R}^{n-1}$ is the unmatched component, and $\bar{B} \in \mathbb{R}^{n\times(n-1)}$ is the nullspace of B.

The matched component can be canceled directly by simply choosing the opposite of $\hat{\sigma}_1$.

Additionally, we apply a low-pass filter, $C_1(s)$ to u_2. Then we have

$$u_2(s) = -C_1(s)\hat{\sigma}_1(s) \tag{2.16}$$

If $C_1(s) = 1$, u_2 can cancel the effects of $\hat{\sigma_1}$ on the predicted state perfectly. However, notice that the adaptive law in (2.10) is a high-gain feedback design. In implementation, such an approach leads to aggressive control signals in both magnitude and rate and can amplify measurement noise and reduce the time-delay margin of the closed-loop system [44]. The introduction of a low-pass filter at this point in the control loop allows us to decouple control and estimation by only canceling the low-frequency components of $\hat{\sigma}_1$. Furthermore, the bandwidth of $C_1(s)$ can be chosen to attenuate frequencies that are too high for the system to respond to as well as those frequencies which are a-priori known to not be reflective of the real uncertainty. This low-pass filter not only ensures that the control signal stays within a reasonable frequency range, but also provides an efficient tool for adjusting the trade-off between performance and robustness [9].

Because $\hat{\sigma}_2$ is unmatched, it cannot be canceled directly by choosing its opposite in the control signal. However, we can perform a dynamic inversion of the state predictor to cancel the effects of $\hat{\sigma}_2$ on $\hat{y}$. Let us decompose (2.11) into the effects on $\hat{y}$ from $\hat{\sigma}_2$ and u_3 and take the Laplace transforms. This yields

$$\hat{y}_1(s) = C(sI - A)^{-1}Bu_3(s) \tag{2.17}$$

$$\hat{y}_2(s) = C(sI - A)^{-1}\bar{B}\hat{\sigma}_2(s) \tag{2.18}$$

Where $\hat{y}_1 \in \mathbb{R}$ and $\hat{y}_2 \in \mathbb{R}$ are the effects on the predicted output from u_3 and $\hat{\sigma}_2$ respectively. We want $\hat{y}_1 + \hat{y}_2 = 0$. u_3 is obtained by substituting (2.17) and (2.18) and solving for u_3. Similar to (2.16), we apply a low-pass filter, $C_2(s)$, to u_3 to mitigate the effects of high-gain

feedback.

$$u_3(t) = -C_2(s)\frac{C(sI - A^{-1})\bar{B}}{C(sI - A^{-1})B}\hat{\sigma}_2(t) \tag{2.19}$$

The total control law is

$$u(t) = K_g r(t) - C_1(s)\hat{\sigma}_1(t) - C_2(s)\frac{C(sI - A^{-1})\bar{B}}{C(sI - A^{-1})B}\hat{\sigma}_2(t) \tag{2.20}$$

The state predictor in (2.6), the adaptive law in (2.10), and the control law in (2.20) comprise the $\mathcal{L}_1$ adaptive controller.

2.5 Simulation Example

To demonstrate $\mathcal{L}_1$'s dependence on sampling time, we will examine a simulation ran at two different time-steps. Consider the system in (2.4) with

$$A = \begin{bmatrix} 0 & 10 \\ -1 & -\sqrt{2} \end{bmatrix} \quad B = \begin{bmatrix} 0 \\ 1 \end{bmatrix} \quad C = \begin{bmatrix} 1 & 0 \end{bmatrix} \tag{2.21}$$

Let $x = \begin{bmatrix} x_1 & x_2 \end{bmatrix}^\top$. Consider the uncertainty

$$\sigma(x,t) = \begin{bmatrix} 0 \\ -x_1 - (0.5 - 0.1x_1^2)x_2 - \frac{2}{1+0.05x_1^2} \end{bmatrix} \tag{2.22}$$

The $\mathcal{L}_1$ controller parameters are

$$C_1(s) = \frac{5}{s+5} \quad C_2(s) = \frac{1}{s+1} \tag{2.23}$$

Figure 2.2 shows reference tracking performance for the $\mathcal{L}_1$ controller at a sampling rate of $T = 0.001$ seconds, and Figure 2.3 shows that for $T = 0.1$ seconds. The performance

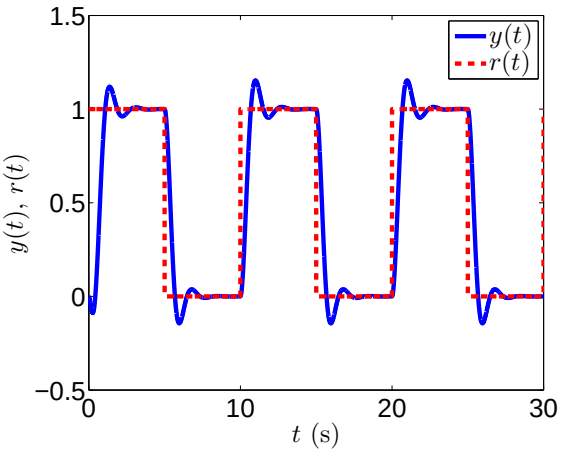

Figure 2.2: Tracking performance with $T = 0.001$ sec

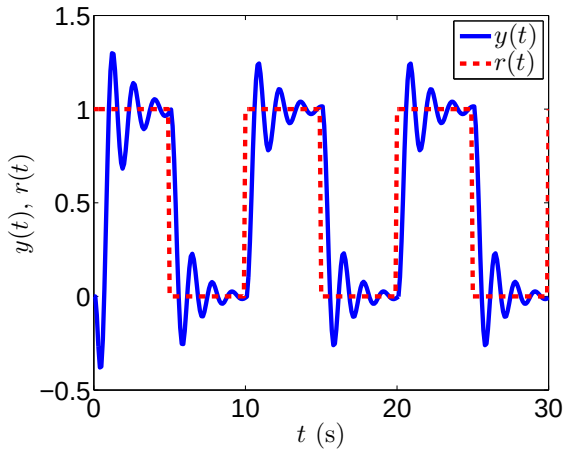

Figure 2.3: Tracking performance with $T = 0.1$ sec

degrades significantly with the decrease in sampling rate. The response in Figure 2.3 has a larger overshoot and is much more oscillatory than that in Figure 2.2. This type of behavior motivates the need for techniques to improve performance at slow sampling rates for fast adaptation-based algorithms. These techniques will be developed and discussed in the following two chapters.

Chapter 3

Artificial Neural Network Adaptive Law

The first of two methods for increasing control performance of fast adaptation-based algorithms in the presence of slow sampling rates is the artificial neural network (ANN) adaptive law. ANNs can be used to represent a nonlinear function as a linear summation of weighted basis functions with an arbitrarily small approximation error. Neural network controller designs have been used to handle systems with nonlinear uncertainties that could not be parameterized linearly [24, 72, 84].

The first rigorous stability proofs of neural network controllers were published by Narendra and Parthsarathy [55]. Some types of neural network controllers that can be found in the literature include back-propagation-type tuning [53, 56], radial basis functions (RBFs) for feedback [74], dead-zone parameter tuning [15, 14], projection-based adaptation [65, 64, 63], e-modification adaptive laws [42], discrete-time systems [73], dynamic ANNs [71], ANNs for general nonlinear systems with full state feedback and output feedback [86, 25], and decentralized control [80]. Some applications in which ANNs have been used are robotic manipulators [43] and aircraft control [7]. ANNs have been used in conjunction with $\mathcal{L}_1$ adaptive control in [81, 10, 18].

This chapter will show that the state prediction error in the $\mathcal{L}_1$ adaptive control architecture is due to both the integration time-step and the actual uncertainty. By adding a Gaussian radial basis function (GRBF) ANN function approximation to the adaptive law, the difference between the actual uncertainty and the uncertainty approximation replaces the actual uncertainty in the prediction error's dependence. As the ANN converges to approximate the uncertainty, the prediction error is reduced. Furthermore, a lack of convergence of the ANN cannot degrade performance.

3.1 Gaussian Radial Basis Function Artificial Neural Network

Any function, $f(x)$, can be expressed as a GRBF ANN with m neurons,

$$f(x) = W\phi(x) + \varepsilon(x), \quad |\varepsilon(x)| \leq \varepsilon^* \tag{3.1}$$

where $W \in \mathbb{R}^{1\times m}$ is the weight vector, $\phi \in \mathbb{R}^m$ is a vector of GRBFs with ith element,

$$\phi_i(x) = \exp\left(-\frac{(x - z_i)^\top (x - z_i)}{\delta_i^2}\right) \tag{3.2}$$

where z_i and δ_i are the center and width of the RBF respectively, ε is the approximation error, and ε^* is the bound of ε. The ANN approximation for $f(x)$ is

$$\hat{f}(x) = \hat{W}\phi(x) \tag{3.3}$$

where $\hat{W} \in \mathbb{R}^{1\times m}$ is the estimated weight vector which is updated via a gradient search.

3.2 Application to $\mathcal{L}_1$ Adaptive Control

To use an ANN adaptive law with $\mathcal{L}_1$ adaptive control, we will reformulate the state predictor in (2.6) as

$$\begin{aligned} \dot{\hat{x}}(t) &= A\hat{x}(t) + B(u(t) + \hat{\sigma}_1(t) + \hat{f}(x)) + \bar{B}\hat{\sigma}_2(t) \\ \hat{y} &= C\hat{x}(t) \quad \hat{x}(0) = 0 \end{aligned} \tag{3.4}$$

$\hat{f}(x)$ will be an approximation for the matched uncertainty. A second ANN could also be used to approximate the unmatched uncertainty, but a single ANN is considered here for ease of analysis. The extension to an additional ANN in the unmatched channel is straight forward.

We will implement a gradient descent algorithm to obtain the update law for $\hat{W}$. Note that many other novel learning methods exist that can be applied here. The gradient descent algorithm is applied for simplicity in arriving at the main result. First, let the error function be defined as

$$E(\hat{W}) = \frac{1}{2}\left(\hat{f}(x) - \sigma_1(x,t)\right)^2 = \frac{1}{2}\left(\hat{W}\phi(x) - \sigma_1(x,t)\right)^2 \tag{3.5}$$

where $\sigma_1 \in \mathbb{R}$ is the matched component of $\sigma(x,t)$, obtained by the decomposition

$$\begin{bmatrix} \sigma_1(x,t) \\ \sigma_2(x,t) \end{bmatrix} = \begin{bmatrix} B & \bar{B} \end{bmatrix}^{-1} \sigma(x,t) \tag{3.6}$$

where $\sigma_2(x,t) \in \mathbb{R}^{n-1}$ is the unmatched component of σ. Taking the derivative of (3.5) results in

$$\frac{dE}{d\hat{W}} = \phi(x)\left(\hat{W}\phi(x) - \sigma_1(x,t)\right) \tag{3.7}$$

With the implementation of the ANN adaptive law, $\hat{\sigma}_1$ becomes an approximation of $\hat{f}(x) -$

$\sigma_1(x,t)$. Therefore, we can rewrite (3.7) as

$$\frac{dE}{d\hat{W}} = \phi(x)\hat{\sigma}_1(t). \tag{3.8}$$

Multiplying the derivative by a learning rate, $k < 0$, results in the update law for $\hat{W}$. Additionally, the projection operator is used to limit the norm of $\hat{W}$. Let $\dot{\bar{W}} = k\phi(x)\hat{\sigma}_1(t)$. The update law is given by

$$\begin{aligned} \dot{\hat{W}} &= \text{Proj}(\hat{W}, \dot{\bar{W}}) \\ &= \begin{cases} \dot{\bar{W}} - \frac{\nabla g(\hat{W})}{||g(\hat{W})||^2} \left(\frac{\nabla g(\hat{W})}{||g(\hat{W})||^2} \right)^\top \dot{\bar{W}} g(\hat{W}) & \text{if } g(\hat{W}) > 0 \text{ and } \dot{\bar{W}}^\top \nabla g(\hat{W}) > 0 \\ \dot{\bar{W}} & \text{otherwise} \end{cases} \end{aligned} \tag{3.9}$$

where

$$g(\hat{W}) = \frac{(\epsilon_{\hat{W}} + 1)\hat{W}\hat{W}^\top - \hat{W}_{\max}^2}{\epsilon_{\hat{W}} \hat{W}_{\max}^2} \tag{3.10}$$

where $\epsilon_{\hat{W}} > 0$ is the projection tolerance bound and $\hat{W}_{\max}$ is the bound for the norm of $\hat{W}$. $\epsilon_{\hat{W}}$ is a tunable parameter that specifies a range of values for $\hat{W}$ for which the projection operator makes $\dot{\hat{W}} \neq \dot{\bar{W}}$. Note that $||\phi(x)||_\infty \leq 1$. Thus, $|\hat{f}(x)| < \hat{W}_{\max}$. Furthermore, because $\hat{f}(x)$ is composed of RBFs, it is a Lipschitz continuous map. Thus $\exists\, L_2 > 0$ such that

$$|\hat{f}(x_1) - \hat{f}(x_2)| \leq L_2 ||x_1 - x_2|| \tag{3.11}$$

With the addition of the ANN adaptive law, u_2 becomes

$$u_2(t) = -C_1(s)(\hat{f}(x) + \hat{\sigma}_1(t)) \tag{3.12}$$

The rest of the $\mathcal{L}_1$ archtitecture remains unchanged.

3.3 Stability Analysis and Tracking Performance

This section will examine the stability and tracking performance for the $\mathcal{L}_1$ adaptive controller with the ANN adaptive law.

Lemma 3.1. *Given*

$$\int_0^T e^{A(T-\tau)}(\hat{z} - z(\tau))d\tau = 0 \tag{3.13}$$

where $z \in \mathbb{R}^n$ is a bounded, continuous signal and $\hat{z} \in \mathbb{R}^n$ is a constant, $\forall\, \epsilon > 0$, $\exists\, T$ and $t_i \in [0, T]$, $i = 1, \ldots, n$ such that

$$|\hat{z}_i(t_i) - z_i| \leq \epsilon \tag{3.14}$$

$$\lim_{T \to 0} |\hat{z}_i(t_i) - z_i| = 0 \tag{3.15}$$

where z_i and $\hat{z}_i$ are the ith elements of z and $\hat{z}$ respectively.

Proof. Since z is continuous, $e^{A(T-\tau)}(\hat{z} - z(\tau))$ is also continuous. The ith element of (3.13) is

$$\int_0^T 1_i^\top e^{A(T-\tau)}(\hat{z} - z(\tau)) = 0 \tag{3.16}$$

(3.16) implies $\exists\, t_i \in [0, T]$ such that

$$1_i^\top e^{A(T-t_i)}(\hat{z} - z(t_i)) = 0 \tag{3.17}$$

Using (3.17), we can express the ith element of $\hat{z} - z(t_i)$ as

$$\hat{z}_i - z_i(t_i) = 1_i^\top(\hat{z} - z(t_i)) - 1_i^\top e^{A(T-t_i)}(\hat{z} - z(t_i)) = 1_i^\top \left(I - e^{A(T-t_i)}(\hat{z} - z(t_i))\right) \tag{3.18}$$

Since

$$\lim_{T \to 0} e^{A(T-t_i)} = I \tag{3.19}$$

along with the facts that $\hat{z}$ is a constant and z is bounded, we can write

$$\lim_{T\to 0} 1_i^\top \left(I - e^{A(T-t_i)}(\hat{z} - z(t_i))\right) = 0 \tag{3.20}$$

and thus

$$\lim_{T\to 0} |\hat{z}_i(t_i) - z_i| = 0 \tag{3.21}$$

Then, $\forall\, \epsilon > 0$, $\exists\, T > 0$ such that

$$\left|1_i^\top \left(I - e^{A(T-t_i)}(\hat{z} - z(t_i))\right)\right| \leq \epsilon \tag{3.22}$$

and thus

$$|\hat{z}_i(t_i) - z_i| \leq \epsilon \tag{3.23}$$

(3.21) and (3.23) constitute proof of Lemma 3.1. □

For the following theorem, we will define several constants. $\forall\, \gamma_\sigma > 0$, T, let

$$\eta(T) = \int_0^T \sqrt{\Lambda_{\max}\left(\Phi(T-\tau)^\top \Phi(T-\tau)\right)} d\tau \gamma_\sigma \tag{3.24}$$

Definition 3.1. *For any matrix $Q_{n\times n}$, the induced 1-norm is defined as*

$$||Q||_1 = \max_{j=1,\ldots,n} \left(\sum_{i=1}^{n} |Q_{ij}|\right) \tag{3.25}$$

Property 3.1. *The induced 1-norm has the property $||Qv||_\infty \leq ||Q||_1 ||v||_\infty \,\forall v \in \mathbb{R}^n$*

$\forall\, \gamma_x$, let

$$\begin{aligned}
\eta_2 &= ||A||_1\gamma_x + ||B||(\gamma_u + L(\gamma_x)\gamma_x + B_1) && (3.26)\\
\eta_3 &= d_{\sigma_x}(\gamma_x)\eta_2 + d_{\sigma_t}(\gamma_x) && (3.27)\\
\eta_4(T) &= 2T\left(||B|||k|||\Gamma||_1\eta(T)\right) + ||A||_1\eta(T) + \epsilon && (3.28)\\
\eta_5(T) &= \left|\left|\left[B \quad \bar{B}\right]\right|\right|_1 \left(\eta_4(T) + ||B||\hat{W}_{\max}\right) && (3.29)
\end{aligned}$$

where

$$\begin{aligned}
\gamma_u &= |K_g|||r||_{\mathcal{L}_\infty} && (3.30)\\
&\quad + \left(||C_1(s)||_{\mathcal{L}_1} + \left|\left|C_2(s)\frac{C(sI-A)^{-1}\bar{B}}{C(sI-A)^{-1}B}\right|\right|_{\mathcal{L}_1}\right)(L(\gamma_x)\gamma_x + B_1 + \eta_5) + \epsilon_0
\end{aligned}$$

where ϵ_0 is an arbitrary positive constant. Let

$$\begin{aligned}
G(s) &= (sI-A)^{-1}B(1-C_1(s)) && (3.31)\\
\gamma_e(T) &= \left|\left|(sI-A)^{-1}\right|\right|_{\mathcal{L}_1}\eta_4(T) && (3.32)\\
\gamma_0(T) &= ||(sI-A)^{-1}B||_{\mathcal{L}_1}\left(|K_g|||r(s)||_{\mathcal{L}_\infty} + \left|\left|C_2(s)\frac{C(sI-A)^{-1}\bar{B}}{C(sI-A)^{-1}B}\right|\right|_{\mathcal{L}_1}\right. && (3.33)\\
&\quad \left.\times(L(\gamma_x)\gamma_x + B_1 + \eta_5) + \hat{W}_{\max}\right) + ||(sI-A)^{-1}\bar{B}||_{\mathcal{L}_1}(L(\gamma_x)\gamma_x + B_1 + \eta_5)
\end{aligned}$$

The stability conditions for the controller are

$$\begin{aligned}
||G(s)||_{\mathcal{L}_1}\left(L(\gamma_x)\gamma_x + B_1 + \eta_5\right) + \gamma_0(T) + \gamma_e(T) &< \gamma_x && (3.34)\\
2||\Gamma||_1\gamma_e + ||B||\hat{W}_{\max} &< \gamma_\sigma && (3.35)
\end{aligned}$$

Theorem 3.1. *Let $\tilde{\sigma}(t) = B\hat{f}(x) - \sigma(t)$. Then for T and $C_1(s)$ such that (3.34) and (3.35)*

are satisfied, if $x(0) < \gamma_x$, $u(0) < \gamma_u$, *and* $\tilde{\sigma}(0) < \gamma_\sigma$, *then*

$$||\tilde{x}||_{\mathcal{L}_\infty} \leq \gamma_e(T) \tag{3.36}$$

$$||x||_{\mathcal{L}_\infty} < \gamma_x \tag{3.37}$$

$$||u||_{\mathcal{L}_\infty} < \gamma_u \tag{3.38}$$

$$||\tilde{\sigma}||_{\mathcal{L}_\infty} < \gamma_\sigma \tag{3.39}$$

Proof. If (3.37), (3.38), and (3.39) do not hold, then since $x(0) < \gamma_x$, $u(0) < \gamma_u$, and $\tilde{\sigma}(0) < \gamma_\sigma$ and $x(t)$, $u(t)$, and $\tilde{\sigma}(t)$ are continuous, $\exists\, t'$ such that

$$||x(t')|| = \gamma_x \tag{3.40}$$

$$||u(t')|| = \gamma_u \tag{3.41}$$

$$||\tilde{\sigma}(t')|| = \gamma_\sigma \tag{3.42}$$

and

$$||x_{t'}||_{\mathcal{L}_\infty} \leq \gamma_x \tag{3.43}$$

$$||u_{t'}||_{\mathcal{L}_\infty} \leq \gamma_u \tag{3.44}$$

$$||\tilde{\sigma}_{t'}||_{\mathcal{L}_\infty} \leq \gamma_\sigma \tag{3.45}$$

With the ANN adaptive law, (2.9) becomes

$$\tilde{x}((i+1)T) = \Phi(T)\tilde{x}(iT) + \int_0^T \Phi(T-\tau)\hat{\sigma}(iT)\,d\tau + \int_0^T \Phi(T-\tau)\tilde{\sigma}(\tau)\,d\tau \tag{3.46}$$

Substituting (2.10) into (3.46) yields

$$\tilde{x}((i+1)T) = \int_0^T \Phi(T-\tau)\tilde{\sigma}(\tau)\,d\tau \tag{3.47}$$

From (3.45) and (3.47), we have

$$||\tilde{x}((i+1)T)|| \leq \eta(T) \tag{3.48}$$

$\forall\, i$ such that $(i+1)T \in [0, t']$.

Note that the adaptive law in (2.10) is designed such that

$$\Phi(T)\tilde{x}(iT) + \int_0^T \Phi(T-\tau)\hat{\sigma}(iT)d\tau = 0 \tag{3.49}$$

By multiplying by -1 and adding $\tilde{x}(iT)$ to each side of (3.49), we can write

$$\tilde{x}(iT) = (I - \Phi(T))\tilde{x}(iT) - \int_0^T \Phi(T-\tau)\hat{\sigma}(iT)d\tau \tag{3.50}$$

(3.50) can also be expressed as

$$\tilde{x}(iT) = -\int_0^T \Phi(T-\tau)(\hat{\sigma}(iT) + A\tilde{x}(iT))d\tau \tag{3.51}$$

From (3.46) we can also write

$$\tilde{x}(iT) = \int_0^T \Phi(T-\tau)\tilde{\sigma}((i-1)T + \tau)d\tau \tag{3.52}$$

Equating the right hand sides of (3.51) and (3.52) yields

$$-\int_0^T \Phi(T-\tau)(\hat{\sigma}(iT) + A\tilde{x}(iT))d\tau = \int_0^T \Phi(T-\tau)\tilde{\sigma}((i-1)T + \tau)d\tau \tag{3.53}$$

and

$$\int_0^T \Phi((i+1)T - \tau)(\hat{\sigma}(iT) + \tilde{\sigma}((i-1)T + \tau) - A\tilde{x}(iT))d\tau = 0 \tag{3.54}$$

It follows from Lemma 3.1 that $\exists\, t_1, \ldots, t_i, \ldots, t_n \in [0, T]$ such that

$$\hat{\sigma}(iT) = \bar{\sigma} - A\tilde{x}(iT) + \epsilon_c \tag{3.55}$$

where $\bar{\sigma}$ is a constant with ith element $-\tilde{\sigma}_i((i-1)T + t_i)$ where $\tilde{\sigma}_i \in \mathbb{R}$ is the ith element of $\tilde{\sigma}$ and $||\epsilon_c||_\infty < \epsilon$. From (3.55) we can also write

$$\hat{\sigma}(iT) + \tilde{\sigma}(iT + \tau) = \bar{\sigma} + \tilde{\sigma}(iT + \tau) - A\tilde{x}(iT) + \epsilon_c \tag{3.56}$$

Thus

$$||\hat{\sigma}(iT) + \tilde{\sigma}(iT + \tau)||_\infty \leq ||\bar{\sigma} + \tilde{\sigma}(iT + \tau)||_\infty + ||A\tilde{x}(iT)||_\infty + \epsilon \tag{3.57}$$

The next step of the proof is to characterize the bound of $||\hat{\sigma}(iT + \tau) + \tilde{\sigma}(iT + \tau)||$. This requires us to first derive the bound for $\tilde{\sigma}$. From Assumptions 2.2 and 2.3 and (3.43), we have

$$||\sigma_{t'}||_{\mathcal{L}_\infty} \leq L(\gamma_x)\gamma_x + B_1 \tag{3.58}$$

Applying (3.43), (3.44), and (3.58) to (2.4) yields

$$||\dot{x}(t)||_\infty \leq \eta_2 \tag{3.59}$$

(3.59) and Assumption 2.4 imply

$$||\dot{\sigma}(x, t)||_\infty \leq \eta_3 \tag{3.60}$$

From (3.49) and (3.48), we can write

$$||\sigma(iT)||_\infty \leq ||\Gamma||_1 \eta(T) \tag{3.61}$$

$\forall\, i$ such that $(i+1)T \in [0, t']$. From (3.3), (3.9) and (3.58) we know that

$$\left|\left|\dot{\hat{f}}(x)\right|\right|_\infty = \left|\left|\dot{\hat{W}}\right|\right|_\infty \leq |k|||\Gamma||_1 \eta(T) \tag{3.62}$$

From the definition of $\tilde{\sigma}$, we have

$$\dot{\tilde{\sigma}}(t) = B\dot{\hat{f}}(x) - \dot{\sigma}(t) \tag{3.63}$$

Then from (3.60), (3.62), and (3.63), we have

$$\left|\left|\dot{\tilde{\sigma}}(t)\right|\right|_\infty = ||B|||k|||\Gamma||_1 \eta(T) + \eta_3 \tag{3.64}$$

Since $\tau \in [0, T)$ and $t_i \in [0, T]$, $i = 1, \ldots, n$,

$$iT + \tau - (i-1)T + t_i \leq 2T \tag{3.65}$$

Thus

$$||\bar{\sigma} + \tilde{\sigma}(iT + \tau)||_\infty \leq 2T\left(||B|||k|||\Gamma||_1 \eta(T)\right) \tag{3.66}$$

(3.48), (3.57), and (3.66) imply

$$||\hat{\sigma}(iT + \tau) + \tilde{\sigma}(iT + \tau)||_\infty \leq 2T\left(||B|||k|||\Gamma||_1 \eta(T)\right) + ||A||_1 \eta(T) + \epsilon \tag{3.67}$$

Since (3.67) holds $\forall\, i$ such that $(i+1)T \leq t$,

$$||(\hat{\sigma} + \tilde{\sigma})_{t'}||_{\mathcal{L}_\infty} \leq \eta_4(T) \tag{3.68}$$

By adding $\hat{\sigma}$ to both sides of the definition of $\tilde{\sigma}$ and solving for $\hat{\sigma}(t) - \sigma(x, t)$, we can write

$$\hat{\sigma}(t) - \sigma(x, t) = \hat{\sigma}(t) + \tilde{\sigma}(t) - B\hat{f}(x) \tag{3.69}$$

Multiplying both sides of (3.69) by $\begin{bmatrix} B & \bar{B} \end{bmatrix}^{-1}$ and applying the bound in (3.67) results in

$$\left|\left|\left(\begin{bmatrix}\hat{\sigma}_1\\ \hat{\sigma}_2\end{bmatrix} - \begin{bmatrix}\sigma_1\\ \sigma_2\end{bmatrix}\right)_{t'}\right|\right|_{\mathcal{L}_\infty} \leq \eta_5 \tag{3.70}$$

Following the definition of the $\mathcal{L}_\infty$-norm, we have

$$\begin{aligned} ||(\hat{\sigma}_1 - \sigma_1)_{t'}||_{\mathcal{L}_\infty} &\leq \eta_5 \\ ||(\hat{\sigma}_2 - \sigma_2)_{t'}||_{\mathcal{L}_\infty} &\leq \eta_5 \end{aligned} \tag{3.71}$$

Substituting (2.20) into (3.4) yields

$$\begin{aligned} \dot{\hat{x}}(t) &= A\hat{x}(t) + BK_g r(t) + (1 - C_1(s))B\hat{\sigma}_1(t) \\ &\quad -C_2(s)\frac{C(sI-A)^{-1}\bar{B}}{C(sI-A)^{-1}B}B\hat{\sigma}_2(t) + B\hat{f}(x) + \bar{B}\hat{\sigma}_2(t) \end{aligned} \tag{3.72}$$

Taking the Laplace transform of (3.72) yields

$$\begin{aligned} \hat{x}(s) &= (sI-A)^{-1}BK_g r(s) + (sI-A)^{-1}(1 - C_1(s))B\hat{\sigma}_1(s) \\ &\quad +(sI-A)^{-1}\left[B\left(C_2(s)\frac{C(sI-A)^{-1}\bar{B}}{C(sI-A)^{-1}B}B\hat{\sigma}_2(s) + \hat{f}(x)\right) + \bar{B}\hat{\sigma}_2(s)\right] \end{aligned} \tag{3.73}$$

and thus

$$||\hat{x}_{t'}||_{\mathcal{L}_\infty} \leq ||G(s)||_{\mathcal{L}_1}||\hat{\sigma}_{1_{t'}}||_{\mathcal{L}_\infty} + ||\zeta_{t'}||_{\mathcal{L}_\infty} \tag{3.74}$$

where $\zeta(t)$ is the signal with Laplace transform $(sI-A)^{-1}B\left(K_g r(s) - C_2(s)\frac{C(sI-A)^{-1}\bar{B}}{C(sI-A)^{-1}B}\hat{\sigma}_2(s) + \hat{f}(x)\right) + (sI-A)^{-1}\bar{B}\hat{\sigma}_2(s)$. (3.58) implies

$$\begin{aligned} ||\sigma_{1_{t'}}||_{\mathcal{L}_\infty} &\leq L(\gamma_x)\gamma_x + B_1 \\ ||\sigma_{2_{t'}}||_{\mathcal{L}_\infty} &\leq L(\gamma_x)\gamma_x + B_1 \end{aligned} \tag{3.75}$$

From the definition of the $\mathcal{L}_\infty$-norm, $||\hat{\sigma}_{1_{t'}}||_{\mathcal{L}_\infty} \leq ||\hat{\sigma}_{1_{t'}}||_{\mathcal{L}_\infty} + ||(\hat{\sigma}_1 - \sigma_1)_{t'}||_{\mathcal{L}_\infty}$, and thus from (3.71),

$$\begin{aligned} ||\hat{\sigma}_{1_{t'}}||_{\mathcal{L}_\infty} &\leq L(\gamma_x)\gamma_x + B_1 + \eta_5(T) \\ ||\hat{\sigma}_{2_{t'}}||_{\mathcal{L}_\infty} &\leq L(\gamma_x)\gamma_x + B_1 + \eta_5(T) \end{aligned} \tag{3.76}$$

(3.76) implies

$$||\zeta_{t'}||_{\mathcal{L}_\infty} \leq \gamma_0(T) \tag{3.77}$$

Combining (3.74) and (3.77) results in

$$||\hat{x}_{t'}||_{\mathcal{L}_\infty} \leq ||G(s)||_{\mathcal{L}_1}||\hat{\sigma}_{1_{t'}}||_{\mathcal{L}_\infty} + \gamma_0 \tag{3.78}$$

Since (3.34) holds, (3.78) implies

$$||\hat{x}_{t'}||_{\mathcal{L}_\infty} < \gamma_x - \gamma_e(T) \tag{3.79}$$

The prediction error dynamics for the $\mathcal{L}_1$ controller with ANN adaptive law are

$$\begin{aligned} \dot{\tilde{x}}(t) &= A\tilde{x}(t) + \hat{\sigma}(t) + B\hat{f}(x) - \sigma(x,t) \\ &= A\tilde{x}(t) + \hat{\sigma}(t) + \tilde{\sigma}(t) \end{aligned} \tag{3.80}$$

(3.80) has the Laplace transform

$$\tilde{x}(s) = (sI - A)^{-1}(\hat{\sigma}(s) + \tilde{\sigma}(s)) \tag{3.81}$$

(3.67) and (3.81) imply

$$||\tilde{x}_{t'}||_{\mathcal{L}_\infty} \leq \gamma_x \tag{3.82}$$

Since $x(t) = \hat{x}(t) + \tilde{x}(t)$, we have

$$||x_{t'}||_{\mathcal{L}_\infty} \leq ||\hat{x}_{t'}||_{\mathcal{L}_\infty} + ||\tilde{x}_{t'}||_{\mathcal{L}_\infty} \tag{3.83}$$

(3.79), (3.82), and (3.83) imply

$$||x_{t'}||_{\mathcal{L}_\infty} < \gamma_x \tag{3.84}$$

which contradicts (3.43). Next, we will find a similar contradiction to (3.44).

From(2.20) and (3.76), we can write

$$\begin{aligned} ||u_{t'}||_{\mathcal{L}_\infty} &\leq |K_g|||r||_{\mathcal{L}_\infty} \\ &+ \left(||C_1(s)||_{\mathcal{L}_1} + \left|\left| C_2(s) \frac{C(sI-A)^{-1}\bar{B}}{C(sI-A)^{-1}B} \right|\right|_{\mathcal{L}_1} \right) (L(\gamma_x)\gamma_x + B_1 + \eta_5) \end{aligned} \tag{3.85}$$

which implies

$$||u_{t'}||_{\mathcal{L}_\infty} < \gamma_u \tag{3.86}$$

which contradicts (3.44).

Finally, we must find a contradiction to (3.45). From the definition of $\tilde{\sigma}$, we can write

$$\hat{\sigma}(t) + \tilde{\sigma}(t) = \hat{\sigma}(t) + B\hat{f}(x) - \sigma(x,t) \tag{3.87}$$

which implies

$$||\tilde{\sigma}_{t'}||_{\mathcal{L}_\infty} \leq ||(\hat{\sigma} + B\hat{f}(x))_{t'}||_{\mathcal{L}_\infty} + ||\sigma(t)|| + ||\hat{\sigma}_{t'}||_{\mathcal{L}_\infty} \tag{3.88}$$

From (2.10) and (3.82) we can write

$$||\hat{\sigma}_{t'}||_{\mathcal{L}_\infty} < ||\Gamma||_1 \gamma_e(T) \tag{3.89}$$

Since (3.35) holds, (3.88) and (3.89) imply

$$||\hat{\sigma}_{t'}||_{\mathcal{L}_\infty} < \gamma_\sigma \tag{3.90}$$

which contradicts (3.45).

Since (3.84), (3.86), and (3.90) contradict (3.43), (3.44), and (3.45) respectively, (3.37), (3.38), and (3.39) must be true. Furthermore, (3.36) follows directly from (3.82) since (3.34) and (3.35) hold. □

Theorem 3.2 will analyze the parameter values for which (3.34) and (3.35) hold. For simplicity, consider a first order low-pass filter for $C_1(s)$,

$$C_1(s) = \frac{\omega_1}{s + \omega_1} \tag{3.91}$$

Theorem 3.2. *$\exists$ a small T and large ω_1 that satisfy (3.34) and (3.35).*

Proof. It is shown in [33] that for the low-pass filter in (3.91)

$$\lim_{\omega_1 \to \infty} ||G(s)||_{\mathcal{L}_1} = 0 \tag{3.92}$$

From the definition of $\eta(T)$, it is clear that $\lim_{T\to 0} \eta(T) = 0$. It follows that

$$\lim_{T\to 0} \eta_5(T) = \left|\left|\begin{bmatrix} B & \bar{B} \end{bmatrix}^{-1}\right|\right|_1 (\epsilon + ||B||\hat{W}_{\max}) \tag{3.93}$$

$$\lim_{T\to 0} \gamma_0(T) = ||(sI - A)^{-1}B||_{\mathcal{L}_1} \Bigg(|K_g|||r||_{\mathcal{L}_\infty} + \left|\left| C_2(s) \frac{C(sI - A)^{-1}\bar{B}}{C(sI - A)^{-1}B} \right|\right|_{\mathcal{L}_1} \times (L(\gamma_x)\gamma_x + B_1) + \hat{W}_{\max} \Bigg) + ||(sI - A)^{-1}\bar{B}||_{\mathcal{L}_1}(L(\gamma_x)\gamma_x + B_1) \tag{3.94}$$

$$\lim_{T\to 0} \gamma_e(T) = ||(sI - A)^{-1}||_{\mathcal{L}_1}\epsilon \tag{3.95}$$

Then $\forall\, \gamma_x > \gamma_0(T) + \gamma_e(T)$, if

$$||G(s)||_{\mathcal{L}_1} < \frac{\gamma_x - \gamma_0(T) - \gamma_e(T)}{(L(\gamma_x)\gamma_x + B_1 + \eta_5(T))} \tag{3.96}$$

then (3.34) can always be satisfied. Furthermore, (3.94) and (3.95) imply $\exists\, T$ such that $\frac{\gamma_x - \gamma_0(T) - \gamma_e(T)}{(L(\gamma_x)\gamma_x + B_1 + \eta_5(T))}$ is a finite positive number. Thus it follows from (3.92) and (3.96) that (3.34) can always be satisfied by increasing ω_1 or reducing T.

By taking the limit as $T \to 0$ of (3.35), we obtain $2||\Gamma||_1\epsilon + ||B||\hat{W}_{\max}$, which is a finite positive number. Thus, $\exists$ a finite positive γ_σ that satisfies (3.35). □

Definition 3.2. *The tracking error between the reference system and the real system is defined as*

$$x_e(t) = x(t) - x_{des}(t) \tag{3.97}$$

Theorem (3.3) will characterize the tracking error bound.

Theorem 3.3. *The error bound between the reference system and the real system is*

$$\begin{aligned} ||x_e||_{\mathcal{L}_\infty} \;\leq\; & ||G(s)||_{\mathcal{L}_1} \left(L(\gamma_x)\gamma_x + B_1 + \eta_5(T) + \hat{W}_{\max} \right) \\ & + \left|\left|(sI - A)^{-1}\right|\right|_{\mathcal{L}_1} \left(\left|\left| C_2(s) \frac{C(sI - A)^{-1}\bar{B}}{C(sI - A)^{-1}B} B \right|\right|_{\mathcal{L}_1} (L(\gamma_x)\gamma_x + B_1 + \eta_5(T)) \right. \\ & \left. + ||B||\hat{W}_{\max} \right) + \left|\left|(sI - A)^{-1}\bar{B}\right|\right|_{\mathcal{L}_1} (L(\gamma_x)\gamma_x + B_1 + \eta_5(T)) + \gamma_e(T) \end{aligned} \tag{3.98}$$

Proof. From the definition of $\tilde{x}$, we can write

$$x(s) = \hat{x}(s) + \tilde{x}(s) \tag{3.99}$$

Substituting (3.73) into (3.99) yields

$$\begin{aligned} x(s) &= (sI-A)^{-1}BK_g r(s) + (sI-A)^{-1}(1-C_1(s))B(\hat{\sigma}_1(s)+\hat{f}(x)) \\ &\quad +(sI-A)^{-1}\left[B\left(C_2(s)\frac{C(sI-A)^{-1}\bar{B}}{C(sI-A)^{-1}B}B\hat{\sigma}_2(s)+\hat{f}(x)\right)+\bar{B}\hat{\sigma}_2(t)\right]+\tilde{x}(s) \end{aligned} \tag{3.100}$$

From (2.5), we can write the Laplace transform of $x_{des}(t)$ as

$$x_{des}(s) = (sI-A)^{-1}BK_g r(s) \tag{3.101}$$

Taking the Laplace transform of (3.97) and substituting in (3.100) and (3.101) yields

$$\begin{aligned} x_e(s) &= (sI-A)^{-1}(1-C_1(s))B\hat{(}\sigma_1(s)+\hat{f}(x)) \\ &\quad +(sI-A)^{-1}\left(C_2(s)\frac{C(sI-A)^{-1}\bar{B}}{C(sI-A)^{-1}B}B\hat{\sigma}_2(s)+B\hat{f}(x)+\bar{B}\hat{\sigma}_2(t)\right)+\tilde{x}(s) \end{aligned} \tag{3.102}$$

By substituting the appropriate bounds into (3.102), we obtain

$$\begin{aligned} ||x_e||_{\mathcal{L}_\infty} &\leq ||G(s)||_{\mathcal{L}_1}\left(L(\gamma_x)\gamma_x+B_1+\eta_5(T)+\hat{W}_{\max}\right) \\ &\quad +\left|\left|(sI-A)^{-1}\right|\right|_{\mathcal{L}_1}\left(\left|\left|C_2(s)\frac{C(sI-A)^{-1}\bar{B}}{C(sI-A)^{-1}B}B\right|\right|_{\mathcal{L}_1}(L(\gamma_x)\gamma_x+B_1+\eta_5(T))\right. \\ &\quad \left.+||B||\hat{W}_{\max}\right)+\left|\left|(sI-A)^{-1}\bar{B}\right|\right|_{\mathcal{L}_1}(L(\gamma_x)\gamma_x+B_1+\eta_5(T))+\gamma_e(T) \end{aligned} \tag{3.103}$$

which proves Theorem 3.3. □

Remark 3.1. *The dynamics of $x_e(t)$ can be expressed as*

$$\begin{aligned} \dot{x}_e(t) &= Ax_e(t) - C_1(s)B\hat{\sigma}_1(t) - C_2(s)\frac{C(sI-A)^{-1}\bar{B}}{C(sI-A)^{-1}B}B\hat{\sigma}_2(t) \\ &\quad -\left(C_1(s)B\hat{f}(x)-\sigma(x,t)\right) \end{aligned} \tag{3.104}$$

For the original $\mathcal{L}_1$ controller without the ANN adaptive law, (3.104) remains true with

$\hat{f}(x) = 0$. *Notice that the magnitude of* x_e *is reduced by the introduction of the ANN adaptive law as long as the ANN converges such that* $0 < |\hat{f}(x)| \leq |\sigma_1(t)|$ *and* $sign(\hat{f}(x)) = sign(\sigma_1(x,t))$. *The gradient descent update law for* $\hat{f}(x)$ *ensures these conditions*

3.4 Simulation Results

In order to illustrate the theoretical results in Section 3.3, we will examine numerical simulations. We will consider the same system dynamics and $\mathcal{L}_1$ controller of Section 2.5 ((2.21) - (2.23))

The ANN adaptive law consists of nine GRBFs with centers equally distributed over the grid $x_1 \in [-3, 3]$, $x_2 \in [-3, 3]$, i.e. the GRBF centers, z_i, consist of all combinations of $x_1 = -3, 0, 3$ and $x_2 = -3, 0, 3$. All GRBF widths are $\delta_i = 2$. The learning rate is $k = 5$, and the projection operator parameters are $\hat{W}_{\max} = 6$ and $\epsilon_W = 0.1$.

The simulation is performed for two scenarios, $T = 0.001$ seconds and $T = 0.1$ seconds. We will look at results for each scenario using both the standard $\mathcal{L}_1$ adaptive controller and the $\mathcal{L}_1$ controller with ANN adaptive law. In the case where T is sufficiently small, the standard $\mathcal{L}_1$ controller performs identically to the ANN controller. However, when T is too large to rely solely on fast adaptation, the ANN controller shows a significant improvement.

3.4.1 Small Time-Step

Here we consider the case where $T = 0.001$ seconds. Figure 3.1 shows the tracking performance, control input, and the adaptive parameters of the standard $\mathcal{L}_1$ controller. Figure 3.2 shows these signals for the ANN controller. Additionally, Figure 3.2d shows the ANN approximation plotted with the estimated signal, σ_1. Notice that the two controllers perform equally well here. In the standard $\mathcal{L}_1$ controller, fast adaptation is able to accurately estimate σ without the need for additional online modeling. Note that in the ANN controller, $\hat{f}(x)$ is able to approximate σ_1 very well. This greatly reduces the magnitude of $\hat{\sigma}$, thereby

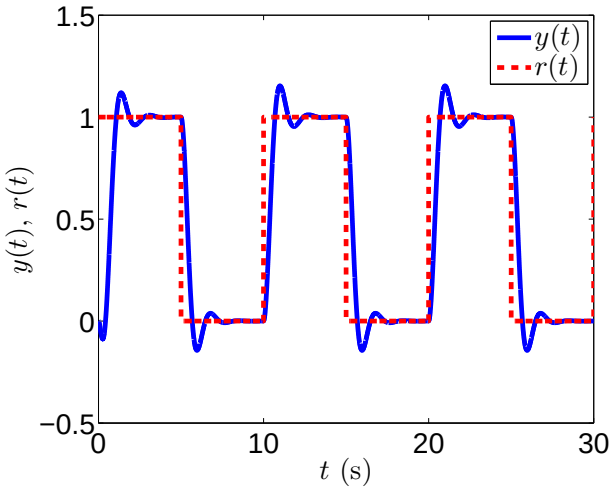

(a) Tracking performance

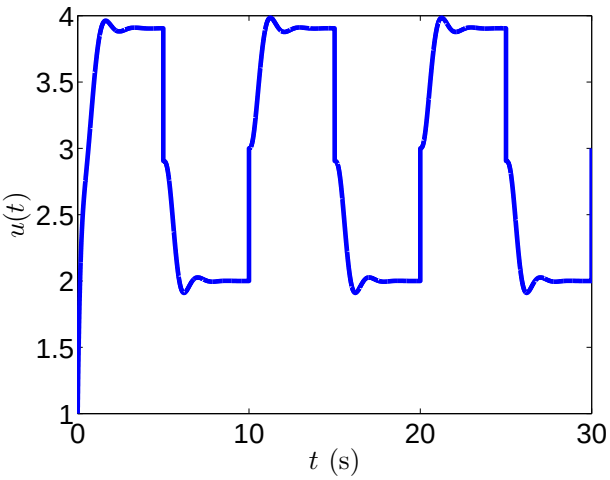

(b) Control input

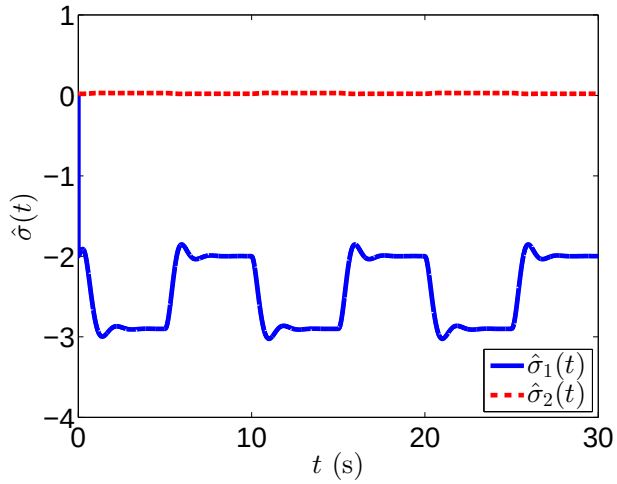

(c) Adaptive parameters

Figure 3.1: Simulation results using the standard $\mathcal{L}_1$ controller with $T = 0.001$ sec

shifting the burden of estimation off of the fast adaptation. The fast adaptation now only estimates high frequency components of the uncertainty.

3.4.2 Large Time-Step

Now we consider the case where $T = 0.1$ seconds. Figures 3.3 and 3.4 show the tracking performance, control input, adaptive parameters for the standard $\mathcal{L}_1$ controller and the ANN controller respectively. Additionally, Figure 3.4d shows the ANN approximation in the ANN controller. By comparing Figure 3.3 to Figure 3.1, we see that the reduction in sampling

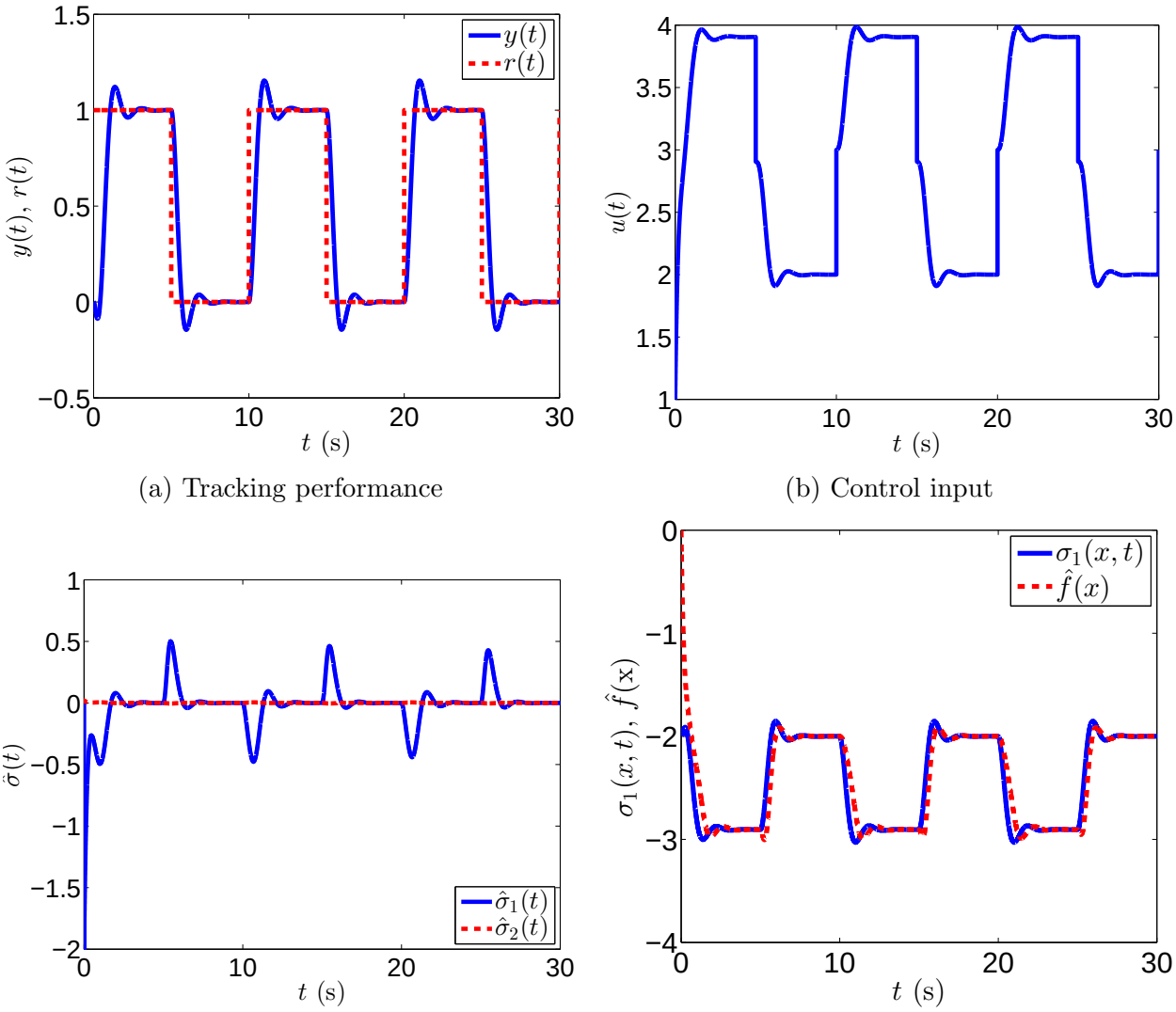

(a) Tracking performance

(b) Control input

(c) Adaptive parameters

(d) ANN approximation

Figure 3.2: Simulation results using the $\mathcal{L}_1$ controller with ANN adaptive law with $T = 0.001$ sec

speed heavily degrades performance. The response is much more oscillatory, and the adaptive law does not accurately estimate σ.

In Figure 3.4, we see much better control performance with the ANN controller compared to the standard $\mathcal{L}_1$ controller. Also, performance does not degrade as drastically from the small T case as with the standard $\mathcal{L}_1$ controller. There is a larger overshoot, but oscillations are damped out quickly once the ANN weights begin to converge. The ANN is still able to accurately estimate σ_1, and magnitude of $\hat{\sigma}$ remains small.

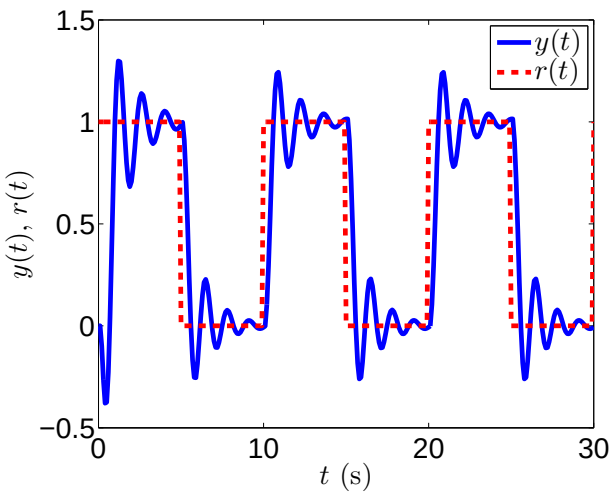

(a) Tracking performance

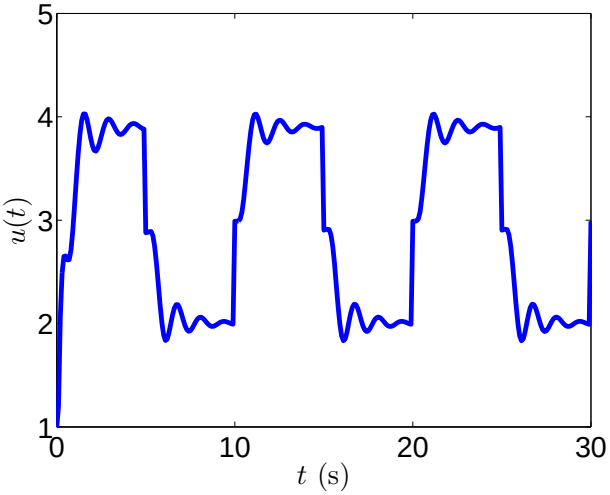

(b) Control input

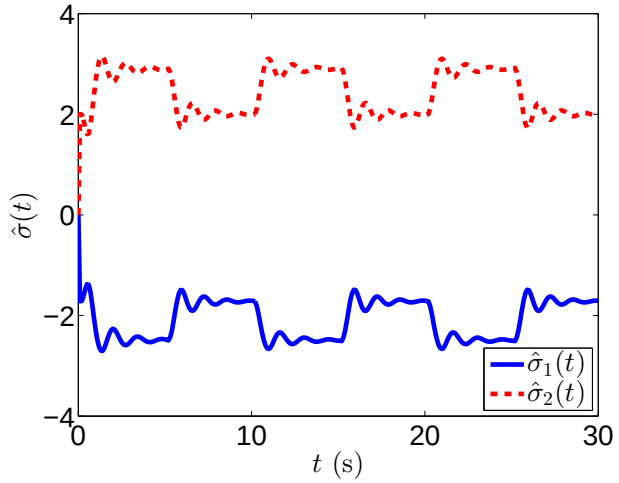

(c) Adaptive parameters

Figure 3.3: Simulation results using the standard $\mathcal{L}_1$ controller with $T = 0.1$ sec

3.4.3 Convergence of Neural Network Weights

By running the simulation for a long period of time, the ANN weights converge to minimize the error function, E. By performing this process offline, the ANN can be trained. Figure (3.5) shows the convergence of the ANN weights over 5000 seconds. The simulation time-step was $T = 0.001$ seconds.

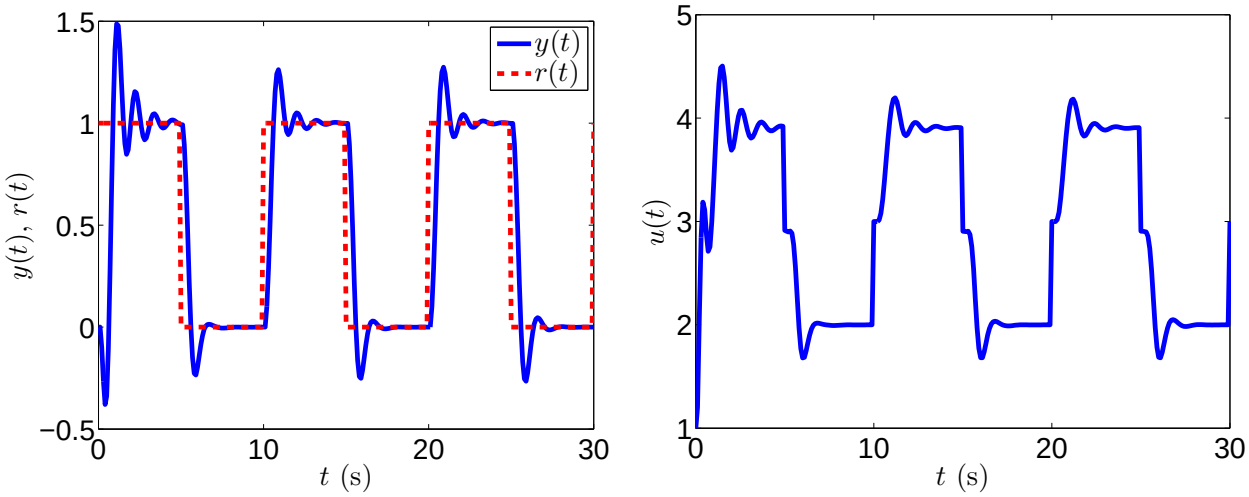

(a) Tracking performance

(b) Control input

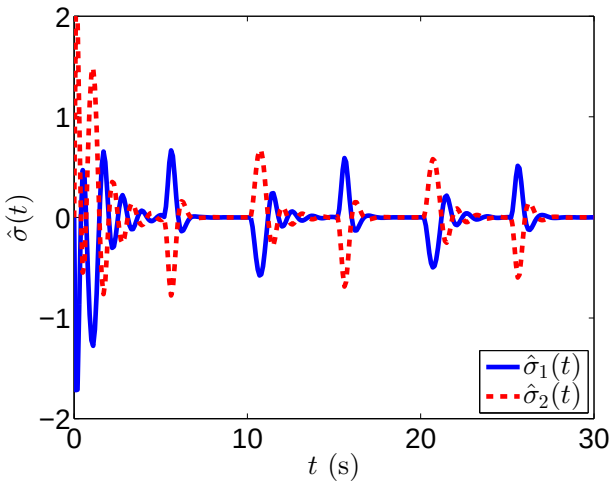

(c) Adaptive parameters

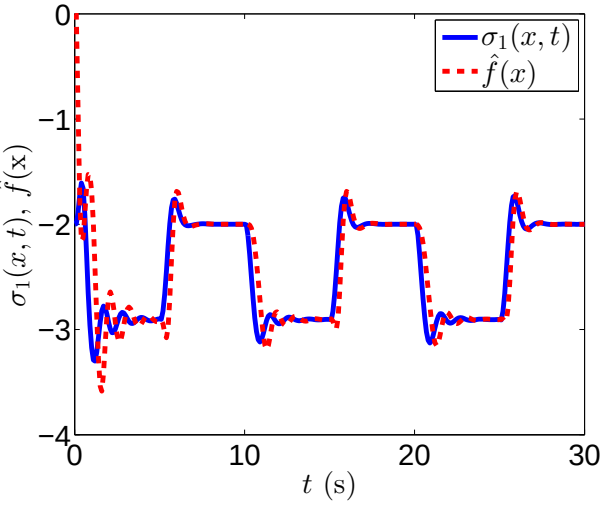

(d) ANN approximation

Figure 3.4: Simulation results using the $\mathcal{L}_1$ controller with ANN adaptive law with $T = 0.1$ sec

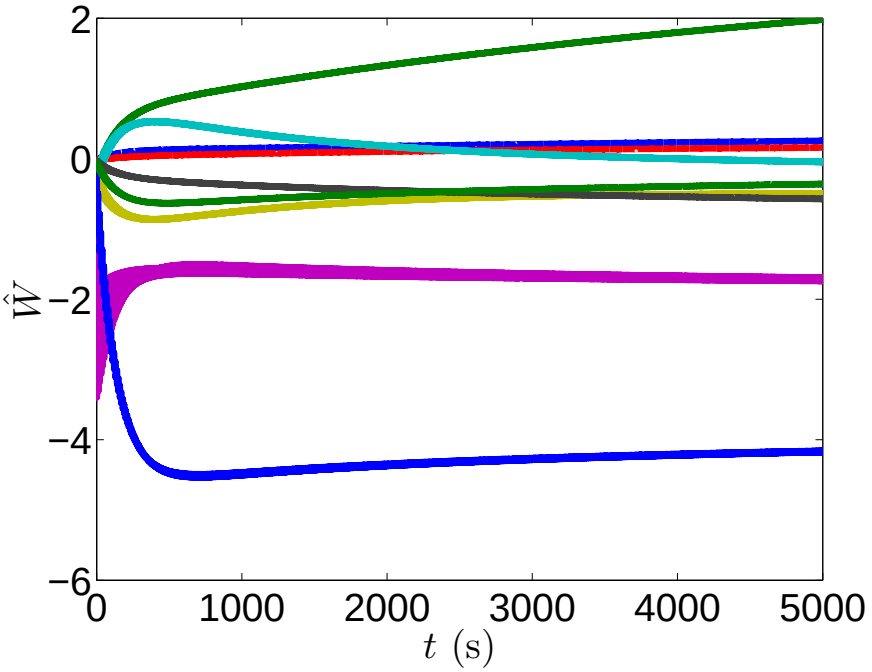

Figure 3.5: ANN weight convergence

Chapter 4

Memorizing Mechanism

The second method that can be used for performance improvement in fast adaptation with slow sampling speeds is known as the memorizing mechanism. In this technique, the previous values of uncertainty estimates are stored by introducing an integrator to the adaptive law. An advantage of this technique over the artificial neural network adaptive law is that the memorizing mechanism is capable of estimating time-varying uncertainties whereas the ANN adaptive law can only deal with state-dependent uncertainties. Furthermore, there are fewer parameters that require tuning in the memorizing mechanism. This method was used to estimate constant biases in system uncertainties in [17]

The memorizing mechanism works by applying a low-pass filter to the total uncertainty estimate, which is the adaptive parameter plus the memory term. We rearrange the equation obtained this way to solve for the memory term, and the result is the application of a linear system to the adaptive parameter. As long as the low-pass filter used has a DC-gain of 1, the resulting linear system will always have an integrator that can be factored out. Since the adaptive parameter is integrated, we refer to the resulting linear system as a memorizing mechanism. If the total uncertainty estimate is very close to the real uncertainty, then because the memory term is a filtered version of it, the magnitude of the fast adaptation parameter will be very small. For simplicity, we will consider the full state feedback $\mathcal{L}_1$

controller described in Chapter 2, however, this tehcnique can easily be applied to more complex versions of the $\mathcal{L}_1$ controller such as those of [12, 11, 13].

4.1 Memorizing Mechanism Design

The memory term is denoted by $\hat{\sigma}_b$. To update the memory term, we apply a low-pass filter, $D(s)$ to the total uncertainty estimate, $\hat{\sigma} + \hat{\sigma}_b$.

$$\hat{\sigma_b}(t) = D(s)(\hat{\sigma}(t) + \hat{\sigma}_b(t)) \tag{4.1}$$

By rearranging (4.1), we obtain the update law for $\hat{\sigma}_b$,

$$\hat{\sigma}_b(t) = \frac{D(s)}{1 - D(s)}\hat{\sigma}(t) \tag{4.2}$$

In general, $D(s)$ has the form

$$D(s) = \frac{\omega^m}{(s + \omega)^m} \tag{4.3}$$

where ω is the filter bandwidth and m is the order of the filter. Then

$$\frac{D(s)}{1 - D(s)} = \frac{\omega^m}{(s + \omega)^m - \omega^m} \tag{4.4}$$

From (4.4), we see that the zero-order term in the denominator cancels out, and thus s can be factored out of the denominator. Thus, $\hat{\sigma}$ is always integrated to generate the memory term. In the case of $m = 1$, (4.2) simply becomes

$$\hat{\sigma}_b(t) = \frac{\omega}{s}\hat{\sigma}(t) \tag{4.5}$$

Note that for constant uncertainties, $\hat{\sigma}$ will converge to zero. In this manner, $\hat{\sigma}_b$ serves as an

estimation of constant biases in uncertainty.

4.2 Application to $\mathcal{L}_1$ Adaptive Control

To use the memorizing mechanism with $\mathcal{L}_1$ adaptive control, the state predictor in (2.6) is reformulated as

$$\begin{aligned} \dot{\hat{x}}(t) &= A\hat{x}(t) + Bu(t) + \hat{\sigma}(t) + \hat{\sigma}_b(t) \\ \hat{y}(t) &= C\hat{x}(t) \quad \hat{x}(0) = 0 \end{aligned} \tag{4.6}$$

Since the total uncertainty estimate is now $\hat{\sigma}(t) + \hat{\sigma}_b(t)$, this is the signal whose effects must be canceled via the control law. We will redefine $\hat{\sigma}_1$ and $\hat{\sigma}_2$ as

$$\begin{bmatrix} \hat{\sigma}_1(t) \\ \hat{\sigma}_2(t) \end{bmatrix} = \begin{bmatrix} B & \bar{B} \end{bmatrix}^{-1} (\hat{\sigma}(t) + \hat{\sigma}_b(t)) \tag{4.7}$$

The rest of the $\mathcal{L}_1$ architecture remains unchanged.

4.3 Stability Analysis and Tracking Performance

This section will examine the stability and tracking performance for the L1 adaptive controller with the memorizing mechanism.

Lemma 4.1. *The transfer function*

$$\frac{s\omega^m}{(s+\omega)^m - \omega^m} \tag{4.8}$$

is stable $\forall$ *positive integers,* m*, and* $\forall\, \omega > 0$*.*

Proof. consider the integral of the system in (4.8),

$$\frac{\omega^m}{(s+\omega)^m - \omega^m} \tag{4.9}$$

This system can be expresses as negative feedback system with the feed-forward transfer function,

$$-D(s) = -\frac{\omega^m}{(s+\omega)^m} \tag{4.10}$$

Consider the root locus for the system in (4.9). The system in (4.10) has m poles at $-\omega$. Thus the root locus of (4.9) has m branches that originate at $-\omega$. (4.10) has no zeros, so each branch of the root locus of (4.9) approaches an asymptote at infinity. The asymptote angles are given by

$$\phi_l = \frac{360^\circ(l-1)}{m} \quad l = 1, 2, 3, \ldots, m \tag{4.11}$$

Note that there is always an asymptote along the real axis to the right. Since there are no zeros in the feed-forward transfer function and the branches all originate from the same point in the complex plane, the root locus is composed of straight lines with angles ϕ_l. Thus, as the feed-forward gain is increased, the branch along $\phi_l = 0^\circ$ will be the first to cross the imaginary access. By substituting $s = 0$ into (4.10), we find that the gain on $-D(s)$ which places 1 pole at the origin is 1. This implies that (4.9) has one marginally stable pole, with all other poles in the left-half complex plane. Multiplying (4.9) by s will cancel the marginally stable pole, and yield the system in (4.8). Thus, all the poles of (4.8) are in the left-half complex plane. □

Some of constants from Section 3.3 will be redefined here. All other constants maintain

the same definition as in Section 3.3.

$$\eta_4(T) = 2T\left(\eta_3 + \left|\left|\frac{sD(s)}{1-D(s)}\right|\right|_{\mathcal{L}_1} ||\Gamma||_1\eta(T)\right) + ||A||_1\eta(T) + \epsilon \tag{4.12}$$

$$\eta_5(T) = \left|\left|\begin{bmatrix} B & \bar{B}\end{bmatrix}^{-1}\right|\right|_1 \eta_4(T) \tag{4.13}$$

$$\begin{aligned}\gamma_0(T) = {} & ||(sI-A)^{-1}B||_{\mathcal{L}_1}\left(|K_g|||r(s)|||_{\mathcal{L}_\infty} + \left|\left|C_2(s)\frac{C(sI-A)^{-1}\bar{B}}{C(sI-A)^{-1}B}\right|\right|_{\mathcal{L}_1}\right. \\ & \left.\times\left(L(\gamma_x)\gamma_x + B_1 + \eta_5(T)\right)\right) + ||(sI-A)^{-1}\bar{B}||_{\mathcal{L}_1}\left(L(\gamma_x)\gamma_x + B_1 + \eta_5(T)\right)\end{aligned} \tag{4.14}$$

The stability conditions for the controller are

$$||G(s)||_{\mathcal{L}_1}\left(L(\gamma_x)\gamma_x + B_1 + \eta_5(T)\right) + \gamma_0 + \gamma_e(T) < \gamma_x \tag{4.15}$$

$$2\left(L(\gamma_x)\gamma_x + B_1\right) + \eta_5(T) + ||\Gamma||_1\gamma_e < \gamma_\sigma. \tag{4.16}$$

Theorem 4.1. *Let $\tilde{\sigma}(t) = \hat{\sigma}_b(t) - \sigma(x,t)$. Then for T, $C_1(s)$, and $D(s)$ such that (4.15) and (4.16) are satisfied, if $x(0) < \gamma_x$, $u(0) < \gamma_u$, and $\tilde{\sigma}_b(0) < \gamma_\sigma$, then*

$$||\tilde{x}||_{\mathcal{L}_\infty} \leq \gamma_e(T) \tag{4.17}$$

$$||x||_{\mathcal{L}_\infty} < \gamma_x \tag{4.18}$$

$$||u||_{\mathcal{L}_\infty} < \gamma_u \tag{4.19}$$

$$||\tilde{\sigma}||_{\mathcal{L}_\infty} < \gamma_\sigma \tag{4.20}$$

Proof. Similar to the proof of Theorem 3.1, we will prove Theorem 4.1 by contradiction. Assume that (4.18), (4.19), and (4.20) are not true. Since $x(0) < \gamma_x$, $u(0) < \gamma_u$, and

$\tilde{\sigma}_b(0) < \gamma_\sigma$, and $x(t)$, $u(t)$, and $\tilde{\sigma}_b(t)$ are continuous, there exists t' such that

$$||x(t')|| = \gamma_x \tag{4.21}$$

$$||u(t')|| = \gamma_u \text{ or} \tag{4.22}$$

$$||\tilde{\sigma}_b(t')|| = \gamma_\sigma \tag{4.23}$$

and

$$||x_{t'}||_{\mathcal{L}_\infty} \leq \gamma_x \tag{4.24}$$

$$||u_{t'}||_{\mathcal{L}_\infty} \leq \gamma_u \tag{4.25}$$

$$||\tilde{\sigma}_{t'}||_{\mathcal{L}_\infty} \leq \gamma_\sigma \tag{4.26}$$

With the memorizing mechanism, (2.9) becomes

$$\tilde{x}((i+1)T) = \Phi(T)\tilde{x}(iT) + \int_0^T \Phi(T-\tau)\hat{\sigma}(iT)\,d\tau + \int_0^T \Phi(T-\tau)\tilde{\sigma}_b(\tau)\,d\tau \tag{4.27}$$

Substituting (2.10) into (4.27) yields

$$\tilde{x}((i+1)T) = \int_0^T \Phi(T-\tau)\tilde{\sigma}_b(iT+\tau)d\tau. \tag{4.28}$$

Thus (3.48) holds for the memorizing mechanism controller $\forall\, i$ such that $(i+1)T \in [0, t']$.

Taking the time derivative of (4.2) in the Laplace domain yields

$$\dot{\hat{\sigma}}_b(t) = \frac{sD(s)}{1-D(s)}\hat{\sigma}(t) \tag{4.29}$$

From Lemma 4.1, we know that $\left|\left|\frac{sD(s)}{1-D(s)}\right|\right|_{\mathcal{L}_1}$ is a finite value. From (3.60) and (4.29), we can deduce

$$||\dot{\hat{\sigma}}_b(t)||_\infty \leq \left|\left|\frac{sD(s)}{1-D(s)}\right|\right|_{\mathcal{L}_1} ||\Gamma||_1 \eta(T) \tag{4.30}$$

From the definition for $\tilde{\sigma}$, we have

$$\dot{\tilde{\sigma}}(t) = \dot{\hat{\sigma}}_b(t) - \dot{\sigma}(t) \tag{4.31}$$

Note that (3.60) holds for the memorizing mechanism controller. Thus, we can write

$$||\dot{\tilde{\sigma}}(t)||_\infty \leq ||\dot{\hat{\sigma}}_b(t)||_\infty + ||\dot{\sigma}(x,t)||_\infty \leq \left|\left|\frac{sD(s)}{1-D(s)}\right|\right|_{\mathcal{L}_1} ||\Gamma||_1 \eta(T) + \eta_3 \tag{4.32}$$

Furthermore, (3.65) holds for the memorizing mechanism controller, from which we can write

$$||\bar{\sigma} + \tilde{\sigma}(iT+\tau)||_\infty \leq 2T \left(\left|\left|\frac{sD(s)}{1-D(s)}\right|\right|_{\mathcal{L}_1} ||\Gamma||_1 \eta(T) + \eta_3 \right) \tag{4.33}$$

(3.67) also holds, which along with (3.48) and (4.33) implies

$$||\hat{\sigma}(iT+\tau) + \tilde{\sigma}(iT+\tau)||_\infty \leq 2T \left(\left|\left|\frac{sD(s)}{1-D(s)}\right|\right|_{\mathcal{L}_1} ||\Gamma||_1 \eta(T) + \eta_3 \right) + ||A||_1 \eta(T) + \epsilon \tag{4.34}$$

With (3.67), (3.68) holds under the redefined η_4 in (4.12).

By adding $\hat{\sigma}$ to both sides of the definition of $\tilde{\sigma}$ and rearranging the equation, we can write

$$\hat{\sigma}(t) + \hat{\sigma}_b(t) - \sigma(x,t) = \hat{\sigma}(t) + \tilde{\sigma}(t) \tag{4.35}$$

Multiplying both sides of (4.35) by $\begin{bmatrix} B & \bar{B} \end{bmatrix}^{-1}$ results in

$$\begin{bmatrix} \hat{\sigma}_1(t) \\ \hat{\sigma}_2(t) \end{bmatrix} - \begin{bmatrix} \sigma_1(x,t) \\ \sigma_2(x,t) \end{bmatrix} = \begin{bmatrix} B & \bar{B} \end{bmatrix}^{-1} (\hat{\sigma}(t) + \tilde{\sigma}(t)) \tag{4.36}$$

Applying the bound in (4.34) results in (3.70) and (3.71) holding for the new definition of η_5 in (4.13).

Substituting (2.20) into (4.6) yields

$$\begin{aligned}\dot{\hat{x}}(t) &= A\hat{x}(t) + BK_g r(s) + (1 - C_1(s))B\hat{\sigma}_1(t) \\ &\quad -C_2(s)\frac{C(sI-A)^{-1}\bar{B}}{C(sI\_A)^{-1}B}B\hat{\sigma}_2(t) + \bar{B}\sigma_2(t)\end{aligned} \tag{4.37}$$

Taking the Laplace transform of (4.37) yields

$$\begin{aligned}\hat{x}(s) &= (sI-A)^{-1}BK_g r(s) + (sI-A)^{-1}(1 - C_1(s))B\hat{\sigma}_1(s) \\ &\quad +(sI-A)^{-1}BC_2(s)\frac{C(sI-A)^{-1}\bar{B}}{C(sI\_A)^{-1}B}B\hat{\sigma}_2(s) + \bar{B}\hat{\sigma}_2(s)\end{aligned} \tag{4.38}$$

and thus

$$||\hat{x}_{t'}||_{\mathcal{L}_\infty} \leq ||G(s)||_{\mathcal{L}_1}||\hat{\sigma}_{1_{t'}}||_{\mathcal{L}_\infty} + ||\zeta_{t'}||_{\mathcal{L}_\infty} \tag{4.39}$$

where $\zeta(t)$ is redefined as the signal with Laplace transform

$$\zeta(s) = (sI-A)^{-1}B\left(K_g r(s) - C_2(s)\frac{C(sI-A)^{-1}\bar{B}}{C(sI-A)^{-1}B}B\hat{\sigma}_2(s)\right) + (sI-A)^{-1}\bar{B}\hat{\sigma}_2(s) \tag{4.40}$$

Note that (3.75) and (3.76) hold for the memorizing mechanism controller, and thus (3.77) holds as well. By following the process for the proof of Theorem 3.1, we can see that (3.84) holds for the memorizing mechanism controller, which contradicts (4.24). Likewise, (3.85) and (3.86) hold, which contradicts (4.25).

From the definition of $\tilde{\sigma}$, we can write

$$\hat{\sigma}(t) + \tilde{\sigma}(t) = \hat{\sigma}(t) + \hat{\sigma}_b(t) - \sigma(x,t) \tag{4.41}$$

which implies

$$||\hat{\sigma}_{t'}|| \leq ||(\hat{\sigma} + \hat{\sigma})_{t'}||_{\mathcal{L}_\infty} + ||\sigma_{t'}||_{\mathcal{L}_\infty} + ||\hat{\sigma}_{t'}||_{\mathcal{L}_\infty} \tag{4.42}$$

Since (3.84) holds, (3.89) holds as well. Along with (4.16), substituting (3.89) into (4.42)

shows that (3.90) holds for the memorizing mechanism controller, which contradicts (4.26).

Since (3.84), (3.86), and (3.90) hold and contradict (4.24), (4.25), and (4.26) respectively, (4.18), (4.19), and (4.20) must be true. Furthermore, (4.17) follows directly from (3.82) since (4.15) and (4.16) hold. □

Theorem 4.2 will analyze the parameter values for which (4.15) and (4.16) hold. For simplicity, consider a first order low-pass filter for $C_1(s)$ as in (3.91)

Theorem 4.2. *$\exists$ a small T and large ω_1 that satisfy (4.15) and (4.16).*

Proof. The following limits can easily be computed.

$$\lim_{T\to 0}\eta_5(T) = \left|\left|\begin{bmatrix} B & \bar{B}\end{bmatrix}^{-1}\right|\right|_1 \epsilon \tag{4.43}$$

$$\lim_{T\to 0}\gamma_0(T) = ||(sI-A)^{-1}B||_{\mathcal{L}_1}\Bigg(|K_g|||r||_{\mathcal{L}_\infty} + \left|\left|C_2(s)\frac{C(sI-A)^{-1}\bar{B}}{C(sI-A)^{-1}B}\right|\right|_{\mathcal{L}_1} \times (L(\gamma_x)\gamma_x + B_1 + \epsilon)\Bigg) + ||(sI-A)^{-1}\bar{B}||_{\mathcal{L}_1}(L(\gamma_x)\gamma_x + B_1 + \epsilon) \tag{4.44}$$

and (3.95) holds for the memorizing mechanism controller. Then $\forall\, \gamma_x > \gamma_0(T) + \gamma_e(T)$, if

$$||G(s)||_{\mathcal{L}_1} < \frac{\gamma_x - \gamma_0(T) - \gamma_e(T)}{(L(\gamma_x)\gamma_x + B_1 + \eta_5(T))} \tag{4.45}$$

then (4.15) can always be satisfied. Furthermore, (4.44) and (3.95) imply $\exists T$ such that $\frac{\gamma_x-\gamma_0(T)-\gamma_e(T)}{(L(\gamma_x)\gamma_x+B_1+\eta_5(T))}$ is a finite positive number. Thus it follows from (3.92) and (4.45) that (4.15) can always be satisfied by increasing ω_1 or reducing T.

By taking the limit as $T \to 0$ of (4.16), we obtain

$$2(L(\gamma_x)\gamma_x + B_1 + \epsilon\left(\left|\left|\begin{bmatrix} B & \bar{B}\end{bmatrix}^{-1}\right|\right|_1 + ||\Gamma||_1\right)$$

which is a finite positive number. Thus, $\exists$ a finite positive γ_σ that satisfies (4.16). □

Theorem (4.3) will characterize the tracking error bound.

Theorem 4.3. *The error bound between the reference system and the real system is*

$$\begin{aligned} ||x_e||_{\mathcal{L}_\infty} &\leq ||G(s)||_{\mathcal{L}_1} \left(L(\gamma_x)\gamma_x + B_1 + \eta_5(T)\right) \\ &+ \left|\left|(sI-A)^{-1}\right|\right|_{\mathcal{L}_1} \left|\left| C_2(s)\frac{C(sI-A)^{-1}\bar{B}}{C(sI-A)^{-1}B}B \right|\right|_{\mathcal{L}_1} \left(L(\gamma_x)\gamma_x + B_1 + \eta_5(T)\right) \\ &+ \left|\left|(sI-A)^{-1}\bar{B}\right|\right|_{\mathcal{L}_1} \left(L(\gamma_x)\gamma_x + B_1 + \eta_5(T)\right) + \gamma_e(T) \end{aligned} \tag{4.46}$$

Proof. Clearly, (3.99) holds for the memorizing mechanism controller. Substituting (4.38) into (3.99) yields

$$\begin{aligned} x(s) &= (sI-A)^{-1}BK_g r(s) + (sI-A)^{-1}(1-C_1(s))B\hat{\sigma}_1(s) \\ &+(sI-A)^{-1}\left[C_2(s)\frac{C(sI-A)^{-1}\bar{B}}{C(sI\_A)^{-1}B}B\hat{\sigma}_2(s) + \bar{B}\hat{\sigma}_2(s)\right] + \tilde{x}(s) \end{aligned} \tag{4.47}$$

Substituting (3.101) and (4.47) into the Laplace transform of (3.97) results in

$$\begin{aligned} x_e(s) &= (sI-A)^{-1}(1-C_1(s))B\hat{\sigma}_1(s) \\ &+(sI-A)^{-1}\left[C_2(s)\frac{C(sI-A)^{-1}\bar{B}}{C(sI\_A)^{-1}B}B\hat{\sigma}_2(s) + \bar{B}\hat{\sigma}_2(s)\right] + \tilde{x}(s) \end{aligned} \tag{4.48}$$

By substituting the appropriate bounds into (4.48), we obtain

$$\begin{aligned} ||x_e||_{\mathcal{L}_\infty} &\leq ||G(s)||_{\mathcal{L}_1} \left(L(\gamma_x)\gamma_x + B_1 + \eta_5(T)\right) \\ &+ \left|\left|(sI-A)^{-1}\right|\right|_{\mathcal{L}_1} \left|\left| C_2(s)\frac{C(sI-A)^{-1}\bar{B}}{C(sI-A)^{-1}B}B \right|\right|_{\mathcal{L}_1} \left(L(\gamma_x)\gamma_x + B_1 + \eta_5(T)\right) \\ &+ \left|\left|(sI-A)^{-1}\bar{B}\right|\right|_{\mathcal{L}_1} \left(L(\gamma_x)\gamma_x + B_1 + \eta_5(T)\right) + \gamma_e(T) \end{aligned} \tag{4.49}$$

which proves Theorem 4.3. □

4.4 Simulation Results

In order to illustrate the theoretical results in Section 4.3, we will examine numerical simulations. We will consider the system in (2.4) with

$$A = \begin{bmatrix} 0 & 10 \\ -1 & -\sqrt{2} \end{bmatrix} \quad B = \begin{bmatrix} 0 \\ 1 \end{bmatrix} \quad C = \begin{bmatrix} 1 & 0 \end{bmatrix} \tag{4.50}$$

Let $x = \begin{bmatrix} x_1 & x_2 \end{bmatrix}^\top$. Consider the uncertainty

$$\sigma(x,t) = \begin{bmatrix} 0.1\sin(2x_1(t)+1)+4 \\ 0.2\sin(x_2(t))+2 \end{bmatrix} \tag{4.51}$$

The memorizing mechanism is implemented with

$$D(s) = \frac{20}{s+20} \tag{4.52}$$

and the $\mathcal{L}_1$ control parameters are

$$C_1(s) = C_2(s) = \frac{20}{s+20} \tag{4.53}$$

As in Section 3.4, the simulation is performed for both small and large time-step scenarios. For the small time-step, we consider $T = 0.0001$ seconds, and for the large time-step case, $T = 0.01$ seconds. We compare results for each scenario using both the standard $\mathcal{L}_1$ adaptive controller and the $\mathcal{L}_1$ controller with memorizing mechanism. In the case where T is sufficiently small, the standard $\mathcal{L}_1$ controller performs identically to the memorizing mechanism controller. However, when T is too large to rely solely on fast adaptation, the memorizing mechanism controller shows a significant improvement.

4.4.1 Small Time-Step

Here, we consider the case where $T = 0.0001$ seconds. Figure 4.1 shows the tracking performance, control input, and the adaptive parameters along with the system uncertainties for the standard $\mathcal{L}_1$ controller. Figure 4.2 shows these signals for the memorizing mechanism controller. Additionally, Figure 4.2c shows the fast adaptation parameters plotted along with the memory terms. Notice that the two controllers perform equally well here. In the standard $\mathcal{L}_1$ controller, fast adaptation is able to accurately estimate σ without the need for additional online modeling. Note that in the memorizing mechanism controller, the fast adaptation parameters quickly converge to a very low magnitude while the memory terms converge to the constant bias of σ. As with the ANN controller in Chapter 3, the burden of estimation is shifted away from the fast adaptation which now only estimates high frequency components of the uncertainty.

4.4.2 Large Time-Step

Now we consider the case where $T = 0.01$ seconds. Figure 4.3 shows the tracking performance, control input, and the adaptive parameters along with the system uncertainties for the standard $\mathcal{L}_1$ controller. Figure 4.4 shows these signals for the memorizing mechanism controller. Additionally, Figure 4.4c shows the fast adaptation parameters plotted along with the memory terms. In Figure 4.3a, we see that the reduction in sampling speed introduces a steady-state error to the reference tracking. Note that the predicted output, $\hat{y}$, in Figure 4.3a does not have this steady-state error. This is indicative that the adaptive law is not accurately estimating the uncertainty, σ. Examining Figure 4.3c confirms that there is indeed an offset between the adaptive parameters and the actual uncertainty.

Figure 4.4 is nearly identical to Figure 4.2. The steady-state error is present in neither the tracking performance nor the uncertainty approximation. This shows that the addition of the memorizing mechanism results in improved robustness to sampling rates up two orders of magnitude slower than the small time-step case.

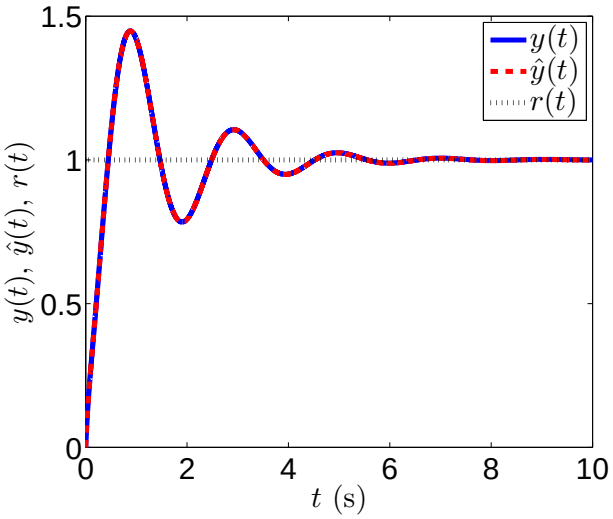

(a) Tracking performance

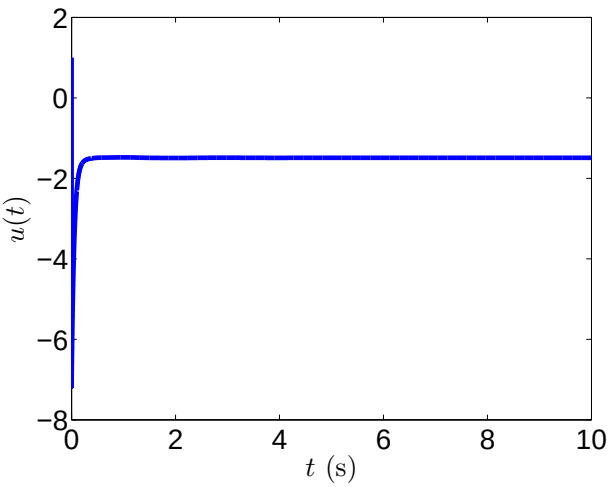

(b) Control input

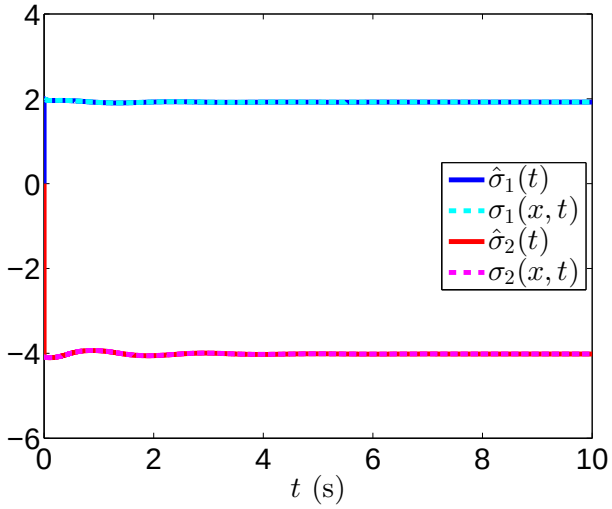

(c) Adaptive parameters

Figure 4.1: Simulation results using the standard $\mathcal{L}_1$ controller with $T = 0.0001$ sec

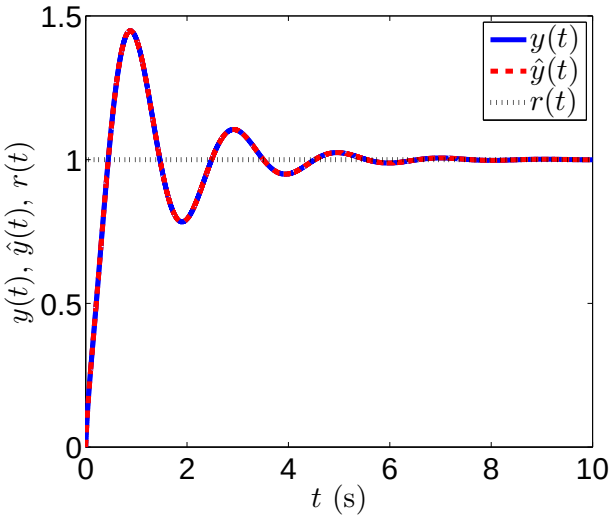

(a) Tracking performance

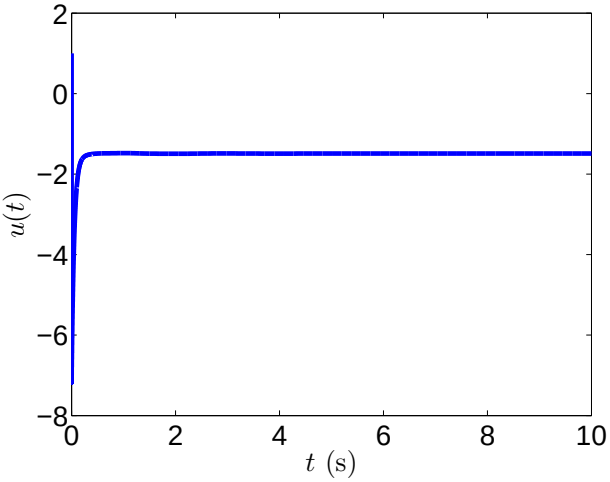

(b) Control input

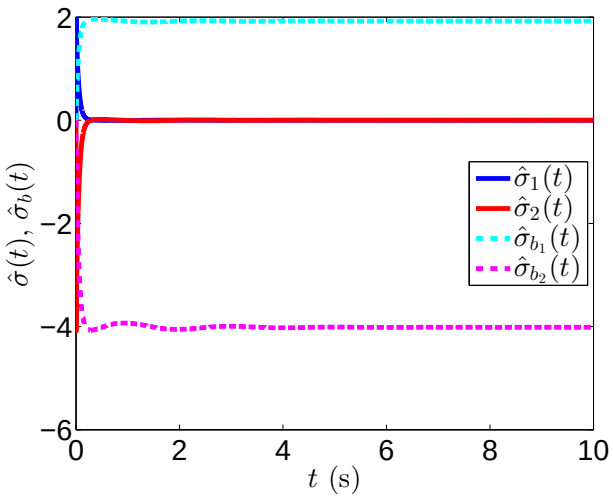

(c) Adaptive parameters

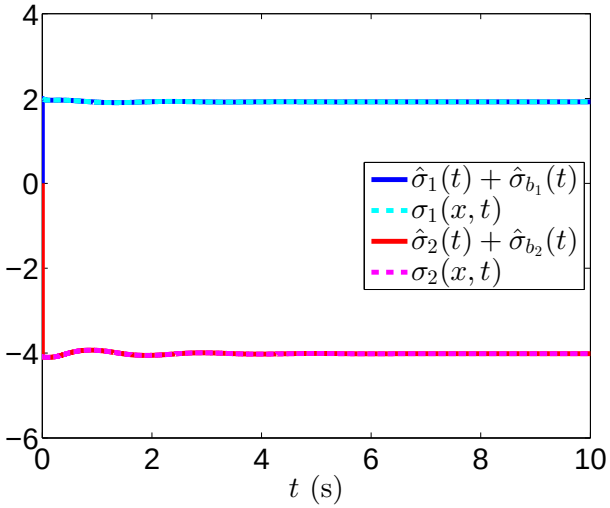

(d) Total uncertainty approximation

Figure 4.2: Simulation results using the $\mathcal{L}_1$ controller with memorizing mechanism with $T = 0.0001$ sec

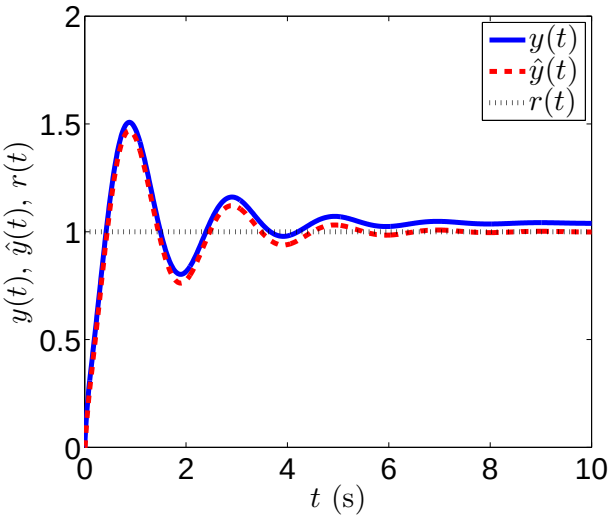

(a) Tracking performance

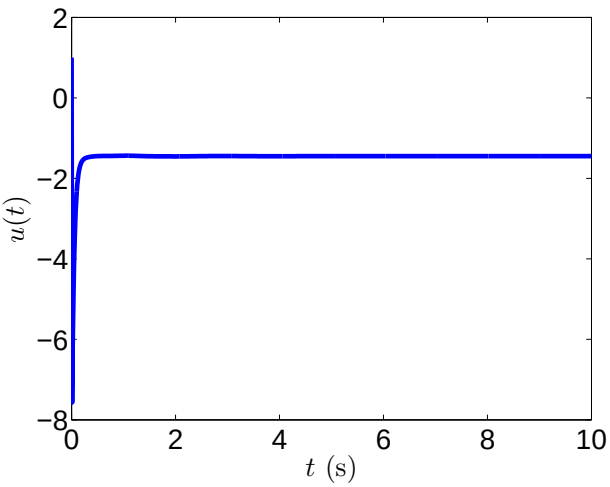

(b) Control input

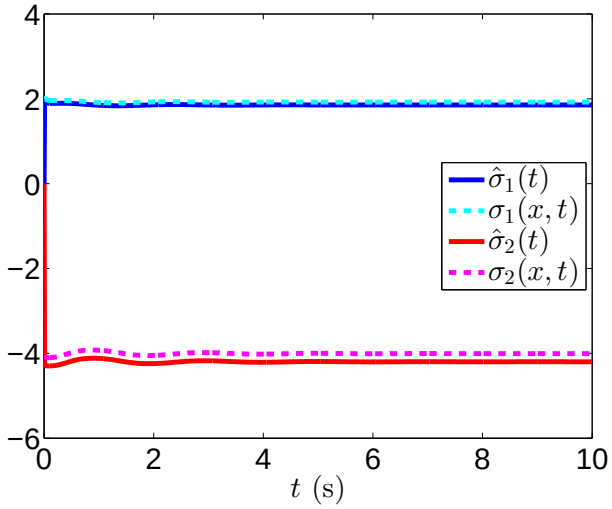

(c) Adaptive parameters

Figure 4.3: Simulation results using the standard $\mathcal{L}_1$ controller with $T = 0.01$ sec

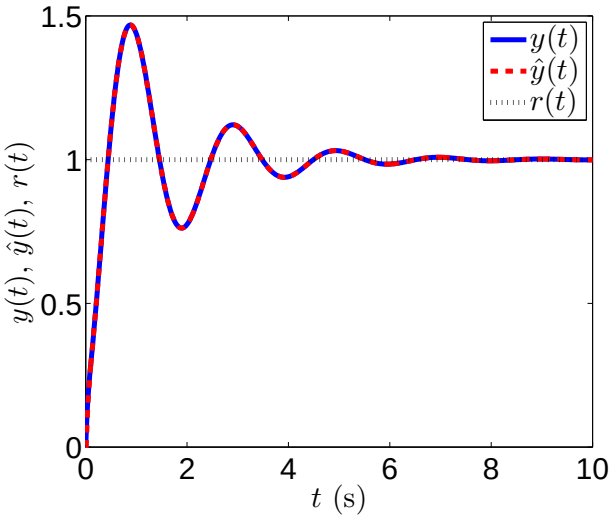

(a) Tracking performance

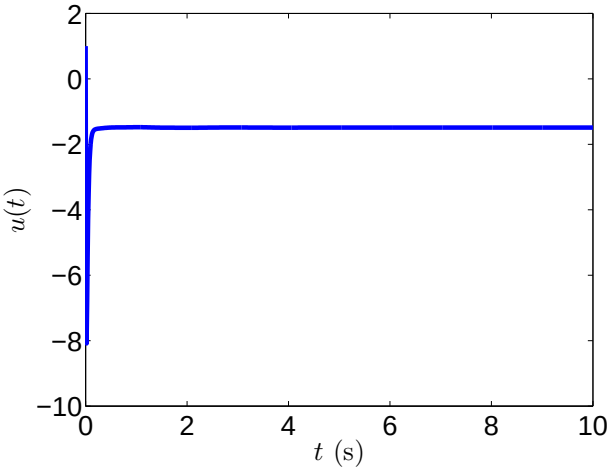

(b) Control input

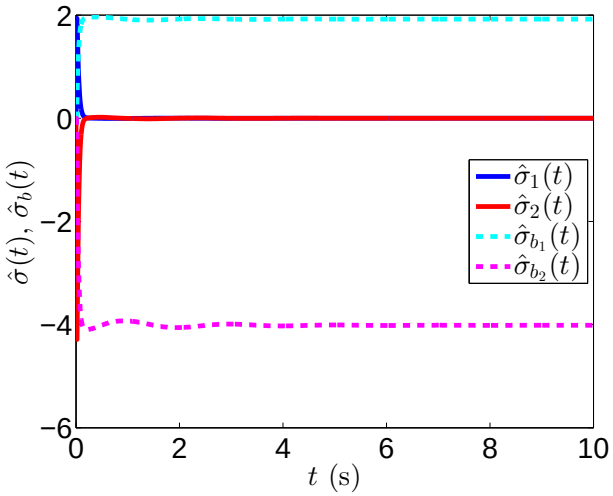

(c) Adaptive parameters

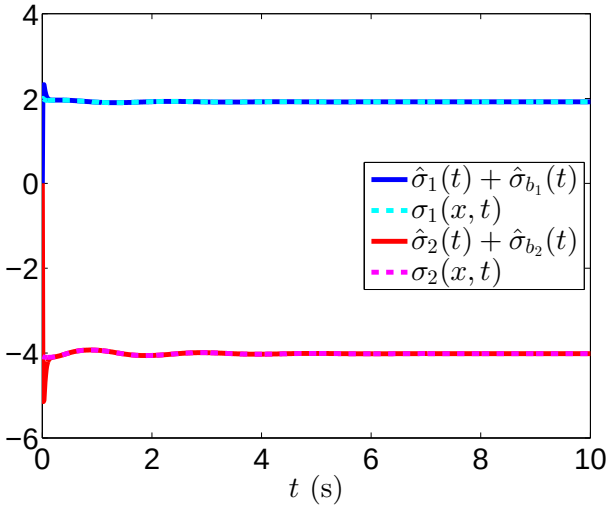

(d) Total uncertainty approximation

Figure 4.4: Simulation results using the $\mathcal{L}_1$ controller with memorizing mechanism with $T = 0.01$ sec

Chapter 5

Fast Adaptation-Based Performance-Seeking Control

This chapter presents a method of using fast adaptation for online optimization. Engineering systems are usually designed to optimize a performance criteria. For example, in jet engines, stator vane settings and nozzle area are selected to optimize fuel efficiency. In reality, every individual engine will deviate somewhat from the optimal design due to manufacturing variability or deterioration due to component age. Performance-seeking control (PSC) is an auxiliary control algorithm designed to compensate for such deviations and re-optimize the system online by contributing small deviations to a baseline input based on feedback and adaptive estimates.

In the late 1970's, NASA investigated performance-seeking control for aircraft propulsion and determined that Powell [67] and Zangwill-Powell [85] optimization techniques were efficient methods [75]. In the early 1990's, NASA conducted flight tests of PSC on board a NASA F-15 aircraft for maximum thrust, minimum turbine inlet temperature, and minimum fuel flow. All three modes demonstrated a performance increase in their respective metrics [58, 26, 27, 60]. In 1997, NASA developed an adaptive performance-seeking controller [38]. This method combined fuzzy model reference learning control [40] with positive gradient

control to perform online optimization

The fast adaptation-based PSC architecture is based on $\mathcal{L}_1$ adaptive control and contains a state predictor, adaptive law, and control law. The block diagram for this structure is shown in Figure 5.1. The state predictor is a dynamic system that attempts to mimic the plant dynamics in the operating region prescribed by the baseline controller. The adaptive law uses fast adaptation to update the adaptive parameters such that the state prediction error is driven to zero. Finally, the control law consists of a gradient search algorithm combined with a Lyapunov-based tracking method. This ensures the state does not deviate from what is prescribed by the baseline input while minimizing the performance metric. Each component of this architecture is elaborated on in the subsequent sections.

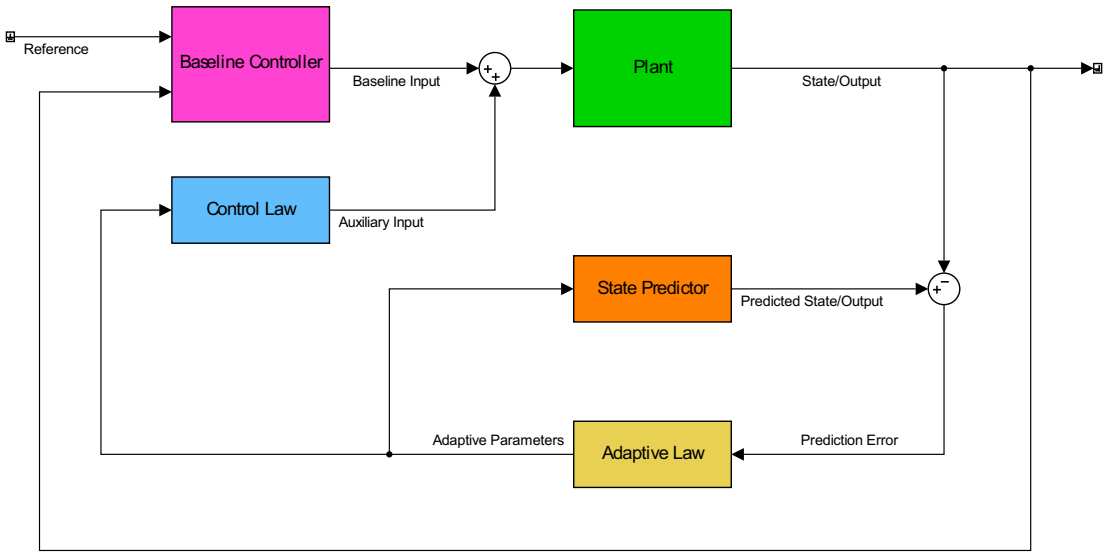

Figure 5.1: Performance-seeking control block-diagram

5.1 Problem Formulation

Let the plant dynamics be given by

$$\begin{aligned} \dot{x}(t) &= Ax(t) + B\sigma(u(t)) \\ y(t) &= Cx(t) \quad x(0) = 0 \end{aligned} \tag{5.1}$$

where $x \in \mathbb{R}^n$ is the deviation in the system state from the reference maintained by the baseline controller, $t \geq 0 \in \mathbb{R}$ is time, $A \in \mathbb{R}^{n \times n}$ is a Hurwitz state matrix, $B \in \mathbb{R}^n$ is the input vector, $\sigma \in \mathbb{R}$ is an unknown, nonlinear control effectiveness function, $u = \begin{bmatrix} u_1 & u_2 \end{bmatrix}^\top$ is the auxiliary control input that the PSC can affect, $y \in \mathbb{R}$ is the deviation in the system output from the reference maintained by the baseline controller, and $C \in \mathbb{R}^{1 \times n}$ is the output matrix.

$\exists$ a continuous implicit relation, $u_1 = f(x, u)$ such that $\frac{\partial^2 f}{\partial u_2^2} \geq 0$. Furthermore, $\frac{\partial \sigma}{\partial u_1} > 0$.

The control objective is to minimize the performance function, $f(x, u)$ whilst regulating x to zero.

5.2 State Predictor

As in the $\mathcal{L}_1$ control architecture, the state predictor is a dynamic model that matches the structure of the plant dynamics in (5.1).

$$\begin{aligned} \dot{\hat{x}}(t) &= A\hat{x}(t) + B\hat{\sigma}(t) \\ \hat{y}(t) &= Cx(t) \quad \hat{x}(0) = 0 \end{aligned} \tag{5.2}$$

where $\hat{x} \in \mathbb{R}^n$ is the predicted state, $\hat{\sigma} \in \mathbb{R}$ is an adaptive parameters, and $\hat{y} \in \mathbb{R}$ is the predicted output.

5.3 Adaptive Law

We use the piece-wise constant adaptive law found in the $\mathcal{L}_1$ architecture. Let $\hat{\sigma}(t) = \hat{\sigma}(iT)$ where i is an integer such that $iT \leq t < (i+1)T$. Let the prediction error be $\tilde{x}(t) = \hat{x}(t) - x(t)$. Subtracting (5.1) from (5.2) results in

$$\dot{\tilde{x}}(t) = A\tilde{x}(t) + B\hat{\sigma}(t) - B\sigma(u(t)) \tag{5.3}$$

The solution to (5.3) over the interval $[iT, (i+1T)]$ is

$$\tilde{x}(t) = \Phi(T)\tilde{x}(iT) + \int_{iT}^{t} \Phi(t-\tau)B\hat{\sigma}(iT)\,d\tau - \int_{iT}^{t} \Phi(t-\tau)B\sigma(u(\tau))\,d\tau \tag{5.4}$$

where τ is a dummy variable and $\Phi(T) = e^{AT}$. At $t = (i+1)T$, (5.4) becomes

$$\tilde{x}((i+1)T) = \Phi(T)\tilde{x}(iT) + \int_{0}^{T} \Phi(T-\tau)B\hat{\sigma}(iT)\,d\tau - \int_{0}^{T} \Phi(T-\tau)B\sigma(u(\tau))\,d\tau \tag{5.5}$$

Note that $\hat{\sigma}(iT)$ does not depend on τ and can thus be taken outside of the integral. We can choose $\hat{\sigma}$ such that its effects on the system drive $\tilde{x}$ to zero at the next time-step by ignoring the third term in (5.3), plugging in $\tilde{x}((i+1)T) = 0$, and solving for $B\hat{\sigma}(iT)$. This results in

$$B\hat{\sigma}(iT) = \Gamma(T)\tilde{x}(iT), \quad \Gamma(T) = -\left[\int_{0}^{T} \Phi(T-\tau)\,d\tau\right]^{-1} \Phi(T) \tag{5.6}$$

Then the adaptive law is

$$\hat{\sigma}(iT) = \frac{1}{||B||}\Gamma(T)\tilde{x}(iT), \quad \Gamma(T) = -\left[\int_{0}^{T} \Phi(T-\tau)\,d\tau\right]^{-1} \Phi(T) \tag{5.7}$$

5.4 Control Law

The control law is composed of a gradient search algorithm to minimize $f(x,u)$ using u_1, and a Lyapunov-based algorithm to regulate x using u_2.

Because $\frac{\partial^2 f}{\partial u_2^2} \geq 0$, $\exists$ a set, $\mathbb{U} \subset \mathbb{R}$ such that

$$u_2^* = \underset{u_2}{\operatorname{argmin}} f(x,u) \quad \forall\, u_2^* \in \mathbb{U} \tag{5.8}$$

Then the goal of the gradient search portion of the control law is to drive u_2 to be in the set $\mathbb{U}$. u_2 is then updated via

$$\dot{u}_2(t) = -k_2 \frac{\partial f}{\partial u_2} \tag{5.9}$$

where $k_2 > 0$ is the update rate. The partial derivative in (5.9) is calculated as

$$\frac{\partial f}{\partial u_2} = \frac{\dot{f}(x(t),u(t))}{\dot{u}_2(t)} \tag{5.10}$$

The goal of the design of u_1 is to regulate x to zero. Since A is Hurwitz, this is achieved when σ is zero. Then the goal becomes the regulation of the nonlinear function, σ to zero. Since σ is unknown, we will design u_1 instead using the adaptive estimate, $\hat{\sigma}$, for feedback. To design the update law for u_1, consider the Lyapunov function

$$V(\hat{\sigma}(t)) = \hat{\sigma}(t)^2 \tag{5.11}$$

The time derivative of $V(\hat{\sigma})$ is

$$\dot{V}(\hat{\sigma}(t)) = \frac{\partial V}{\partial \hat{\sigma}} \frac{\partial \hat{\sigma}}{\partial u_1} \dot{u}_1(t) \tag{5.12}$$

From (5.11), we can write $\frac{\partial V}{\partial \hat{\sigma}}$ as

$$\frac{\partial V}{\partial \hat{\sigma}} = 2\hat{\sigma}(t) \tag{5.13}$$

Then

$$\dot{V}(\hat{\sigma}(t)) = 2\hat{\sigma}(t)\hat{\sigma}\frac{\partial\hat{\sigma}}{\partial u_1}\dot{u}_1(t) \tag{5.14}$$

Since $\frac{\partial\sigma}{\partial u_1} > 0$, we can use the certainty equivalence principle to state $\frac{\partial\hat{\sigma}}{\partial u_1} > 0$. Then in order to make $\dot{V} \leq 0$, we can choose $\dot{u}_1$ to have the opposite sign of $\hat{\sigma}$. As in $\mathcal{L}_1$ adaptive control, the adaptive parameter is low-pass filtered prior to generating control inputs in order to recover the robustness lost from the high-gain feedback of fast adaptation.

$$\dot{u}_1(t) = -k_1 C(s)\hat{\sigma}(t) \tag{5.15}$$

where $k_1 > 0$ is the update rate and $C(s)$ is a low-pass filter.

5.5 Simulation Results

In this section, the performance-seeking control design is verified via a numerical simulation. Consider the system in (5.1) with

$$\begin{aligned} A &= \begin{bmatrix} 0 & 1 \\ -1 & -\sqrt{2} \end{bmatrix} \quad B = \begin{bmatrix} 0 & 1 \end{bmatrix}^\top \\ C &= \begin{bmatrix} 1 & 0 \end{bmatrix} \quad \sigma(u(t)) = (u_1(t)+1)\exp\left(-\frac{(u_2(t)-5)^2}{25}\right) - 0.5 \end{aligned} \tag{5.16}$$

The simulation is performed with a time-step of $T = 0.002$ seconds. The performance function is

$$f(x(t), u(t)) = \frac{u_1(t)+1}{x_1(t)+10} \tag{5.17}$$

Note that in the nonlinearity, σ, $\exp\left(-\frac{(u_2(t)-5)^2}{25}\right)$ is a Gaussian radial basis function with a center at $u_2 = 5$. Thus the effectiveness of u_1 is maximized at $u_2 = 5$. In conjunction with having u_1 in the denominator of (5.17), this means the optimum solution for the PSC is drive u_2 to 5 so that the minimum magnitude u_1 can be used for regulation.

The PSC parameters are

$$C(s) = \frac{100}{s+100} \quad k_1 = 1 \quad k_2 = 5 \tag{5.18}$$

Since the time-derivative $\dot{f}(x,u)$ is calculated numerically, $f(x,u)$ is low-pass filtered through $\frac{20}{s+20}$ before taking the derivative.

Figure 5.2 shows the simulation results. Figure 5.2a shows the state regulation performance along with the predicted state. We can see that the state prediction tracks the real state closely over the duration of the simulation and the states are regulated to a small magnitude within the first 30 seconds. Figure 5.2b shows the control inputs. After an initial transient, u_2 converges to the optimal value of 5 after 60 seconds, and u_1 converges to a value lower than its initial value. Figure 5.2c shows the time-histories of the nonlinearity σ and its adaptive estimate, $\hat{\sigma}$. The adaptive parameter tracks the actual nonlinearity closely through the simulation's duration, thus the adaptive law performs as desired. Finally, Figure 5.2d shows the time history of the performance function. After the initial transient, the performance function converges to a value of 0.05, lower than its initial value of 0.1.

The simulation scenario provided here can be considered analogous to a jet engine performance-seeking problem. The performance function is an analogy to specific fuel consumption, and the two control inputs are analogous to fuel flow rate and engine nozzle area. It is known that an optimum point exists between fuel flow and nozzle area for an engine outputting a constant thrust. This simulation demonstrates the viability of fast adaptation-based performance-seeking control for real-world fuel optimization problems.

5.5.1 Sampling Time Constraints and Memorizing Mechanism

The simulation results in Figure 5.2 used a time-step of 0.002 seconds or a sampling rate of 500 Hz. This is a very fast rate and is likely not implementable in many real-time applications. If we slow down the sampling rate to 200 Hz, the PSC does not converge. This

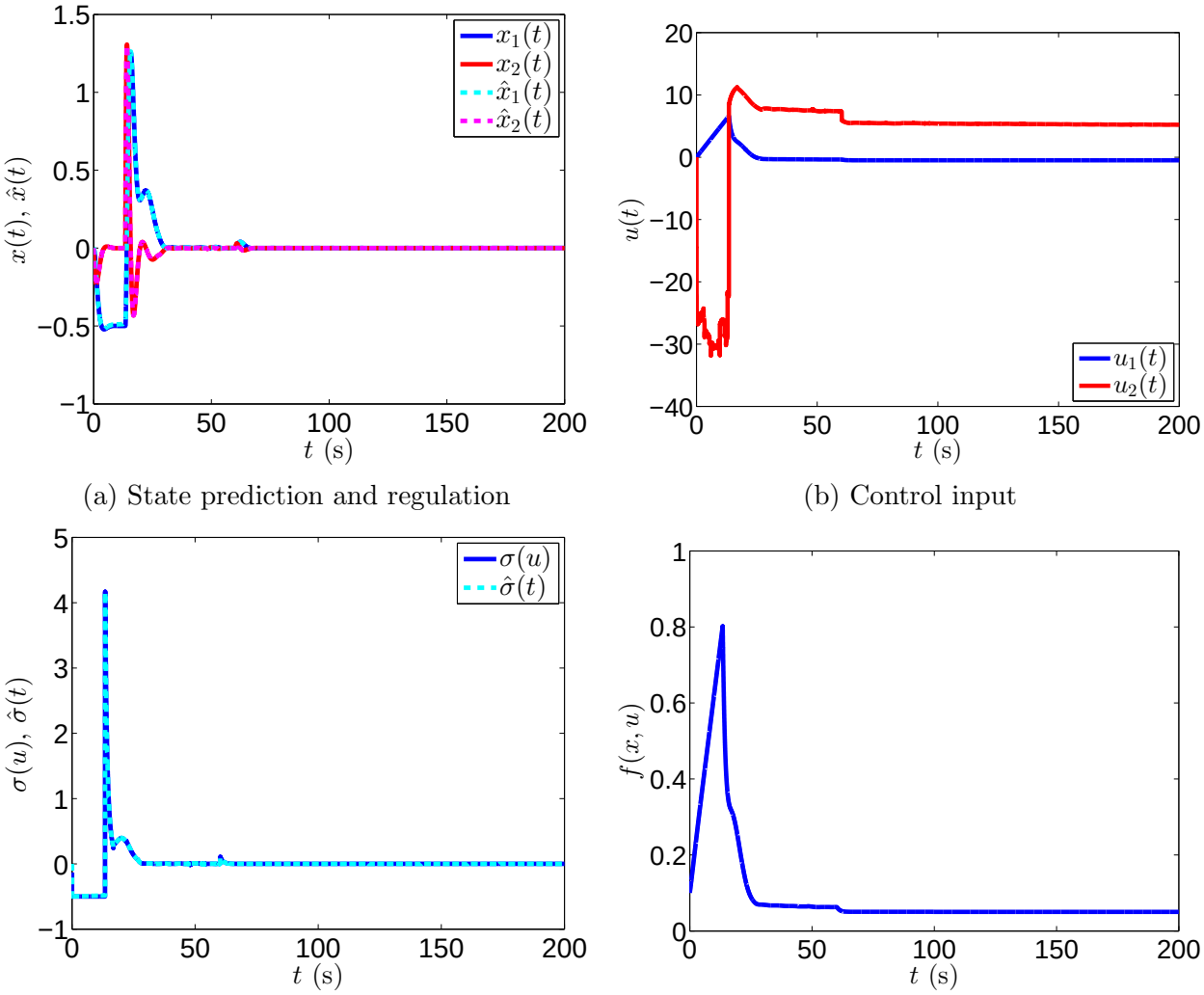

(a) State prediction and regulation

(b) Control input

(c) Nonlinearity and adaptive parameter

(d) Performance function

Figure 5.2: Performance-seeking control simulation results

is shown in Figure 5.3.

Figure 5.3a shows that x_2 has a steady-state error of -0.5, and the prediction $\hat{x}_2$ diverges from the real state. Figure 5.3b shows that u_2 does not converge, and u_1 increases throughout the duration of the simulation. Figure 5.3c shows that $\hat{\sigma}$ diverges from the nonlinearity, σ. Figure 5.3d shows that the performance function increases over time.

Either the ANN adaptive law or the memorizing mechanism from previous chapters can be applied to recover the performance in the presence of slow sampling speeds. Here we will

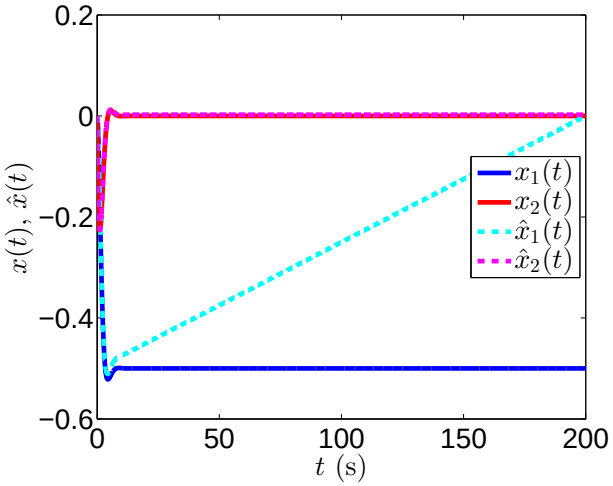

(a) State prediction and regulation

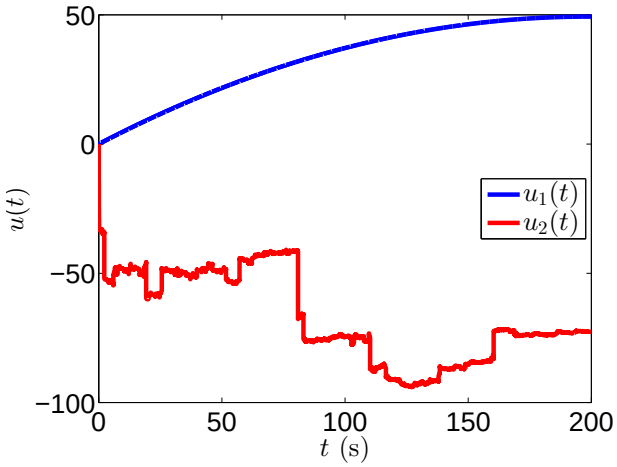

(b) Control input

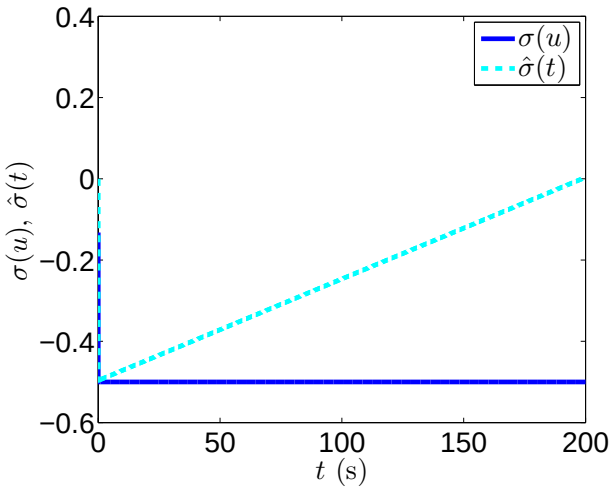

(c) Nonlinearity and adaptive parameter

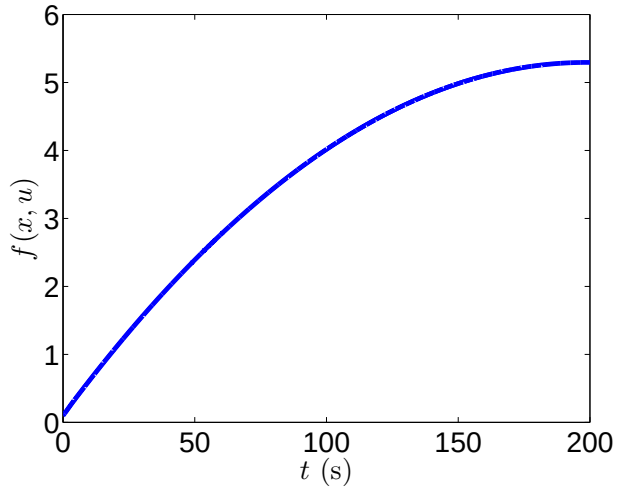

(d) Performance function

Figure 5.3: Performance-seeking control simulation results at $T = 0.005$ seconds

apply the memorizing mechanism with a first-order filter,

$$D(s) = \frac{2.6}{s + 2.6} \tag{5.19}$$

This entails replacing $\hat{\sigma}(t)$ in (5.2), (5.9), and (5.15) with $(\hat{\sigma}(t) + \hat{\sigma}_b(t))$. Simulation results for the PSC with memorizing mechanism at a time-step of 0.005 seconds are shown in Figure 5.4

From Figure 5.4 we see that the memorizing mechanism makes the difference between convergence and divergence for the PSC at the slowed down sampling rate. Figure 5.4a shows

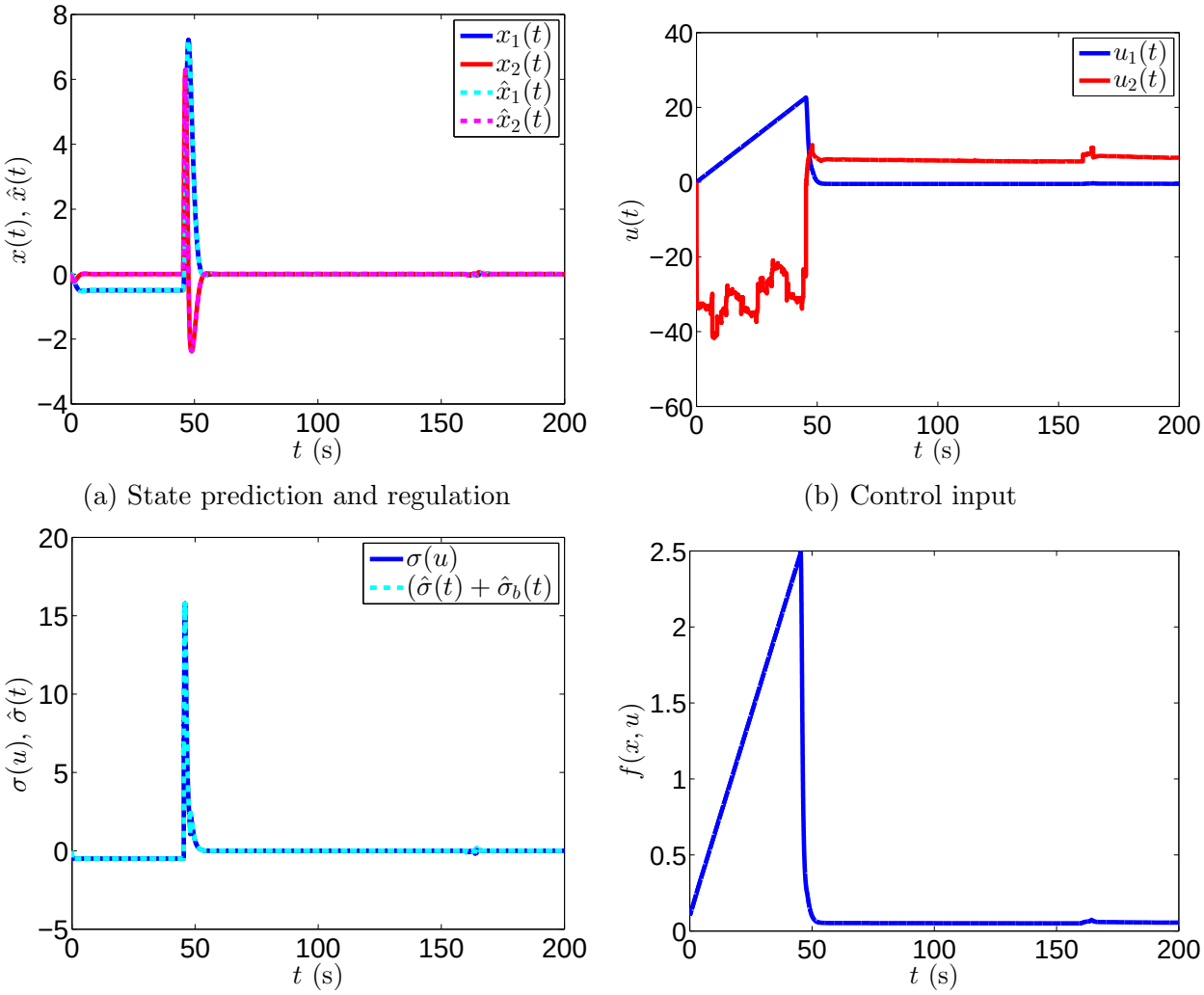

(a) State prediction and regulation

(b) Control input

(c) Nonlinearity and adaptive parameter

(d) Performance function

Figure 5.4: Performance-seeking control with memorizing mechanism simulation results at $T = 0.005$ seconds

that both states are now regulated after an initial transient, and steady-state is reached at approximately 55 seconds. Figure 5.4b shows convergence of u_2 to the optimal value of 5 once steady-state is reached, and u_1 decreases to a value lower than its initial condition. Figure 5.4c shows that the total uncertainty approximation of $(\hat{\sigma} + \hat{\sigma}_b)$. Figure 5.4d shows that the performance function converges to 0.05, the same optimal value reached in Figure 5.2d.

This example supports the application of the techniques in Chapters 3 and 4 to increase performance wherever the fast adaptive law of $\mathcal{L}_1$ control is used.

Chapter 6

Case Study I: Pressure Regulation of Aircraft Air Management Systems

This chapter describes the application of $\mathcal{L}_1$ adaptive control to the problem of pressure regulation in aircraft air management systems using an engine bleed valve. The pressure-regulating valve is part of a larger air management system (AMS) which includes control valves for temperature and flow rates and a heat exchanger or precooler.

The AMS aboard commercial aircraft are used to supply air at desired pressures, temperatures, and flow rates to various other systems throughout the aircraft. There are typically four control valves involved in the AMS - a high-pressure engine bleed valve, low-pressure engine bleed valve, temperature control valve, and flow control valve. Figure 6.1 shows the schematic design of a typical AMS. The two engine bleed valves are used for pressure regulation, and these are the most difficult to control. A pressure-regulating engine bleed valve is shown in Figure 6.2. The dynamic relationship between valve angle and downstream pressure is highly nonlinear, and control performance is very sensitive to manufacturing variability. Some parameters can vary so greatly that a traditional PI controller tuned for the nominal parameter values will experience a significant degradation in tracking performance. Some of the systems parameters known to have such an effect are the orifice size upstream

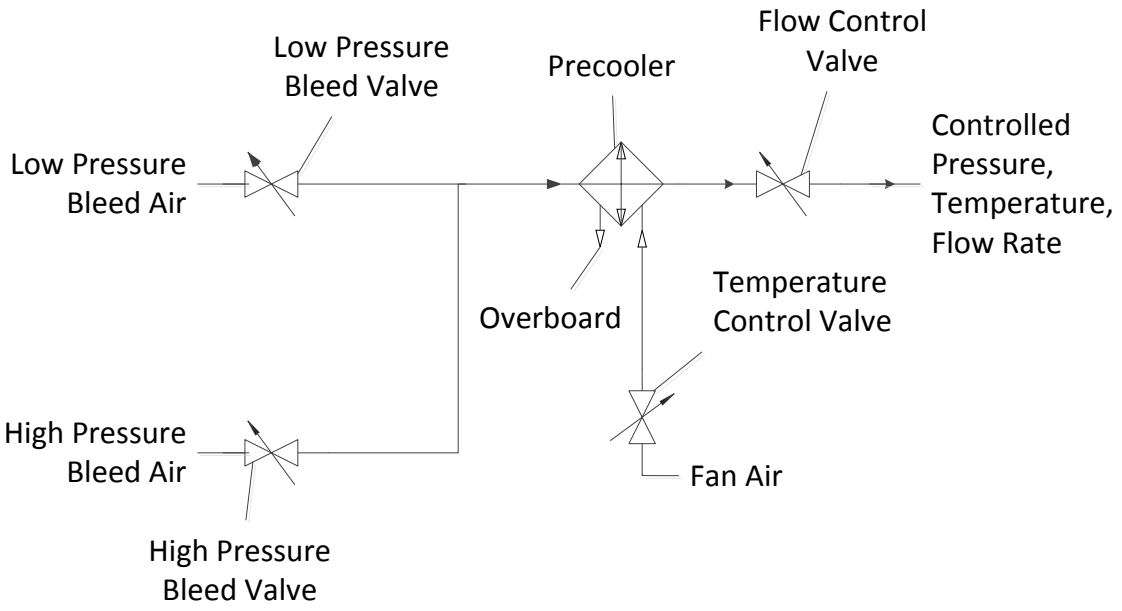

Figure 6.1: Schematic of a typical air management system

and downstream of the torque motor used to drive the valves, the pressure drop across the precooler, and the valve friction coefficients.

The majority of the previous literature involving AMS control deals with temperature control [32, 77, 79, 78]. [62] studies optimal design of AMS without considerations of feedback control and excludes valve dynamics from the system model. Furthermore, the current literature neglects the effects of valve hysteresis caused by backlash and dry friction. These are the primary nonlinearities in the system, which cause valve oscillations under linear controllers. This constitutes an increase in the number of duty cycles of the valve and a decrease in the part's useable life. These effects establish a need for a more robust controller design.

This chapter applies an $\mathcal{L}_1$ adaptive controller to the pressure regulation valve. $\mathcal{L}_1$ control was first applied to AMS pressure regulation in [19]. First a system model is developed for the valve dynamics and the relationship between valve angle and downstream pressure. Next the algorithm is applied to this model. Finally, simulation results are presented and compared to an industry standard PI controller.

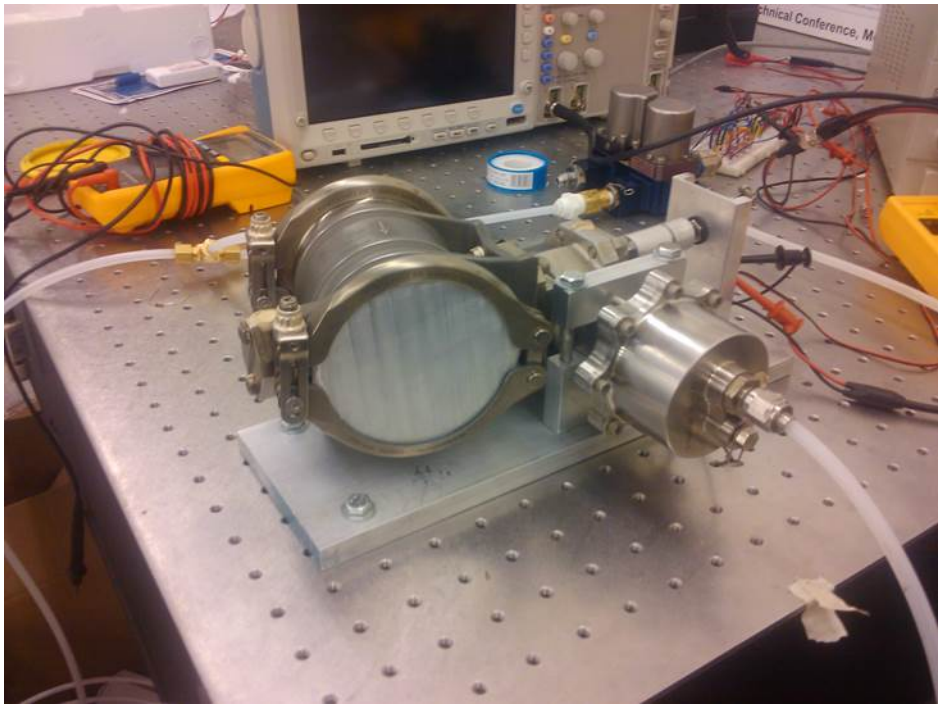

Figure 6.2: Pressure-regulating engine bleed valve

6.1 System Description

A typical AMS uses both high-pressure and low-pressure engine bleed valves for pressure regulation. However, these valves do not operate simultaneously. The high-pressure valve is activated only when the inlet pressure to the low-pressure valve is lower than the desired reference pressure. In this situation, the low-pressure valve operates in a fully open state. Thus, a single valve will be modeled. The following model is an extension of that found in [32, 77, 79, 78]. A hysteresis effect due to backlash and dry friction is added as well as effects from unknown disturbances.

The control valve is modeled as a first-order lag subject to unknown disturbances with

hysteresis in the input,

$$\begin{aligned} \bar{\beta} &= (u_{hyst}(s) + \bar{\sigma}(s))\frac{K_v}{\tau_v s + 1} \\ \beta &= \begin{cases} \pi/2 & \text{if } \bar{\beta} \geq \pi/2 \\ \beta_{min} & \text{if } \bar{\beta} \leq \beta_{min} \\ \bar{\beta} & \text{otherwise} \end{cases} \end{aligned} \tag{6.1}$$

where $\bar{\beta}$ is the linear model valve angle, u_{hyst} is the control signal after hysteresis is applied, $\bar{\sigma}$ is a disturbance in the control input, K_v is the valve gain, τ_v is the valve time-constant, β is the actual valve angle, and β_{min} is the minimum valve angle. The hysteresis model is

$$u_{hyst}(t) = \lim_{dt \to 0} \begin{cases} u_{hyst}(t-dt) - \frac{1/2}{w} & \text{if } u(t) > u_{hyst}(t-dt) + \frac{1}{2}w \\ u_{hyst}(t-dt) + \frac{1/2}{w} & \text{if } u(t) < u_{hyst}(t-dt) - \frac{1}{2}w \\ u_{hyst}(t-dt) & \text{otherwise} \end{cases} \tag{6.2}$$

where u is the control input and w is the width of the hysteresis loop. u is an electrical current supplied to the valve's torque motor.

The valve area is

$$A = \frac{\pi d^2}{4}(1 - \cos\beta) \tag{6.3}$$

The relationship between valve area and downstream pressure is obtained from the equation for an isentropic expansion process for variable area duct flow,

$$\begin{aligned} W &= 0.05593 A P_u \sqrt{\frac{2\gamma g}{T_u(\gamma - 1)R}\left(\phi^{1/\gamma} - \phi^{(1+\gamma)/\gamma}\right)} \\ \phi &= \begin{cases} 0.5283 & \text{if } P_d/P_u < 0.5283 \\ P_d/P_u & \text{otherwise} \end{cases} \end{aligned} \tag{6.4}$$

where W is the mass flow rate in kg/s, A is the valve area in m^2, P_u is the upstream pressure in Pa, $\gamma = 1.4$ is the ratio of specific heat at constant pressure to specific heat at constant volume for air, $g = 9.8066$ m/s^2 is the acceleration due to gravity, T_u is the upstream temperature in K, $R = 287.16$ m^2/(s^{2}K) is the gas constant for air, ϕ is the ratio of downstream pressure to upstream pressure, and P_d is the downstream pressure. While W and T_u are controlled by their respect valves, for the purposes of this model, they will be considered constant parameters. (6.1), (6.2), (6.3), (6.4) make up a model that relates downstream pressure to the input current to the valve's torque motor.

6.2 $\mathcal{L}_1$ Controller

To fit the problem into the $\mathcal{L}_1$ control framework, we will express the pressure dynamics as

$$\dot{P}_d(t) = AP_d(t) + Bu(t) + \sigma(t) \tag{6.5}$$

where $A \in \mathbb{R}$ is a state gain, $B \in \mathbb{R}$ is an input gain, and $\sigma(t) \in \mathbb{R}$ is a term lumping all nonlinearities and uncertainties together.

6.2.1 State Predictor

The state predictor follows the structure of (6.5) and utilizes the memorizing mechanism of Chapter 4. This results in

$$\dot{\hat{P}}_d(t) = A\hat{P}_d(t) + Bu(t) + \hat{\sigma}(t) + \hat{\sigma}_b(t) \tag{6.6}$$

where $\hat{P}_d$ is the predicted downstream pressure, $\hat{\sigma}$ is the fast adaptation parameter, and $\hat{\sigma}_b$ is the memory term.

6.2.2 Adaptive Law

Using the techniques in Section 2.3 results in the piecewise constant adaptive law

$$\hat{\sigma}(iT) = -\left[\int_0^T \Phi(T-\tau)d\tau\right]^{-1} \Phi(T)\tilde{P}_d(iT) \tag{6.7}$$

where $\Phi(T) = e^{AT}$ and $\tilde{P}_d(t) = \hat{P}_d(t) - P_d(t)$. For the memorizing mechanism, we use a first-order filter which results in the update law

$$\hat{\sigma}_b(s) = \hat{\sigma}(s)\frac{\omega}{s} \tag{6.8}$$

where ω is the bandwidth of the memory term.

6.2.3 Control Law

Since the state of the AMS is a scalar, the implementation of (2.14) results in

$$u_1(t) = -\frac{A}{B}r(t) \tag{6.9}$$

where $r(t)$ is the desired reference pressure.

With the use of the memorizing mechanism, $u_2(t)$ must cancel the effects of $(\hat{\sigma}(t)+\hat{\sigma}_b(t))$. Since there are no unmatched uncertainties, this can be done directly by choosing the signal's opposite scaled by $1/B$. Additionally, we apply low-pass filter, $C(s)$, to $u_2(t)$. Then we have

$$u_2(t) = -C(s)\frac{1}{B}(\hat{\sigma}(t) + \hat{\sigma}_b(t)). \tag{6.10}$$

Since there are no unmatched uncertainties, the control signal is composed of only the components u_1 and u_2.

The final step of the control law design is to limit the control signal to an acceptable range for the actuator. Let $\bar{u}(t) = u_1(t)+u_2(t)$. With the actuator limits applied, the control

law is then

$$u(t) = \begin{cases} u_{max} & \text{if } \bar{u}(t) \geq u_{max} \\ u_{min} & \text{if } \bar{u}(t) \leq u_{min} \\ \bar{u}(t) & \text{otherwise} \end{cases} \tag{6.11}$$

6.3 PI Controller

The performance of the $\mathcal{L}_1$ controller will be compared to that of a PI controller as PI control is the industry standard for AMS. The PI controller is defined as

$$e(t) = r(t) - P_d(t) \tag{6.12}$$

$$\bar{u}(s) = K_p e(s) + \frac{K_i}{s} e(s) \tag{6.13}$$

where $e(t)$ is the tracking error, K_p is the proportional gain, and K_i is the integral gain. Additionally, (6.11) is applied to limit the torque motor current.

6.4 Simulation Results

The simulation is performed for the constant flow rate $W = 0.8314$ kg/s, constant temperature $T_u = 297.22$ K, and upstream pressure $P_u = 4.826 \times 10^5$ Pa. The valve diameter is $d = 0.1016$ m. Theses plant parameters result in the mapping from β to P_d shown in Figure 6.3. This results in $\beta_{min} = 0.7091$ rad.

The hysteresis loop width is 1.75×10^{-3} A. The input-output relation of the hysteresis model is shown in Figure 6.4 for an input of $u = 0.025 + 0.003\sin(t)$ A.

The valve parameters are $K_v = 27$ rad/A and $\tau = 1$ s. The limits on torque motor

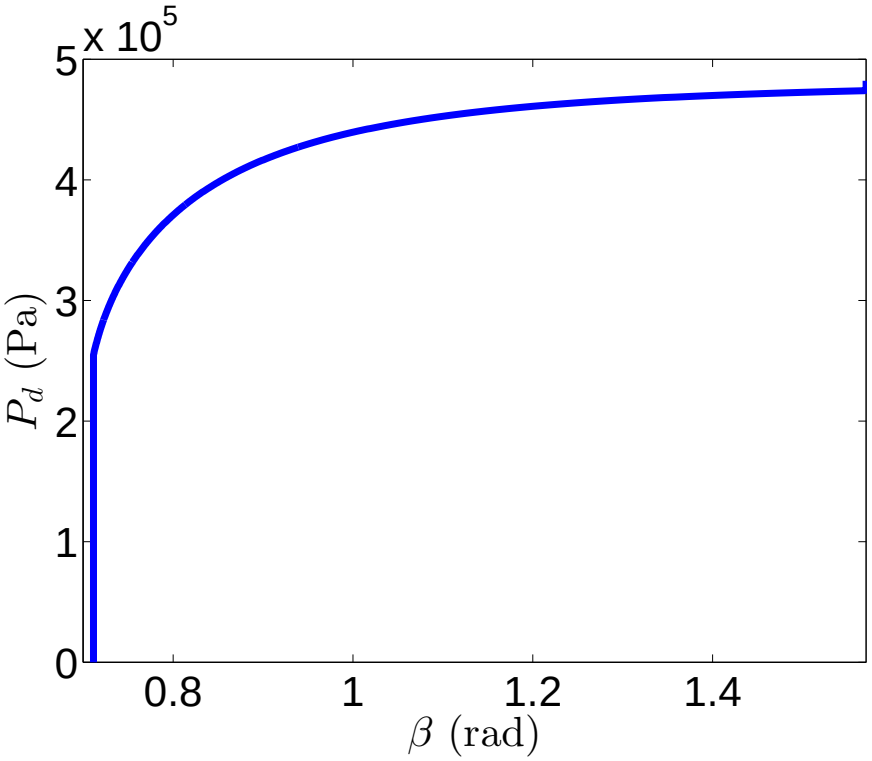

Figure 6.3: Mapping from β to P_d for $W = 0.8314$ kg/s, $T_u = 297.22$ K

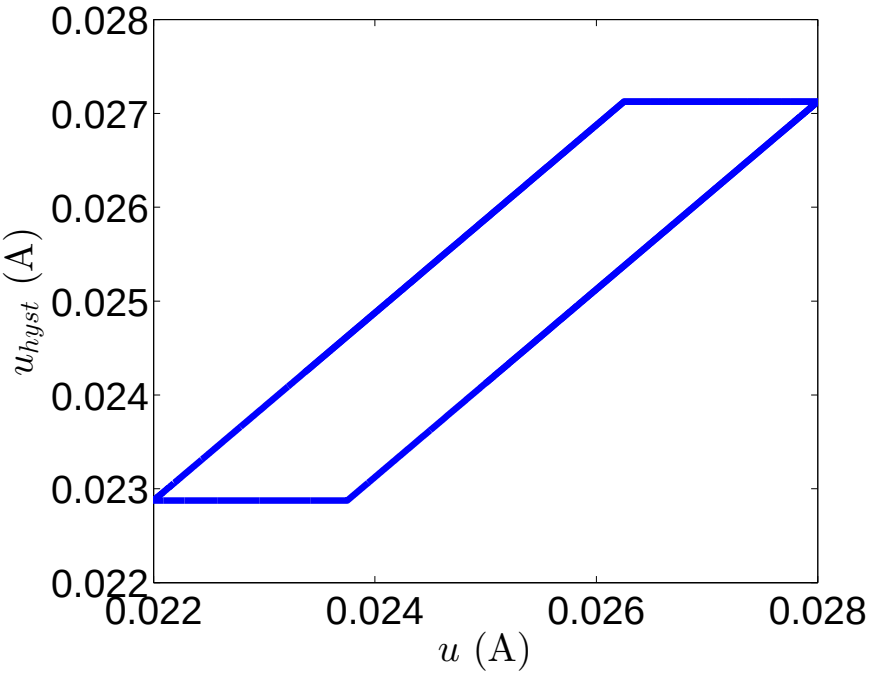

Figure 6.4: Hysteresis loop

current are $u_{min} = 0$, $u_{max} = 0.050$ A, and the valve is subject to a disturbance of

$$\bar{\sigma}(t) = 0.02 \sin(2t) \text{ A} \tag{6.14}$$

The reference pressure for the simulation case is $r = 3.103 \times 10^5$ Pa

6.4.1 $\mathcal{L}_1$ Adaptive Control

The $\mathcal{L}_1$ control parameters are $A = -7$ s^{-1}, $B = 6.894 \times 10^6$ Pa/(As), $T = 0.002$ s, $\omega = 1$ rad/s, and $C(s) = \frac{512}{s+512}$. The $\mathcal{L}_1$ simulation results are shown in Figure 6.5. Figure 6.5a shows the reference pressure tracking performance. Figure 6.5b shows the control input generated by the controller as well as the input to the valve transfer function which is affected by hysteresis. Figure 6.5c shows the time-history of the valve angle. The $\mathcal{L}_1$ controller is able to track the desired pressure and attenuate the effects of the disturbance, $\bar{\sigma}$. Furthermore, the valve's motion is smooth and not oscillatory.

6.4.2 PI Control

The PI control parameters are $K_p = 1$ A/Pa and $K_i = 1$ C/Pa. Simulation results for the AMS under PI control are shown in Figure 6.6. Reference pressure tracking is shown in Figure 6.6a. The control input along with the hysteretic valve input is shown in Figure 6.5b, and the valve angle time-history is shown in Figure 6.6c. The PI controller is able to track the reference pressure, however the response contains high-frequency oscillations that are propagated through as a result of hysteresis in the input. Furthermore, the disturbance, $\bar{\sigma}$ is not well attenuated as in the $\mathcal{L}_1$ case. In Figure 6.6b, we see that the control input is constantly bouncing between the limits u_{min} and u_{max}. Additionally, the valve motion under PI control consists of high-frequency chatter, which shortens the lifespan of the component.

Remark 6.1. *The example of this chapter shows the benefit of $\mathcal{L}_1$ control in systems with highly nonlinear dynamics. Linear controllers are not able to mitigate the effects of nonlin-*

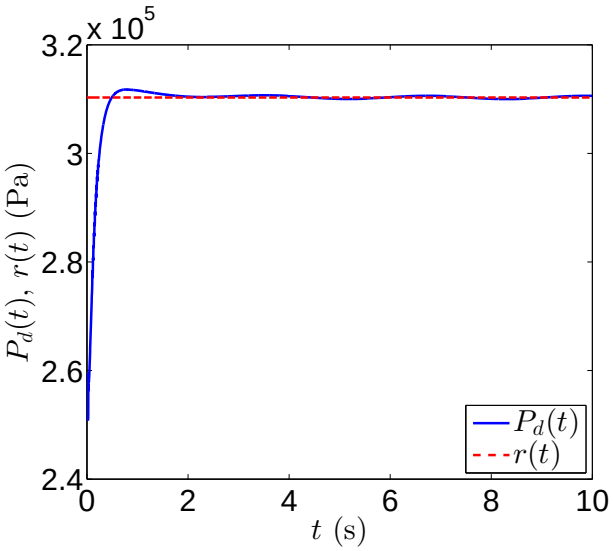

(a) Tracking performance

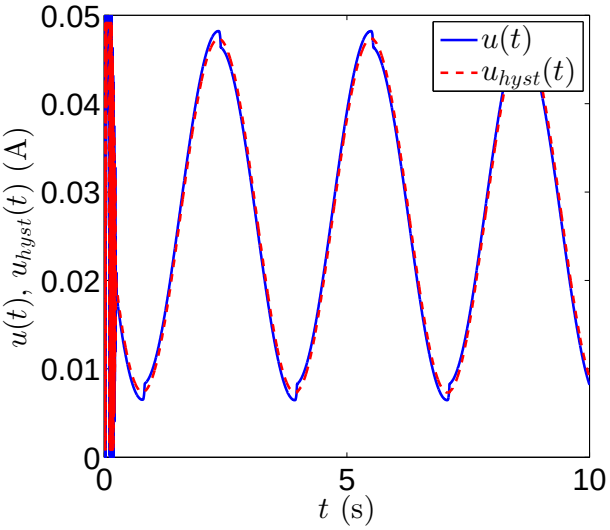

(b) Control input with hysteresis

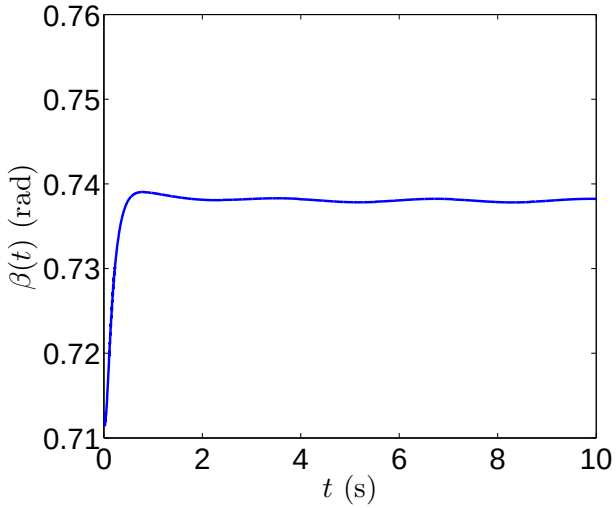

(c) Valve angle

Figure 6.5: Simulation results using $\mathcal{L}_1$ adaptive controller

earities such as hysteresis and the mapping from valve angle to downstream pressure. This quality also means that adaptive control can increase the life of parts in mechanical systems by attenuating nonlinear dynamics which would otherwise cause high loads on actuators.

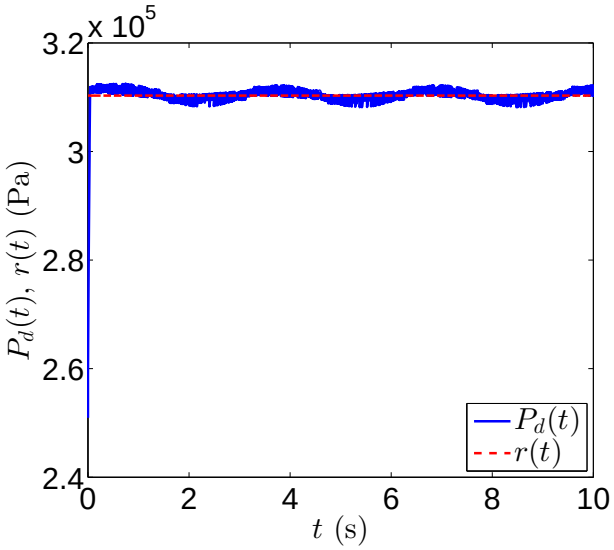

(a) Tracking performance

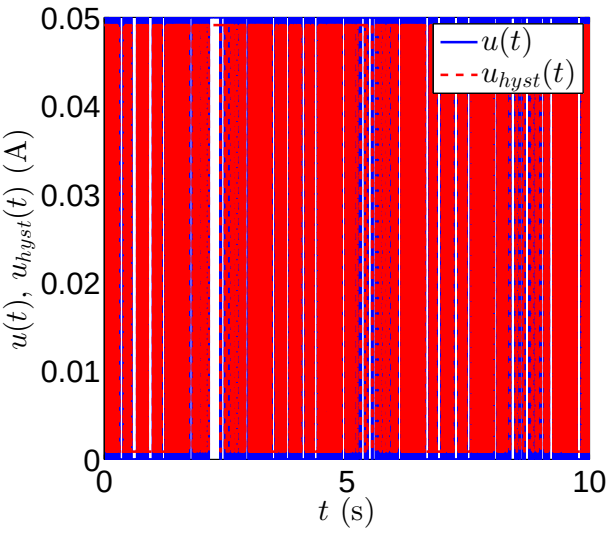

(b) Control input with hysteresis

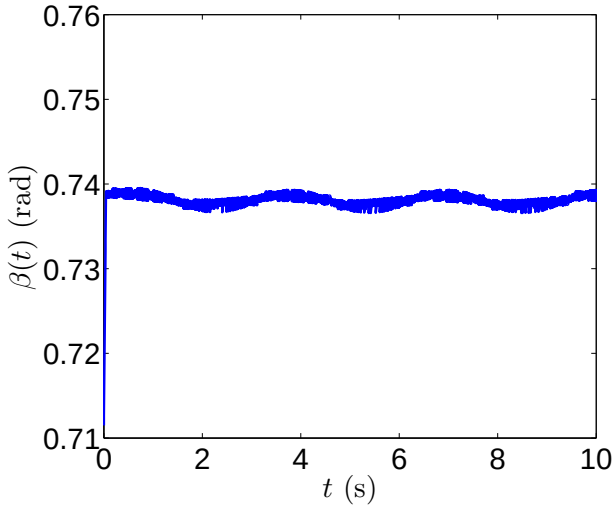

(c) Valve angle

Figure 6.6: Simulation results using PI controller

Chapter 7

Case Study II: Satellite Orbit Stabilization

This chapter develops an $\mathcal{L}_1$ adaptive control algorithm for the orbit stabilization of a man-made Earth-orbiting satellite. There are several potential sources of model uncertainties and unknown disturbances which man-made satellites are subject to. Disturbance forces on satellite dynamics are both internal and external to the system. External disturbances arise from phenomena such as variations in the Earth's gravitational and magnetic fields, aerodynamic drag, or solar radiation pressure. Internal disturbances can come from objects inside the satellite such as payload or propellant shifting around or from effects of the satellite's structural mechanics. All of these examples are difficult to directly measure. Thus, it is advantageous to enlist estimation schemes such as fast adaptation to cancel the effects of disturbances and unmodeled dynamics.

Both passive and active methods are used for satellite actuators. These devices are used to stabilize the satellite's orbit and achieve trajectory tracking goals. Passive methods make use of the environmental forces like gravity, Earth's magnetic field, drag, and the solar radiation pressure. Alternatively, active actuators include micro-thrusters, reaction wheels, and momentum gyros. In this chapter, we will consider a satellite with the capability of

generating a thrust vector in whatever direction is necessary for stabilizing the desired orbit.

Throughout the chapter, we will present the Kepler orbit model for satellite dynamics, develop the $\mathcal{L}_1$ adaptive controller for a micro-thruster satellite, and show simulation results. The simulation results for the $\mathcal{L}_1$ controller will be compared to a proportional-derivative (PD) controller.

7.1 Satellite Dynamics

We will adapt the satellite dynamic model found in [16]. Let the reference coordinate system be defined in an inertial frame with an origin at the center of Earth. The x-axis points toward the vernal equinox, the intersection of Earth's equatorial plane and the orbital plane in which the earth orbits the sun. The z-axis points toward Earth's north pole, and the right-hand rule defines the y-axis in a direction orthogonal to the other two axes. Assume that Earth is spherical and uniform. The satellite's position in the earth-centered inertial coordinates satisfies the equation of motion,

$$\ddot{\vec{r}}(t) = -\frac{\mu}{r^3(t)}\vec{r}(t) + f(t) + u(t) \tag{7.1}$$

where $\vec{r} \in \mathbb{R}^3$ is the satellite's position vector, $\mu \triangleq 398,600 km^3/s$ is Earth's gravitational parameter, $r \triangleq ||\vec{r}||$ is the distance between the satellite and the center of the earth, $f \in \mathbb{R}^3$ is the disturbance force acting on the satellite, and $u \in \mathbb{R}^3$ is the satellite's thrust. The radial component of the satellite's velocity is given by

$$v_r \triangleq \frac{\vec{v} \cdot \vec{r}}{r} \tag{7.2}$$

where $\vec{v} \in \mathbb{R}^3$ is the velocity vector. The satellite's specific angular momentum is given by

$$\vec{h} = \vec{r} \times \vec{v} \tag{7.3}$$

The orbit's inclination is given by

$$i \triangleq \cos^{-1}\left(\frac{h_z}{h}\right) \tag{7.4}$$

where h_z is the z-component of the angular momentum. The eccentricity is

$$\vec{e} \triangleq \frac{1}{\mu}\left[\left(v^2 - \frac{\mu}{r}\right)\vec{r} - rv_r\vec{v}\right]. \tag{7.5}$$

where $v \triangleq ||\vec{v}||$. Let $\vec{n} \in \mathbb{R}^3$ be the unit vector pointing towards the ascending node of the orbit. Then the longitude of the ascending node is given by

$$\Omega \triangleq \begin{cases} \cos^{-1}(n_x) & n_y \geq 0 \\ 2\pi - \cos^{-1}(n_x) & n_y < 0 \end{cases}, \tag{7.6}$$

where n_x and n_y are the x and y-components respectively of $\vec{n}$. and the argument of perigee is given by

$$\omega \triangleq \begin{cases} \cos^{-1}\left(\frac{\vec{n}\cdot\vec{e}}{e}\right) & e_z > 0 \\ 2\pi - \cos^{-1}\left(\frac{\vec{n}\cdot\vec{e}}{e}\right) & e_z < 0 \end{cases}, \tag{7.7}$$

where $e = ||\vec{e}||$ and e_z is the z-component of $\vec{e}$. For equatorial orbits, $\omega = \cos^{-1}\left(\frac{e_x}{e}\right)$. The true anomaly is given by

$$\nu \triangleq \begin{cases} \cos^{-1}\left(\frac{\vec{e}\cdot\vec{r}}{er}\right) & v_r > 0 \\ 2\pi - \cos^{-1}\left(\frac{\vec{e}\cdot\vec{r}}{er}\right) & v_r < 0 \end{cases}, \tag{7.8}$$

with the convention that $\nu = \cos^{-1}\left(\frac{r_x}{r}\right)$ for a circular orbit. The eccentric anomaly is given by

$$E = \cos^{-1}\left(\frac{1 - r/a}{e}\right), \tag{7.9}$$

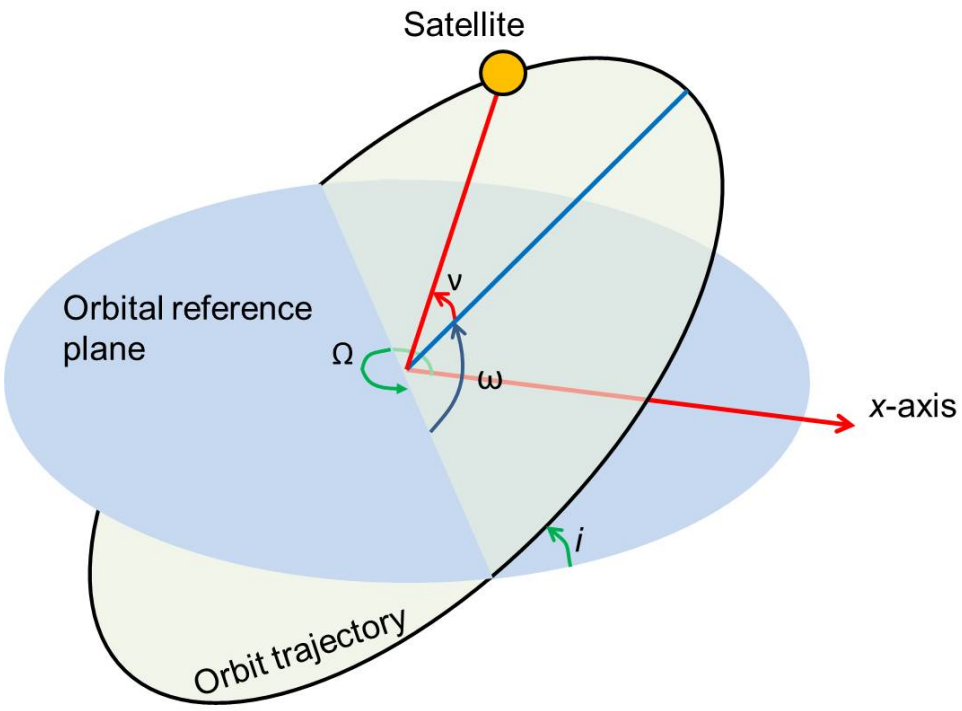

Figure 7.1: Satellite orbital plane

where a is the orbit's major axis given by

$$a = \frac{1}{\frac{2}{r} - \frac{v^2}{\mu}} \tag{7.10}$$

The mean anomaly is given by

$$M = E - e \sin E \tag{7.11}$$

Finally, the orbital period is given by

$$T = 2\pi \sqrt{\frac{a^3}{\mu}} \tag{7.12}$$

Note that the satellite position is fully defined by the parameter set $\{i, \Omega, \omega, T, e, \nu\}$. The angles $\{i, \Omega, \omega\}$ transform the inertial frame to the orbital frame while T and e define the size and shape of the orbit. Finally, ν defines the satellite's position along the orbit. Figure 7.1 shows a visualization of the angles that define the orbital plane and the satellite's position.

7.2 Application of $\mathcal{L}_1$ Adaptive Control

To apply $\mathcal{L}_1$ control to satellite orbit stabilization, we will create three control loops - one for each Cartesian coordinate. The control objective is for the satellite to track a reference trajectory defined by an idealized orbit,

$$\ddot{\vec{r}}_{ref}(t) = -\frac{\mu}{r_{ref}^3(t)}\vec{r}_{ref}(t) \tag{7.13}$$

where $\vec{r}_{ref}$ is the reference trajectory and $r_{ref} = ||\vec{r}_{ref}||$. The reference orbit's orientation and shaped are given by the eccentricity magnitude, e_{ref}, major axis, a_{ref}, longitude of the ascending node, Ω_{ref}, inclination, i_{ref}, argument of perigee, and ω_{ref}. The state predictor, adaptive law, and control law are designed as follows.

7.2.1 State Predictor

Let the state predictor be

$$\begin{aligned} \dot{\hat{X}}_i(t) &= A_i\hat{X}_i(t) + B_i u_i(t) + \hat{\sigma}_i(t) \\ \hat{Y}_i(t) &= C_i\hat{X}_i(t) \end{aligned} \tag{7.14}$$

where $i = 1, 2, 3$. The predicted states are

$$\hat{X}_1 = \begin{bmatrix} \hat{r}_x \\ \dot{\hat{r}}_x \end{bmatrix}, \quad \hat{X}_2 = \begin{bmatrix} \hat{r}_y \\ \dot{\hat{r}}_y \end{bmatrix}, \quad \hat{X}_3 = \begin{bmatrix} \hat{r}_z \\ \dot{\hat{r}}_z \end{bmatrix} \tag{7.15}$$

where $\begin{bmatrix} \hat{r}_x & \hat{r}_y & \hat{r}_z \end{bmatrix}^\top$ is the prediction of $\vec{r}$, and the predicted outputs are

$$\hat{Y}_1 = \hat{r}_x, \quad \hat{Y}_2 = \hat{r}_y, \quad \hat{Y}_3 = \hat{r}_z \tag{7.16}$$

The control inputs are

$$u_1 = u_x, \quad u_2 = u_y, \quad u_3 = u_z \tag{7.17}$$

From (7.1), we see that the real system dynamics are nonlinear due to r^3 in the denominator. Therefore, the state matrices, $A_i \in \mathbb{R}^{2\times 2}$ are parameters to be tuned. The input matrices are $B_i = \begin{bmatrix} 0 & 1 \end{bmatrix}^\top$ and the output matrices are $C_i = \begin{bmatrix} 1 & 0 \end{bmatrix}$. Finally, by comparing (7.1) to (7.14), we see that $\begin{bmatrix} \hat{\sigma}_{1_2} & \hat{\sigma}_{2_2} & \hat{\sigma}_{3_2} \end{bmatrix}^\top$ is an adaptive estimate of the unknown disturbance forces acting on the satellite.

7.2.2 Adaptive Law

Let

$$X_1 = \begin{bmatrix} r_x \\ \dot{r}_x \end{bmatrix}, \quad X_2 = \begin{bmatrix} r_y \\ \dot{r}_y \end{bmatrix}, \quad X_3 = \begin{bmatrix} r_z \\ \dot{r}_z \end{bmatrix}. \tag{7.18}$$

Then we can define the prediction error as $\tilde{X}_i = \hat{X}_i - X_i$. Then we can directly apply the adaptive law from Section 2.3 according to

$$\begin{aligned} \Phi_i(T) &= e^{A_i T} \\ \Gamma_i(T) &= -\left[\int_0^T \Phi_i(T-\tau)\, d\tau\right]^{-1} \Phi_i(T) \\ \hat{\sigma}_i(jT) &= \Gamma_i(T)\tilde{X}_i(jT) \end{aligned} \tag{7.19}$$

where j is the number of elapsed time-steps.

7.2.3 Control Law

Note that the matched and unmatched components of the uncertainty estimates, $\hat{\sigma}_i$ are their second and first elements, $\hat{\sigma}_{i_2}$ and $\hat{\sigma}_{i_1}$ respectively. Then we can apply the control law from Section 2.4 as

$$\bar{u}_i(t) = K_g r_{ref_i}(t) - C_{i_1}(s)\hat{\sigma}_{i_2} - C_{i_2}(s)\frac{C_i(sI - A_i^{-1})\begin{bmatrix} -1 & 0 \end{bmatrix}^\top}{C_i(sI - A_i^{-1})B_i} \tag{7.20}$$

where $\bar{u}$ is a control signal generated by the $\mathcal{L}_1$ controller and not subject to the physical actuator limits of the satellite thrusters, $C_{i_1}(s)$ and $C_{i_2}(s)$ are the low-pass filters used to recover robustness in the presence of the high-gain feedback adaptive law. Of course, the control input must be limited to remain within the range of thrust achievable by the satellite thrusters. This is done as follows

$$u(t) = \begin{cases} u_{max}\frac{\bar{u}(t)}{||\bar{u}(t)||} & \text{if } ||\bar{u}(t)|| \geq u_{max} \\ \bar{u}(t) & \text{otherwise} \end{cases} \tag{7.21}$$

where $u_{max} \in \mathbb{R}$ is the maximum thrust magnitude of the satellite. (7.21) preserves the direction of the three-dimensional thrust vector, $u = \begin{bmatrix} u_x & u_y & u_z \end{bmatrix}^\top$, while limiting its magnitude to remain less than or equal to u_{max}.

7.3 PD Controller

The performance of the $\mathcal{L}_1$ controller will be compared to that of a PD controller. The PD controller is defined as

$$e_i(t) = r_{ref_i}(t) - Y_i(t) \tag{7.22}$$

$$\bar{u}_i(s) = K_p e_i(s) + s K_d e_i(s) \tag{7.23}$$

where $e_i(t)$ is the tracking error for control loop i, $Y_i(t) = C_i X_i(t)$ is the output for control loop i, K_p is the proportional gain, and K_d is the derivative gain. The PD control input is also limited to remain within the actuator limits according to (7.21)

7.4 Simulation Results

In this section, simulation results are presented for a satellite first with no disturbances and then in the presence of unknown, nonlinear disturbance forces. The control performance of the $\mathcal{L}_1$ controller is compared to that of the PD controller.

For each of the simulation scenarios, we will consider a circular, sun-synchronus reference orbit. In a sun-synchronus orbit, the shadows cast by features on the Earth's surface do not change from the satellite's perspective. Sun-synchronus orbits have applications in reconnaissance and weather-based missions [21]. The reference orbit parameters are

$$e_{ref} = 0, \quad a_{ref} = 35,000 \text{ km}, \quad \Omega_{ref} = 0, \quad i_{ref} = \pi/6, \quad \omega_{ref} = \pi/8 \tag{7.24}$$

The initial conditions for the reference orbit trajectory are

$$\nu_{ref_0} = \pi/8 \tag{7.25}$$

$$\vec{r}_{ref_0} = \begin{bmatrix} 24,749 & 0 & 24,749 \end{bmatrix}^\top \text{ km}$$

$$\vec{v}_{ref_0} = \begin{bmatrix} -1.1931 & 2.9226 & 1.1931 \end{bmatrix}^\top \text{ km/s} \tag{7.26}$$

In each case, the controlled satellite's initial orbit is defined by

$$e_0 = 0, \quad a_0 = 34,300 \text{ km}, \quad \Omega_0 = 0, \quad i_0 = \pi/6, \quad \omega_0 = 0.3927 \tag{7.27}$$

with the initial conditions

$$\begin{aligned} \nu_{ref_0} &= \pi/8 \qquad (7.28) \\ \vec{r}_{ref_0} &= \begin{bmatrix} 24,254 & 0 & 24,254 \end{bmatrix}^\top \text{ km} \\ \vec{v}_{ref_0} &= \begin{bmatrix} -1.1931 & 2.9226 & 1.1931 \end{bmatrix}^\top \text{ km/s} \qquad (7.29) \end{aligned}$$

The $\mathcal{L}_1$ controller parameters are

$$A_i = \begin{bmatrix} 0 & 1 \\ -1 & -100 \end{bmatrix}, \quad C_{i_1}(s) = C_{i_2}(s) = \frac{0.05}{s + 0.05}, \quad T = 0.01 \text{ s}, \quad \forall i \tag{7.30}$$

The PD controller parameters are

$$K_p = 2 \text{ s}^{-2}, \quad K_d = 2 \text{ s}^{-1} \tag{7.31}$$

7.4.1 Example 1: No Disturbance

The first simulation case considers the dynamics in (7.1) with $f(t) = \begin{bmatrix} 0 & 0 & 0 \end{bmatrix}^\top$.

Figure 7.2 shows the orbital trajectory of the satellite with the $\mathcal{L}_1$ controller. Figure 7.3 shows the time-history of the magnitude of the position vector, r, along with the magnitude of the reference position vector, r_{ref}. Note that since the reference orbit is circular, r_{ref} is constant. Because of this, we can view Figure 7.3 as a step response plot.

Figure 7.4 shows the orbital trajectory of the satellite with the PD controller. Figure 7.5 shows the time-history of the magnitude of the position vector, r, along with the magnitude

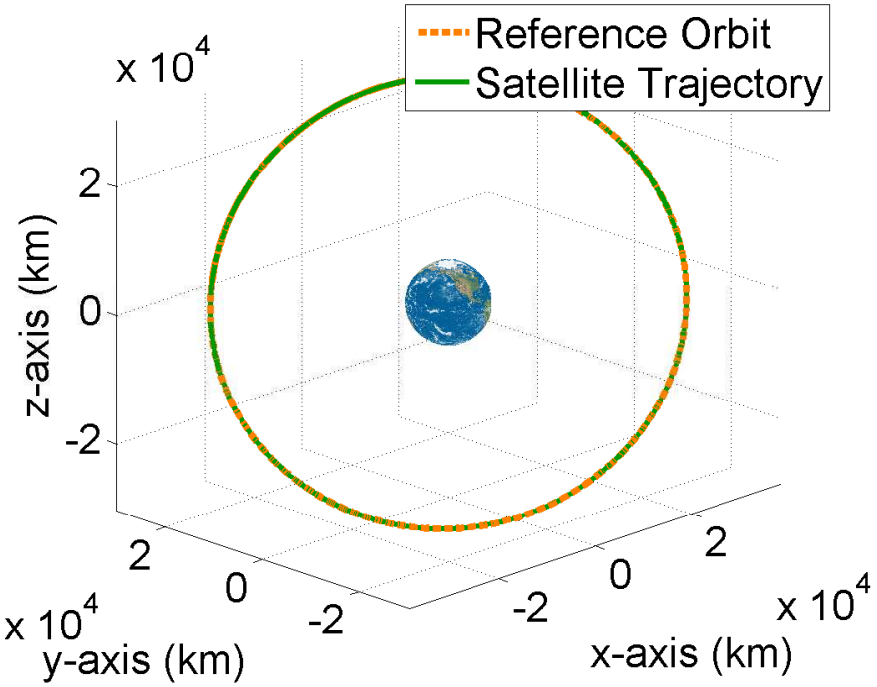

Figure 7.2: Orbital trajectory for satellite under $\mathcal{L}_1$ control with no disturbances

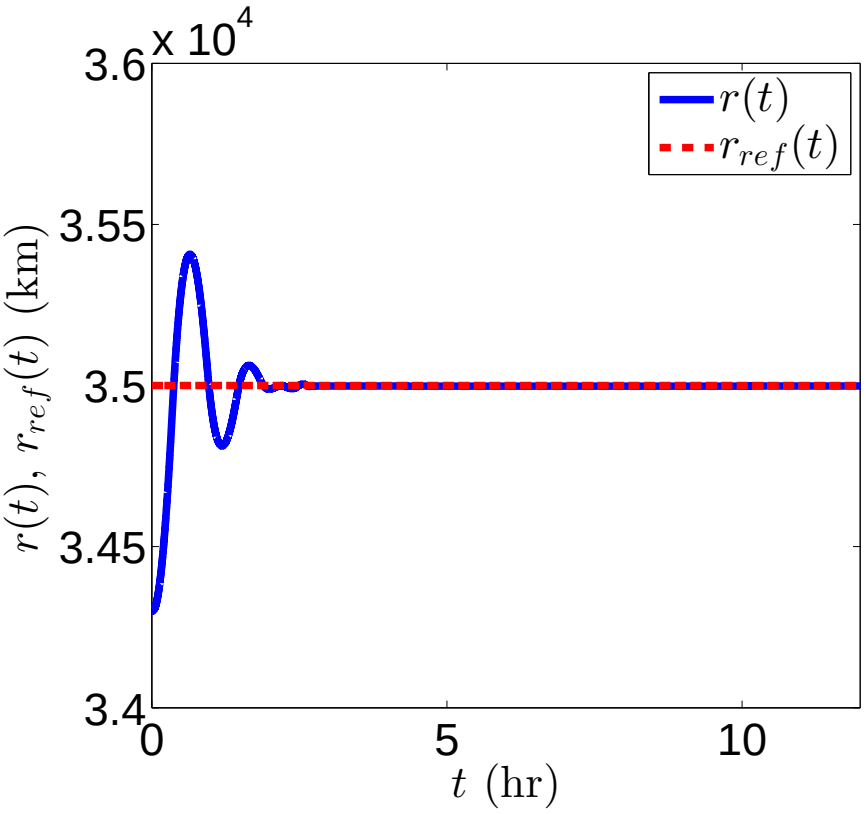

Figure 7.3: Time-history of satellite and reference trajectory distance to center of Earth under $\mathcal{L}_1$ control with no disturbances

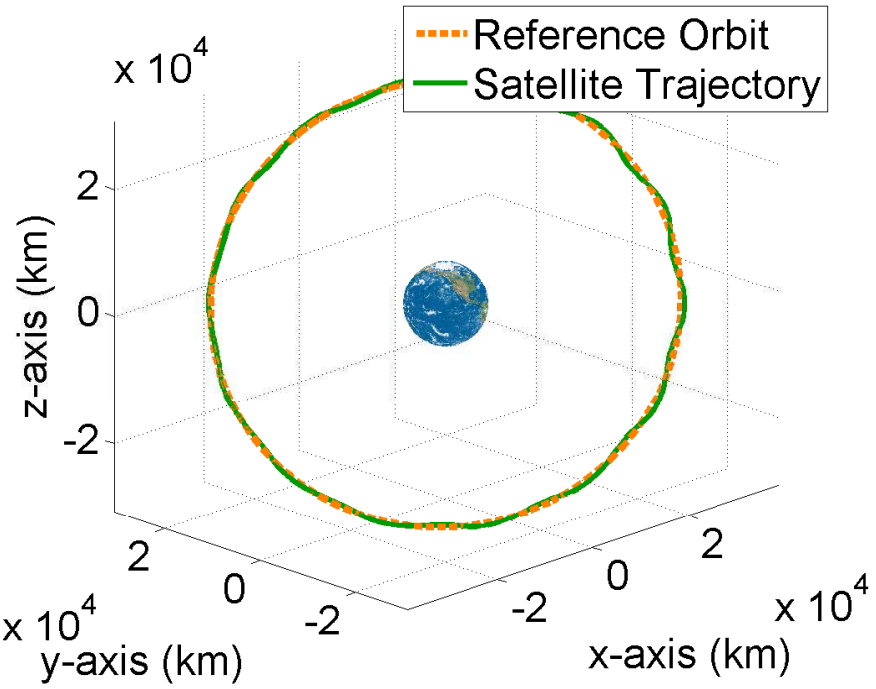

Figure 7.4: Orbital trajectory for satellite under PD control with no disturbances

of the reference position vector, r_{ref}.

Although the PD controller stabilizes the orbit, the response is quite oscillatory. The $\mathcal{L}_1$ controller holds the desired trajectory much more closely.

7.4.2 Example 2: Rejection of Unknown Disturbance Forces

Now the same simulation is performed with the disturbance force

$$f(t) = \begin{bmatrix} 10^{-4}\sin(t) + 5 \times 10^{-4} \\ 5 \times 10^{-4} \\ 3 \times 10^{-4}\sin(2t) \end{bmatrix} \text{N/kg} \tag{7.32}$$

Figure 7.6 shows the orbital trajectory of the satellite with the $\mathcal{L}_1$ controller, and figure 7.7 shows the time-history of the magnitude of the position vector, r, along with the magnitude of the reference position vector, r_{ref}.

Figure 7.8 shows the orbital trajectory of the satellite with the PD controller, and fig-

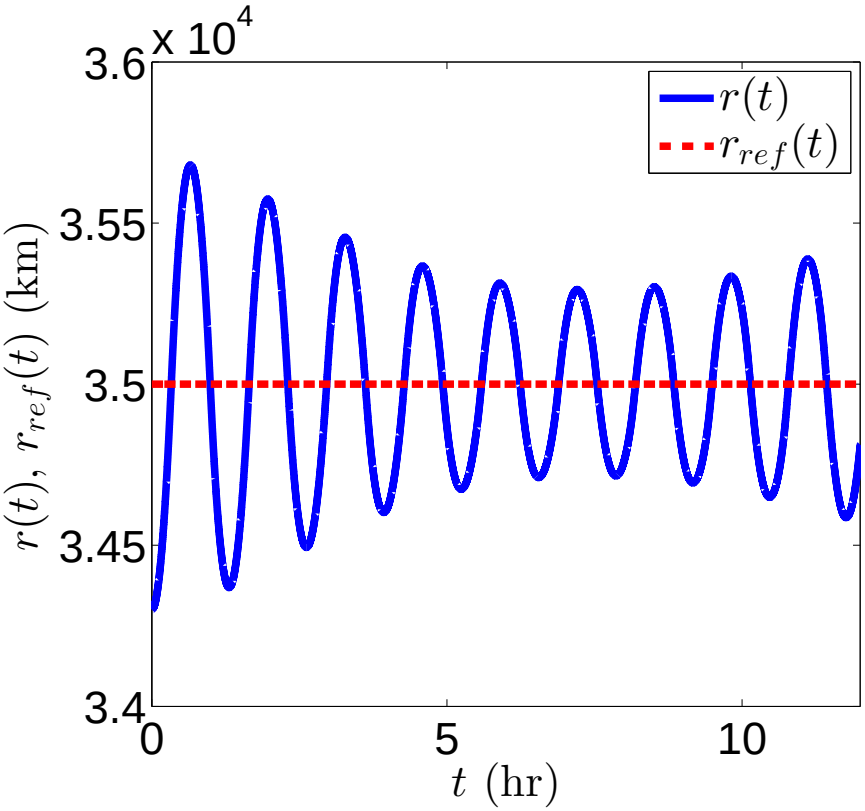

Figure 7.5: Time-history of satellite and reference trajectory distance to center of Earth under PD control with no disturbances

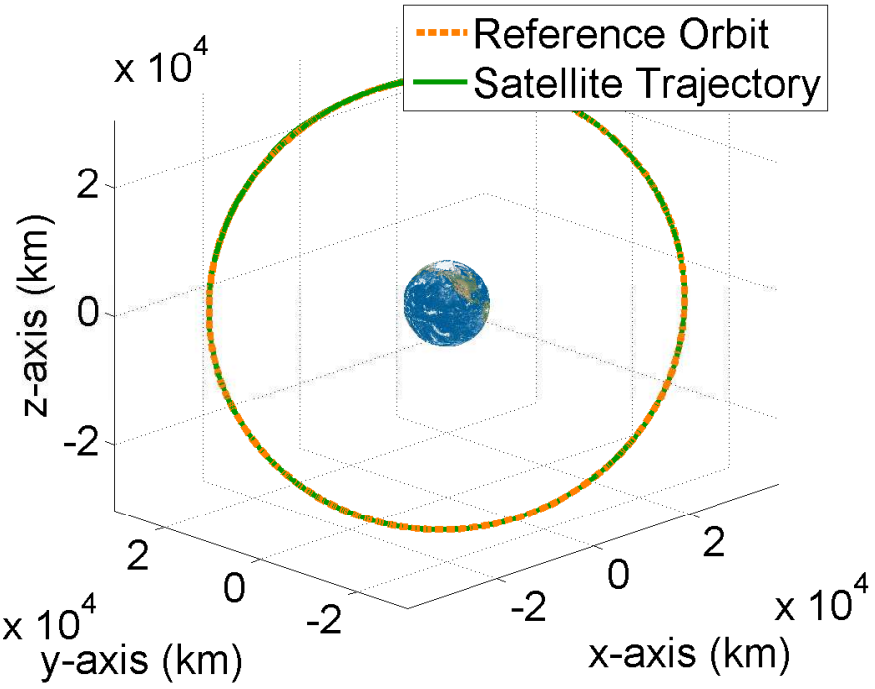

Figure 7.6: Orbital trajectory for satellite under $\mathcal{L}_1$ control with disturbance

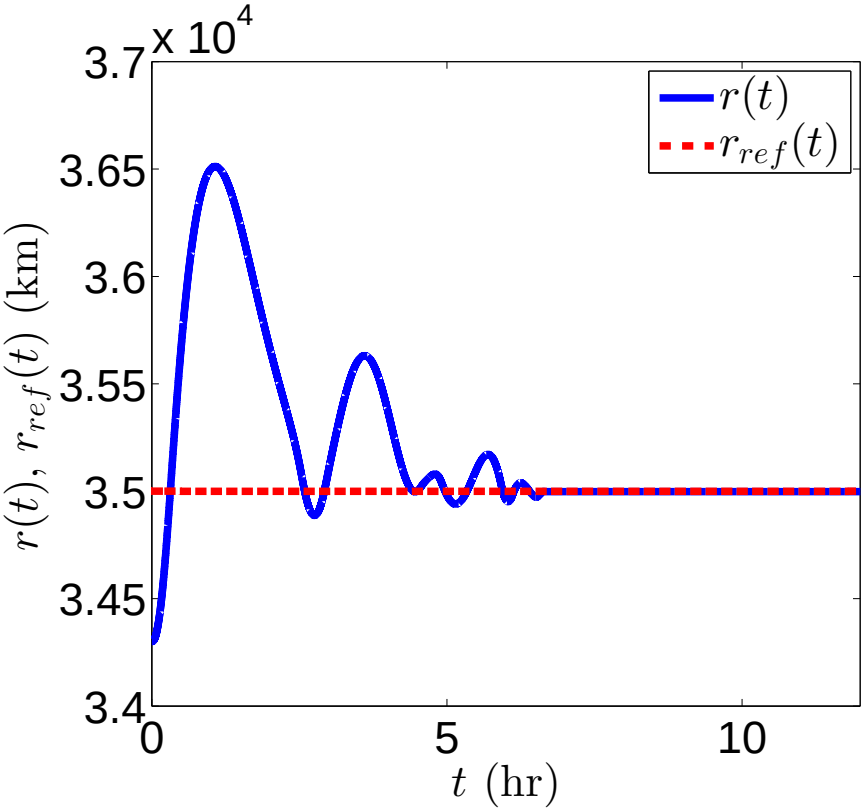

Figure 7.7: Time-history of satellite and reference trajectory distance to center of Earth under $\mathcal{L}_1$ control with disturbance

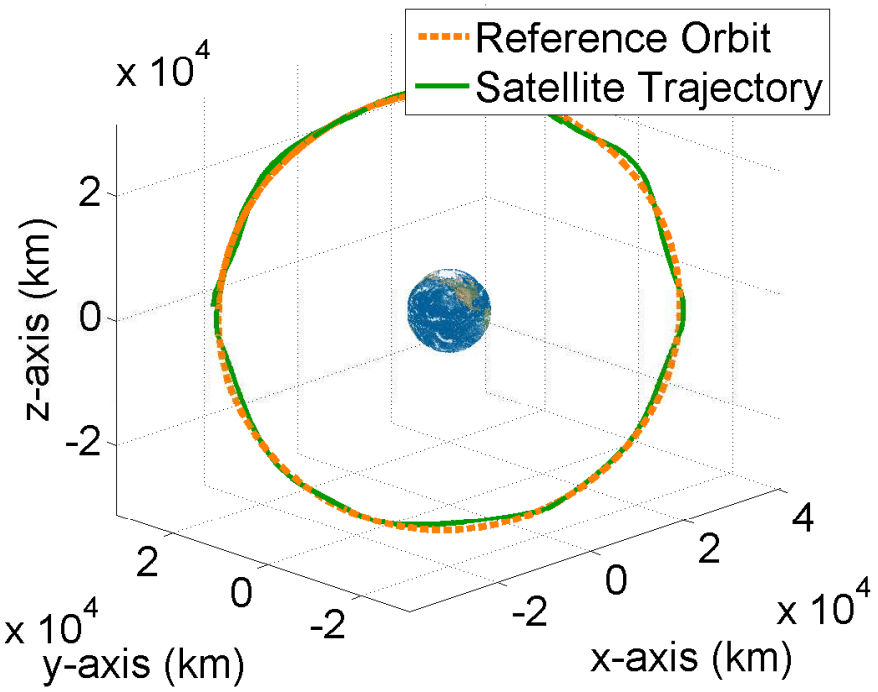

Figure 7.8: Orbital trajectory for satellite under PD control with disturbance

ure 7.9 shows the time-history of the magnitude of the position vector, r, along with the magnitude of the reference position vector, r_{ref}.

In this case, the PD controller is not able to reject the disturbance force while the $\mathcal{L}_1$ controller rejects it after the initial transient and successfully stabilizes the orbit.

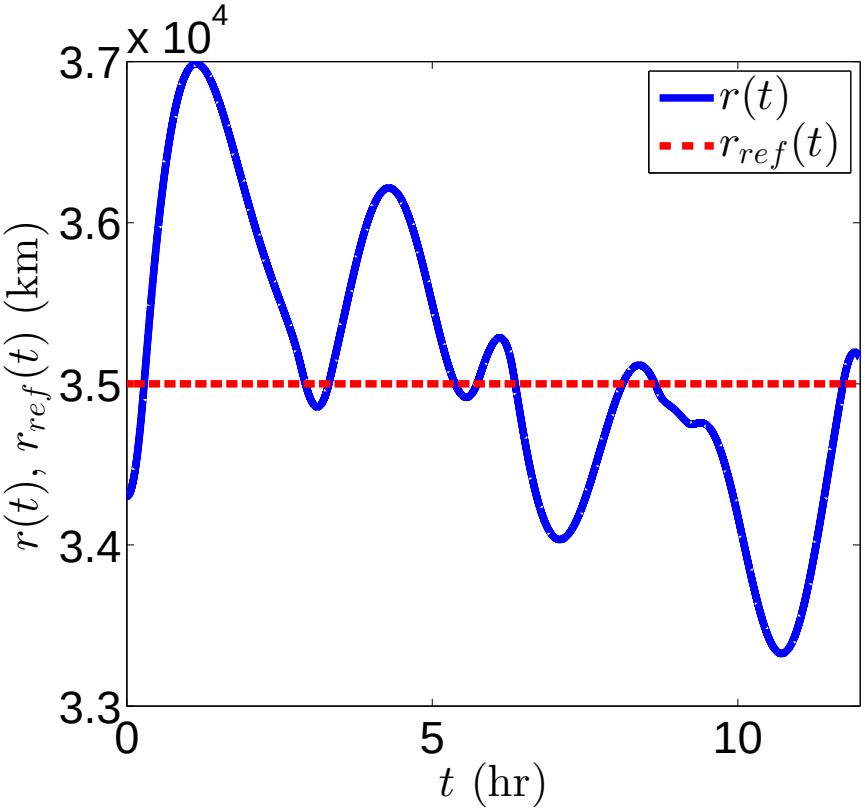

Figure 7.9: Time-history of satellite and reference trajectory distance to center of Earth under PD control with disturbance

Chapter 8

Conclusions and Future Work

To summarize the dissertation thus far, Chapter 1 provided an overview of the history of control theory research while Chapter 2 presented the $\mathcal{L}_1$ adaptive control architecture. A simulation example in Chapter 2 provided evidence for the dependence of $\mathcal{L}_1$ control performance on the controller's sampling rate. Two unique methods for improving performance at slow sampling rates were developed and analyzed: the artificial neural network adaptive law in Chapter 3 and the memorizing mechanism in Chapter 4. The closed-loop stability conditions were derived and proven to exist for both of these methods, and simulation examples were provided which showed a performance improvement over the traditional $\mathcal{L}_1$ controller at slow sampling rates. Chapter 5 presented a performance-seeking controller based on the $\mathcal{L}_1$ architecture. Simulation results were presented where the controller found an optimal control input to minimize the performance function. Additionally, the memorizing mechanism was applied to the performance-seeking controller to preserve the results at a slower sampling rate. Next, two case studies were presented. Chapter 6 developed $\mathcal{L}_1$ control for pressure regulation in an aircraft air management system. The system dynamics contained nonlinearities and hysteresis due to friction in the control valve. The $\mathcal{L}_1$ controller exhibited improved performance over a proportional-integral controller. In Chapter 7, the $\mathcal{L}_1$ architecture was applied to satellite orbit stabilization. The controller was able to track the desired

trajectory much more closely than a proportional-derivative controller which was unable to reject disturbance forces.

This dissertation has provided two effective solutions to a previously unsolved issue in fast adaptation-based control algorithms. Until now, sampling rate has been a limiting factor in the application of such controllers to real-world systems. With the artificial neural network adaptive law or memorizing mechanism, this barrier can now be overcome. Furthermore, a novel method for online optimization of a performance function provides a new way to recover performance in systems that are degraded as a result of age. These effects are not easily measured, thus an adaptive method such as the one within this dissertation is desirable. Lastly, the two case studies in this dissertation extend the range of systems to which fast adaptation-based algorithms have been applied.

Some of the methods in this dissertation have been the subject of industry-sponsored investigations. Adaptive control for aircraft air management systems was studied in conjunction with United Technologies Aerospace Systems. The algorithms were applied to a high fidelity air management system simulation and to a physical test rig with flowing air. Performance-seeking control was developed with impetus from Pratt & Whitney for the application of aircraft jet engines. The performance-seeking controller was exercised on a high-fidelity jet engine model developed by NASA Glenn Research Center [1].

8.1 Future Developments

One future theoretical development in $\mathcal{L}_1$ adaptive control is a method for online adaptation of the bandwidth of the low-pass filters in the control law. The filter bandwidths currently must be tuned on a case-by-case basis to handle disturbances of various frequencies. When the bandwidth is decreased, the response becomes slower and the ability to handle high-frequency disturbances decreases. When the bandwidth is increased, the ability to track a reference trajectory is increased, but the system time-delay margin is decreased. An online

bandwidth adaptation scheme would allow for increased performance when the disturbance frequency is high, and increased robustness when the disturbance frequency is low. Furthermore, such a scheme eliminates the filter bandwidth as a tuning parameter, and provides a more systematic method for designing an $\mathcal{L}_1$ controller.

Shape memory alloys (SMAs) are a type of metal that has a shape dependent on temperature and thermal stress [22]. These materials are of interest for engineering applications due to their ability to undergo plastic strains yet recover their initial shape when subject to the appropriate loading and temperature. Applications include energy absorption, sensing, and actuation. The shape change occurs as a result of a two-phase transformation in the metal's crystalline structure. This is a thermodynamically irreversible process, and thus results in temperature hysteresis. The hysteretic behavior of SMAs makes control difficult, however $\mathcal{L}_1$ adaptive control is capable of handling such nonlinearities as shown in Chapter 6. There has recently been interest in applying $\mathcal{L}_1$ control to SMA actuators which are desirable for their high power to mass ratio, easy maintainability, high reliability, and silent actuation. Fast adaptation is a prime candidate to deal with the untoward effects of hysteresis and other unmodeled dynamics.

Following the successful flight of $\mathcal{L}_1$ adaptive control as a flight control system for NASA's AirSTAR test vehicle [30] , shown in Figure 8.1, there is momentum in the idea of using $\mathcal{L}_1$ control for unmanned aerial vehicles (UAVs). $\mathcal{L}_1$ control is currently being studied as the flight control system for NASA's GL-10 aircraft [69, 29], shown in Figure 8.2. This is a vertical takeoff and land (VTOL), tilt-wing UAV with distributed electric propulsion. Figure 8.3 shows how the vehicle's wing tilts to transition from hover or takeoff mode to forward flight or cruise mode. The modes are vastly different, indicating a need for adaptive control.

$\mathcal{L}_1$ adaptive control was first applied to multi-agent systems in [47] and [48], and this concept was extended in [46]. A recent research effort by NASA Langley Research Center and the National Institute of Aerospace is investigating reconfigurable linked aircraft systems. This entails a group of small UAVs that physically connect to each other during flight with

Figure 8.1: NASA AirSTAR test vehicle

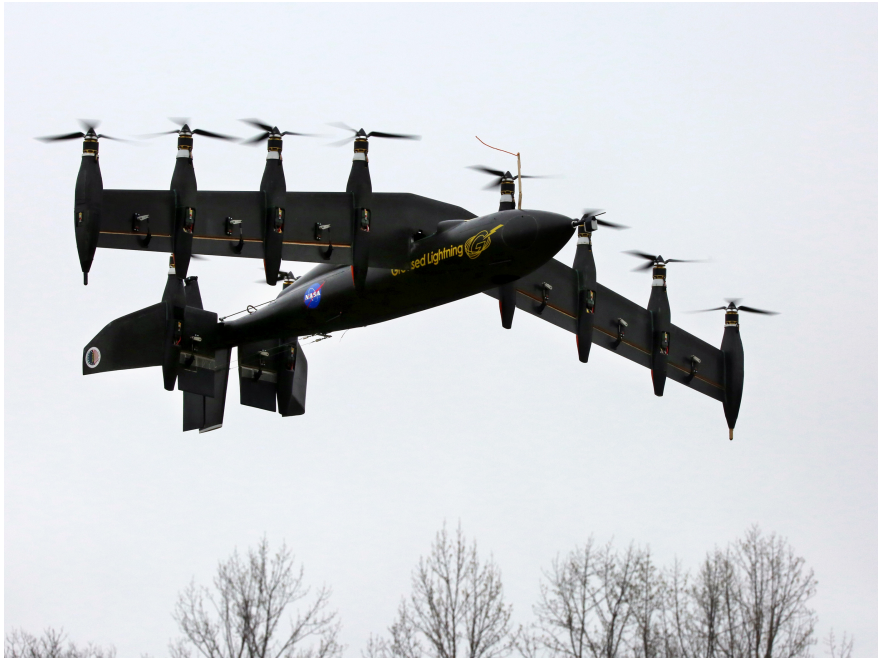

Figure 8.2: NASA GL-10 aircraft

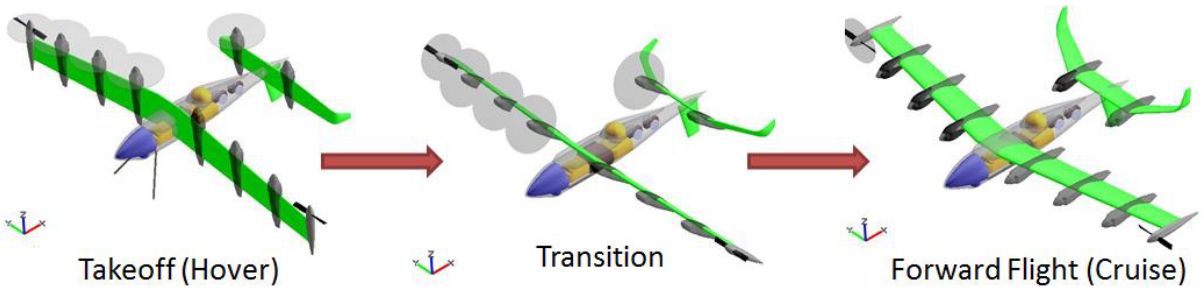

Figure 8.3: NASA GL-10 transition from hover to forward flight

Figure 8.4: Multi-modal linked aircraft system

the ability to reconfigure and complete a wide range of multi-modal missions. An example of such a system is shown in Figure 8.4. Here, a system of three fixed wing vehicles are flying with docked wingtips to increase aerodynamic efficiency. Such a system could make use of adaptive cooperative control as this is a time-varying multi-agent system with much uncertainty.

In summary, the contributions made in this dissertation have furthered the ability of fast adaptation-based control algorithms to be applied to real world systems with limited sampling rates. There still exist theoretical developments to be made in these fast adaptation-

based algorithms, and there is a breadth of new applications to be studied.

Bibliography

[1] Aim laboratory. http://aim.engr.uconn.edu/projects.html. Accessed: 2016-06-20.

[2] George Biddell Airy. *On the Disturbances of Pendulums and Balances, and on the Theory of Escapements*. publisher not identified, 1826.

[3] Karl J Astrom. Adaptive control around 1960. *Control Systems, IEEE*, 16(3):44–49, 1996.

[4] Richard Bellman. Dynamic programming and lagrange multipliers. *Proceedings of the National Academy of Sciences*, 42(10):767–769, 1956.

[5] Richard Bellman and Robert Kalaba. *Mathematical Trends in Control Theory*. Dover, 1964.

[6] Hendrik W Bode. Feedback: The history of an idea. In *Proceedings of the Symposium on Active Networks and Feedback Systems, Polytechnic Press*, 1960.

[7] Anthony J Calise and Rolf T Rysdyk. Nonlinear adaptive flight control using neural networks. *Control Systems, IEEE*, 18(6):14–25, 1998.

[8] A Callender, Douglas R Hartree, and A Porter. Time-lag in a control system. *Philosophical Transactions of the Royal Society of London. Series A, Mathematical and Physical Sciences*, 235(756):415–444, 1936.

[9] Chengyu Cao and N. Hovakimyan. Stability margins of $\mathcal{L}_1$ adaptive controller: Part ii. In *American Control Conference, 2007. ACC '07*, pages 3931 –3936, July 2007.

[10] Chengyu Cao and Naira Hovakimyan. Novel neural network adaptive control architecture with guaranteed transient performance. *Neural Networks, IEEE Transactions on*, 18(4):1160–1171, 2007.

[11] Chengyu Cao and Naira Hovakimyan. $\mathcal{L}_1$ adaptive controller for nonlinearities: Part i. 2008.

[12] Chengyu Cao and Naira Hovakimyan. $\mathcal{L}_1$ adaptive output feedback controller for non-strictly positive real reference systems with applications to aerospace examples. In *AIAA Guidance, Navigation, and Control Conference and Exhibit*, 2008.

[13] Chengyu Cao and Naira Hovakimyan. $\mathcal{L}_1$ adaptive output-feedback controller for non-strictly-positive-real reference systems: missile longitudinal autopilot design. *Journal of guidance, control, and dynamics*, 32(3):717–726, 2009.

[14] Fu-Chuang Chen and Hassan K Khalil. Adaptive control of nonlinear systems using neural networks. *International Journal of Control*, 55(6):1299–1317, 1992.

[15] Fu-Chuang Chen and Chen-Chung Liu. Adaptively controlling nonlinear continuous-time systems using multilayer neural networks. *Automatic Control, IEEE Transactions on*, 39(6):1306–1310, 1994.

[16] H. Chen, G. Chen, E. Blasch, and K. Pham. Comparison of several space target tracking filters. In P. Moteghedi L. Cox, editor, *Sensors and Systems for Space Applications III*, pages APM–241. SPIE, 2009.

[17] John Cooper and Chengyu Cao. $\mathcal{L}_1$ adaptive controller with additional uncertainty bias estimation. In *Control and Decision Conference (CCDC), 2013 25th Chinese*, pages 607–611. IEEE, 2013.

[18] John Cooper, Jiaxing Che, and Chengyu Cao. The use of learning in fast adaptation algorithms. *International Journal of Adaptive Control and Signal Processing*, 28(3-5):325–340, 2014.

[19] John R Cooper, Chengyu Cao, and Jiong Tang. Control of a nonlinear pressure-regulating engine bleed valve in aircraft air management systems. In *ASME 2013 Dynamic Systems and Control Conference*, pages V001T15A013–V001T15A013. American Society of Mechanical Engineers, 2013.

[20] Vladimir Dobrokhodov, Oleg Yakimenko, Kevin D Jones, Isaac Kaminer, Eugene Bourakov, Ioannis Kitsios, and Mariano Lizarraga. New generation of rapid flight test prototyping system for small unmanned air vehicles. In *AIAA Modeling and Simulation Technologies Conference and Exhibit*, page 6567, 2007.

[21] Ali Elahidoost, John Cooper, Chengyu Cao, and Khanh Pham. Satellite orbit stabilization using $\mathcal{L}_1$ adaptive control. In *AIAA Guidance, Navigation, and Control Conference*, page 4923, 2012.

[22] Mohammad H Elahinia and Hashem Ashrafiuon. Nonlinear control of a shape memory alloy actuated manipulator. *Journal of vibration and acoustics*, 124(4):566–575, 2002.

[23] Walter R Evans. Graphical analysis of control systems. *American Institute of Electrical Engineers, Transactions of the*, 67(1):547–551, 1948.

[24] Shuzhi Sam Ge and Cong Wang. Adaptive neural control of uncertain mimo nonlinear systems. *Neural Networks, IEEE Transactions on*, 15(3):674–692, 2004.

[25] Shuzhi Sam Ge and Jin Zhang. Neural-network control of nonaffine nonlinear system with zero dynamics by state and output feedback. *Neural Networks, IEEE Transactions on*, 14(4):900–918, 2003.

[26] Glenn B Gilyard and John S Orme. Subsonic flight test evaluation of a performance seeking control algorithm on an f-15 airplane. 1992.

[27] Glenn B Gilyard and John S Orme. Performance seeking control: program overview and future directions. 1993.

[28] Graham Goodwin, P Ramadge, and P Caines. Discrete-time multivariable adaptive control. *Automatic Control, IEEE Transactions on*, 25(3):449–456, 1980.

[29] Irene M Gregory, Kasey Ackerman, Steve Snyder, and Paul Rothhaar. Adaptive control for tilt-wing vtol uav. In *2015 American Control Conference (ACC)*, pages 2535–2535. IEEE, 2015.

[30] Irene M Gregory, Chengyu Cao, Enric Xargay, Naira Hovakimyan, and Xiaotian Zou. $\mathcal{L}_1$ adaptive control design for nasa airstar flight test vehicle. In *AIAA Guidance, Navigation, and Control Conference, Chicago, IL*, 2009.

[31] Philip C Gregory. Air research and development command plans and programs. In *Proc. Self Adaptive Flight Control Symp*, pages 8–15. OH: Wright-Patterson Air Force Base, 1959.

[32] Peter Hodal and Guangjun Liu. Bleed air temperature regulation system: modeling, control, and simulation. In *Control Applications, 2005. CCA 2005. Proceedings of 2005 IEEE Conference on*, pages 1003–1008. IEEE, 2005.

[33] Naira Hovakimyan, Chengyu Cao, Evgeny Kharisov, Enric Xargay, and Irene M Gregory. Adaptive control for safety-critical systems. *Control Systems, IEEE*, 31(5):54–104, 2011.

[34] P Ioannou and Petar Kokotovic. Robust redesign of adaptive control. *Automatic Control, IEEE Transactions on*, 29(3):202–211, 1984.

[35] Petros A Ioannou and Petar V Kokotovic. Instability analysis and improvement of robustness of adaptive control. *Automatica*, 20(5):583–594, 1984.

[36] Hubert Maxwell James, Nathaniel B Nichols, Ralph Saul Phillips, and CH Dowker. *Theory of servomechanisms*, volume 25. McGraw-Hill New York, 1947.

[37] Ri E Kalman. Design of a self-optimising control system. *Trans. ASME*, 80:468–478, 1958.

[38] George Kopasakis. *Adaptive performance seeking control using fuzzy model reference learning control and positive gradient control*. National Aeronautics and Space Administration, 1997.

[39] Miroslav Krstic, Ioannis Kanellakopoulos, Petar V Kokotovic, et al. *Nonlinear and adaptive control design*, volume 8. John Wiley & Sons New York, 1995.

[40] Jeffery R Layne and Kevin M Passino. Fuzzy model reference learning control for cargo ship steering. *Control Systems, IEEE*, 13(6):23–34, 1993.

[41] D. J. Leith and W.E. Leithead. Survey of gain-scheduling analysis & design. *International Journal of Control*, 73:1001–1025, 2000.

[42] Frank L Lewis, A Yeşildirek, and Kai Liu. Neural net robot controller: Structure and stability proofs. *Journal of Intelligent and Robotic Systems*, 12(3):277–299, 1995.

[43] Frank L Lewis, Aydin Yesildirek, and Kai Liu. Multilayer neural-net robot controller with guaranteed tracking performance. *Neural Networks, IEEE Transactions on*, 7(2):388–399, 1996.

[44] Dapeng Li, Vijay Patel, Chengyu Cao, Naira Hovakimyan, and Kevin Wise. Optimization of the time-delay margin of $\mathcal{L}_1$ adaptive controller via the design of the underlying filter. In *AIAA Guidance, Navigation and Control Conference and Exhibit*, page 6646, 2007.

[45] Jie Luo and Chengyu Cao. $\mathcal{L}_1$ adaptive output feedback controller for a class of nonlinear systems. In *Decision and Control and European Control Conference (CDC-ECC), 2011 50th IEEE Conference on*, pages 5425–5430. IEEE, 2011.

[46] Jie Luo and Chengyu Cao. Consensus in multi-agent systems with nonlinear uncertainties under a fixed undirected graph. *International Journal of Control, Automation and Systems*, 12(2):231–240, 2014.

[47] Jie Luo, John Cooper, Chengyu Cao, and Khanh Pham. Cooperative adaptive control of a two-agent system. In *2012 American Control Conference (ACC)*, pages 2413–2418. IEEE, 2012.

[48] Jie Luo, John Cooper, Chengyu Cao, and Khanh Pham. Cooperative adaptive control of a two-agent system. *International Journal of Control*, 86(1):127–138, 2013.

[49] A Lyapunov. Probleme general de la stabilite du mouvement, commun. soc. math. kharkov (1892, 1893). *Annals of Mathematical Studies*, 17.

[50] J Clerk Maxwell. On governors. *Proceedings of the Royal Society of London*, 16:270–283, 1867.

[51] Otto Mayr. *The origins of feedback control*. 1975.

[52] D.C. McFarlane and K. Glover. A loop shaping design procedure using synthesis. *IEEE Transactions on Automatic Control*, 37(6):759–769, June 1992.

[53] W Thomas Miller, Paul J Werbos, and Richard S Sutton. *Neural networks for control*. MIT press, 1995.

[54] Eli Mishkin and Ludwig Braun. *Adaptive control systems*. McGraw-Hill, 1961.

[55] Kumpati S Narendra and Kannan Parthasarathy. Identification and control of dynamical systems using neural networks. *Neural Networks, IEEE Transactions on*, 1(1):4–27, 1990.

[56] Kumpati S Narendra and Kannan Parthasarathy. Gradient methods for the optimization of dynamical systems containing neural networks. *Neural Networks, IEEE Transactions on*, 2(2):252–262, 1991.

[57] Kumpatis Narendra and Anuradham Annaswamy. A new adaptive law for robust adaptation without persistent excitation. *Automatic Control, IEEE Transactions on*, 32(2):134–145, 1987.

[58] SG Nobbs, SW Jacobs, and DJ Donahue. Development of the fi. l-envelope performance seeking control algorithm. 1992.

[59] Harry Nyquist. Regeneration theory. *Bell System Technical Journal*, 11(3):126–147, 1932.

[60] John S Orme and Timothy R Conners. Supersonic flight test results of a performance seeking control algorithm on a nasa f-15 aircraft. *AIAA Paper*, pages 94–3210, 1994.

[61] PC Parks. Liapunov redesign of model reference adaptive control systems. *Automatic Control, IEEE Transactions on*, 11(3):362–367, 1966.

[62] Isabel Pérez-Grande and Teresa J Leo. Optimization of a commercial aircraft environmental control system. *Applied thermal engineering*, 22(17):1885–1904, 2002.

[63] Marios M Polycarpou. Stable adaptive neural control scheme for nonlinear systems. *Automatic Control, IEEE Transactions on*, 41(3):447–451, 1996.

[64] Marios M Polycarpou and Petros A Ioannou. Modelling, identification and stable adaptive control of continuous-time nonlinear dynamical systems using neural networks. In *American Control Conference, 1992*, pages 36–40. IEEE, 1992.

[65] Marios M Polycarpou and Petros A Ioannou. Neural networks as on-line approximators of nonlinear systems. In *Decision and Control, 1992., Proceedings of the 31st IEEE Conference on*, pages 7–12. IEEE, 1992.

[66] Lev Semenovich Pontryagin. Optimal regulation processes. *Uspekhi Matematicheskikh Nauk*, 14(1):3–20, 1959.

[67] Michael JD Powell. An efficient method for finding the minimum of a function of several variables without calculating derivatives. *The computer journal*, 7(2):155–162, 1964.

[68] Charles E Rohrs, Lena Valavani, Michael Athans, and Gunter Stein. Robustness of adaptive control algorithms in the presence of unmodeled dynamics. In *Decision and Control, 1982 21st IEEE Conference on*, pages 3–11. IEEE, 1982.

[69] Paul M Rothhaar, Patrick C Murphy, J Bacon Barton, Irene M Gregory, Jared A Grauer, Ronald C Busan, and Mark A Croom. Nasa langley distributed propulsion vtol tilt-wing aircraft testing, modeling, simulation, control, and flight test development. In *14th AIAA Aviation Technology, Integration, and Operations Conference, Atlanta, GA*, 2014.

[70] Edward John Routh. *A treatise on the stability of a given state of motion: particularly steady motion*. Macmillan and Company, 1877.

[71] George A Rovithakis and Manolis A Christodoulou. Adaptive control of unknown plants using dynamical neural networks. *Systems, Man and Cybernetics, IEEE Transactions on*, 24(3):400–412, 1994.

[72] George A Rovithakis and Manolis A Christodoulou. Direct adaptive regulation of unknown nonlinear dynamical systems via dynamic neural networks. *Systems, Man and Cybernetics, IEEE Transactions on*, 25(12):1578–1594, 1995.

[73] Nader Sadegh. A perceptron network for functional identification and control of nonlinear systems. *Neural Networks, IEEE Transactions on*, 4(6):982–988, 1993.

[74] Robert M Sanner and Jean-Jacques E Slotine. Gaussian networks for direct adaptive control. *Neural Networks, IEEE Transactions on*, 3(6):837–863, 1992.

[75] Kurt Seldner. Performance-seeking controls. In *NASA Conference Publication 2137*, page 11, 1979.

[76] B Shachcloth and RL Butchart. Synthesis of model reference adaptive control systems by lyapunov's second methods. *IFAC Aymposium, Jeddinglon*, 1965.

[77] Lan Shang and Guangjun Liu. Optimal control of a bleed air temperature regulation system. In *Mechatronics and Automation, 2007. ICMA 2007. International Conference on*, pages 2610–2615. IEEE, 2007.

[78] Lan Shang and Guangjun Liu. Sensor and actuator fault detection and isolation for a high performance aircraft engine bleed air temperature control system. *Control Systems Technology, IEEE Transactions on*, 19(5):1260–1268, 2011.

[79] Lan Shang, Guangjun Liu, and Peter Hodal. Development of high performance aircraft bleed air temperature control system with reduced ram air usage. *Control Systems Technology, IEEE Transactions on*, 18(2):438–445, 2010.

[80] Jeffrey T Spooner and Kevin M Passino. Decentralized adaptive control of nonlinear systems using radial basis neural networks. *Automatic Control, IEEE Transactions on*, 44(11):2050–2057, 1999.

[81] Jiang Wang, Chengyu Cao, Vijay V Patel, Naira Hovakimyan, and Eugene Lavretsky. $\mathcal{L}_1$ adaptive neural network controller for autonomous aerial refueling with guaranteed transient performance. In *AIAA Guidance, Navigation, and Control Conference, Keystone, CO*, 2006.

[82] Norbert Wiener. Generalized harmonic analysis. *Acta Mathematica*, 55(1):117–258, 1930.

[83] Enric Xargay, Naira Hovakimyan, Vladimir Dobrokhodov, Roman Statnikov, Isaac Kaminer, Chengyu Cao, and Irene Gregory. $\mathcal{L}_1$ adaptive flight control system: sys-

tematic design and verification and validation of control metrics. In *AIAA Guidance, Navigation, and Control Conference*, page 7773, 2010.

[84] Haojian Xu and Petros A Ioannou. Robust adaptive control for a class of mimo nonlinear systems with guaranteed error bounds. *Automatic Control, IEEE Transactions on*, 48(5):728–742, 2003.

[85] Willard I Zangwill. Minimizing a function without calculating derivatives. *The Computer Journal*, 10(3):293–296, 1967.

[86] T Zhang, SS Ge, and CC Hang. Adaptive output feedback control for general nonlinear systems using multilayer neural networks. In *American Control Conference, 1998. Proceedings of the 1998*, volume 1, pages 520–524. IEEE, 1998.